PL-TR-91-2059(II)

AD-A236 984

HIGH FREQUENCY ARRAY STUDIES OF LONG RANGE
Lg PROPAGATION AND THE CAUSES OF Lg BLOCKAGE
AND ATTENUATION IN THE EURASIAN CONTINENTAL CRATON

Douglas R. Baumgardt

ENSCO, Inc.
5400 Port Royal Road
Springfield, Virginia 22151-2388

21 March 1991

Final Report (Volume II)
29 September 1989-30 January 1991

DTIC
ELECTE
JUN 13 1991
E

APPROVED FOR PUBLIC RELEASE; DISTRIBUTION UNLIMITED

PHILLIPS LABORATORY
AIR FORCE SYSTEMS COMMAND
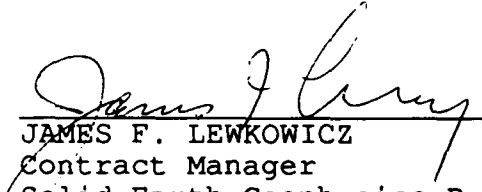HANSCOM AIR FORCE BASE, MASSACHUSETTS 01731-5000
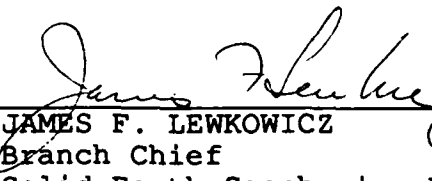
91-01983

91 6 12 062

This technical report has been reviewed and is approved for
publication.

JAMES F. LEWKOWICZ
Contract Manager
Solid Earth Geophysics Branch
Earth Sciences Division

JAMES F. LEWKOWICZ
Branch Chief
Solid Earth Geophysics Branch
Earth Sciences Division

DONALD H. ECKHARDT, Director
Earth Sciences Division

REPORT DOCUMENTATION PAGE

1a. REPORT SECURITY CLASSIFICATION UNCLASSIFIED			1b. RESTRICTIVE MARKINGS N/A
2a. SECURITY CLASSIFICATION AUTHORITY			3. DISTRIBUTION/AVAILABILITY OF REPORT Approved for public release;
2b. DECLASSIFICATION/DOWNGRADING SCHEDULE			Distribution unlimited
4. PERFORMING ORGANIZATION REPORT NUMBER(S) SAS-TR-91-50			5. MONITORING ORGANIZATION REPORT NUMBER (S) PL-TR-91-2059 (II)
6a. NAME OF PERFORMING ORGANIZATION ENSCO, Inc.		6b. OFFICE SYMBOL (If applicable)	7a. NAME OF MONITORING ORGANIZATION Phillips Laboratory
6b. ADDRESS (CITY, STATE, AND ZIP CODE) 5400 Port Royal Road Springfield, VA 22151-2388			7b. ADDRESS (CITY, STATE, AND ZIP CODE) Hanscom AFB, MA 01731-5000
8a. NAME OF FUNDING/SPONSORING ORGANIZATION		8b. OFFICE SYMBOL	9. PROCUREMENT INSTRUMENT IDENTIFICATION NUMBER F19628-89-C-0030

8c. ADDRESS (City, State, and Zip Code)	10. SOURCE OF FUNDING NUMBERS			
	PROGRAM ELEMENT	PROJECT NO.	TASK NO.	ACCESSION NO. WORK UNIT
	62714E	9A10	DA	BA

11. TITLE (Include Security Classification)
High Frequency Array Studies of Long Range Lg Propagation and
the Causes of Lg Blockage and Attenuation in the Eurasian Continental Craton

12. PERSONAL AUTHOR(S).
Dr. Douglas R. Baumgardt

13. TYPE OF REPORT Final Vol II	13b. TIME COVERED FROM 9/29/89 TO 1/30/91	14. DATE OF REPORT (Year, Month, Day) 1991 March 21	15. PAGE COUNT 136

16. SUPPLEMENTARY NOTATION

17. COSATI CODES			18. SUBJECT TERMS (Continue on reverse if necessary and identify by block number)
FIELD	GROUP	SUB-GROUP	Lg, Blockage, Sedimentary Basins, Scattering, Frequency
			Wavenumber Analysis, Ray Tracing

19. ABSTRACT (Continue on reverse if necessary and identify by block number)

It is usually assumed that Lg waves should propagate efficiently to far regional distances in continental shield regions because of the high crustal Q. However, analyses of Lg waves from presumed Soviet weapons tests and PNEs in the Soviet platform recorded at regional and far regional distances exhibit large variations in amplitude. Determinations of Lg Q from the spectral slope are generally high, characteristic of shield regions, and do not correlate with variations in the Lg amplitudes. Incoherent beam and continuous FK analyses of Lg and pre-Lg coda waves indicate that partial blockages are associated with enhancement of the pre-Lg coda, which appears to be produced by increased scattering. The following are examples of partial or complete blockages of Lg waves from these events:

20. DISTRIBUTION/AVAILABILITY OF ABSTRACT ☐ UNCLASSIFIED/UNLIMITED ☒ SAME AS REPORT ☐ DTIC USERS	21. ABSTRACT SECURITY CLASSIFICATION UNCLASSIFIED	
22a. NAME OF RESPONSIBLE INDIVIDUAL James Lewkowicz	22b. TELEPHONE (Include Area Code)	22c. OFFICE SYMBOL PL/LWH

DD FORM 1473, 84 MAR

19.

(1) Nearly complete blockage of Lg from Novaya Zemlya explosions recorded at the NORESS, NORSAR and ARCESS arrays, but not at the Graefenburg array.

(2) Nearly complete blockage of Lg from Azgir and Astrakhan events recorded at NORESS and NORSAR arrays.

(3) Partial blockage of Lg from Semipalatinsk events recorded at ARCESS, but less blockage for Lg recorded at NORSAR, NORESS, and Graefenburg.

(4) Partial blockage of Lg and pre-Lg coda enhancements from PNEs with propagation paths which cross the northern Ural Mountains.

(5) Partial blockage of Lg from PNEs within, or with paths that cross the northern Ural Mountains and the Timan-Pechora Synaclese, a sedimentary basin in the northwestern USSR.

In order to associate Lg amplitude variations with propagation-path characteristics, crustal cross-sections for each Lg-propagation path have been made, assuming that Lg propagates along the great-circle path from source to receiver. The crustal thickness along the path has been estimated from the topographic cross-section, assuming isostatic compensation. For the upper crust, cross-sections of total sediment thickness were estimated from isopach maps assembled by the USGS. We have found that in every instance of partial or complete Lg blockage, the great-circle path of Lg from the source to receiver crosses completely contained sedimentary basins and adjacent topographic discontinuities. Lg blockages do not seem to be related to variations in total crustal thickness. Blockages result from basins where there are unusually thick sediments, usually in excess of 10 km, where the basin is fully contained and the sediments pinch out at the edges of the basin, and/or where there are topographic inhomogeneities at the edges of the basin which may scatter both Sn and Lg waves. Less blockage has been observed for events which occurred inside sedimentary basins themselves, where the basin sediments are not usually thick, or where the sediments thin very gradually with distance. Ray tracing plots show that low velocities in the sediments cause the Lg modes to be delayed and diverted. Repeated reverberations of shear waves, believed to compose the Lg modes, in the low Q sediments may further reduce the amplitudes of Lg waves which propagate through the structure. Sn modes seem to be unaffected, since they presumably are diving waves in the upper mantle and propagate beneath the sedimentary basin. The effects of Lg blockages due to geological heterogeneities such as these need to be taken into account whenever Lg amplitudes are used for yield estimation and event identification.

TABLE OF CONTENTS

SUMMARY

OBJECTIVES

The primary objective of this research has been to investigate the cause of observed variations in the amplitude of Lg waves, which propagate to far regional distances in the Eurasian continental craton. It is usually assumed that Lg waves should propagate efficiently to far regional distances in continental-shield regions because of the high crustal Q. This study follows up earlier research (Baumgardt, 1985 (ʾ, b); Baumgardt, 1987) which has shown that Lg waves, recorded at NORSAR from PNEs in the Soviet Union, exhibit significant amplitude variations that do not seem to relate to crustal-Q variations. The approach has been to try to relate the Lg amplitude variations to the geological and geophysical characteristics of the propagation path, in the form of geologic isopach maps and crustal cross-sections. The goal has been to determine what salient features of the propagation path may cause Lg amplitude variations, due to scattering and blockage effects.

SUMMARY OF RESULTS

Two major studies of Lg propagation have been made under this project. The first study is an investigation of the nature of Lg propagation from the Soviet test site at Novaya Zemlya as recorded by array sensors to the south, including the new regional arrays ARCESS and NORESS, and the teleseismic Graefenburg array, located near the recently installed GERESS regional array. This study is important because of the recently announced intention of the Soviet Union to shift their underground nuclear testing activities from the test site near Semipalatinsk to Novaya Zemlya. The second study follows up earlier ones (Baumgardt, 1985b; Baumgardt, 1987) of long range Lg propagation from nuclear explosions in the platform and shield regions of the Soviet Union. The present study gives geological interpretations of the efficiency of Lg propagation.

Blockage of Lg Waves from Novaya Zemlya

Section 1.0 of this report describes the results of the analysis of *Lg* waves from the Soviet test site at Novaya Zemlya. This study has shown that *Lg* waves from Novaya Zemlya, recorded at the Scandinavian arrays, NORSAR, NORESS, and ARCESS, are clearly blocked. An initial study using the regional arrays, reported in the special issue of the Seismological Society of America bulletin devoted to regional arrays (Baumgardt, 1990), showed that weak *Lg* waves are recorded at the ARCESS and NORESS arrays, but that stronger *Lg* waves are recorded at the Graefenburg array. Section 1.0 describes a follow-up study, which includes analysis of more ARCESS data and additional data from the NORSAR array, shows that the *Lg* blockage may be caused by the Barents sedimentary basin beneath the Barents Sea. "Early *Lg*" waves can be observed at both arrays, which may be caused by *Sn*-to-*Lg* mode conversions from the vertical interface of the Barents Sea sediments and the Kola Peninsula, where no sediments exist. Crustal cross-sections through the region have been made which show that the sediment thicknesses may reach 15 km. Ray tracing plots show that low velocities in the sediments cause the *Lg* modes to be delayed and diverted. Repeated reverberations of shear waves, believed to compose the *Lg* modes, in the low *Q* sediments may further reduce the amplitudes of *Lg* waves, which propagate through the structure. *Sn* modes seem to be unaffected, since they presumably are diving waves in the upper mantle and propagate beneath the sedimentary basin.

Geological Interpretation of Lg Propagation in the Soviet Union

Section 2.0 of this report presents an analysis of the geological heterogeneity along various *Lg* propagation paths which traverse the Soviet Union and the effect of this heterogeneity on the propagation efficiency of *Lg* along the paths. In this study, geological crustal cross-sections were made for several long-range *Lg* propagation paths through the Soviet Union and analyzed to interpret the propagation path features which may be responsible for the observed efficiency or

inefficiency of *Lg* propagation through the region. *Lg* waves appear to be severely blocked by heterogeneities in the upper crust resulting from sedimentary basins in the Soviet shield and platform regions. The biggest effects were produced by the Pechora, Caspian, and Ural Basins. Blockages seem to result from basins where there are unusually thick sediments, usually in excess of 10 km, where the basin is fully contained and the sediments pinch out at the edges of the basin, and/or where there are topographic inhomogeneities at the edge of the basin which may scatter both *Sn* and *Lg* waves. Less blockage has been observed for events which occurred inside sedimentary basins themselves, where the basin sediments are not usually thick, or where the sediments thin very gradually with distance. The Ural Mountains and the adjacent sedimentary seem to partially block *Lg* waves, although the central Urals may pose more of a block than the southern Urals.

OVERALL CONCLUSIONS

The overall conclusion of this study is that heterogeneity in the upper crust, sometimes referred to as the "granitic layer," seems to be the primary factor in the blockage of *Lg*. Whenever a large part of the granitic layer is replaced in a confined region, like in a basin, by lower velocity sediments, such that there is a large velocity contrast between the basin sediments and the surrounding granitic rocks, *Lg* waves appear to be trapped in the basin and are attenuated by repeated reverberations in the basin. As a result, *Lg* waves are delayed, diverted, scattered, and hence, blocked, such that their recorded amplitudes are much reduced compared with what is expected from anelastic attenuation. The effects of *Lg* blockages need to be taken into account whenever *Lg* amplitudes are used for yield estimation and event identification.

1.0 CAUSE OF THE BLOCKAGE AND SCATTERING OF LG WAVES FROM PRESUMED NUCLEAR EXPLOSION AT NOVAYA ZEMLYA

1.1 INTRODUCTION

The Lg phase has assumed critical importance in test ban treaty monitoring, both for yield estimation and event identification. In yield estimation, Lg amplitudes have been shown to provide improved precision for relative yield estimation (Hansen et al, 1990), although methods for path correcting Lg amplitudes for estimation of absolute yields, such as the $Lg \, Q$ correction method of Nuttli (1988), are still uncertain. In seismic discrimination, recent studies have shown that explosions and earthquakes may be separable, based on the latter having higher Lg excitation relative to P than the former (Bennett et al, 1989; Baumgardt and Young, 1990). In both these applications, the proper use of Lg amplitude measurements for seismic source characterization requires that propagation path effects on Lg amplitudes be understood.

In 1989, the Soviet Union announced its intention to shift its weapons testing activities from the western Kazakh test site near Semipalatinsk to the Arctic island of Novaya Zemlya. As a result of this decision, increased attention has been placed on regional propagation, particularly Lg phase propagation, from Novaya Zemlya to regional stations.

The Novaya Zemlya test sites are within regional distances to the regional arrays, ARCESS (10°) and NORESS (21°), and Lg waves would normally be expected to be recorded at these two arrays from explosions at these two test sites. However, Baumgardt (1990) has shown that Lg is almost completely missing at ARCESS and very poorly recorded at NORESS. The most likely explanation for this Lg "blockage" is that Lg must cross the Barents Sea from the Novaya Zemlya island to Scandinavia. Geological evidence from the Soviet literature indicates that the Barents Sea is underlain by a sedimentary basin, with sediment thicknesses on the order of 15 km. Baumgardt (1990) suggested that this laterally heterogeneous structure causes a breakdown in the Lg crustal

1

waveguide across which the phase does not propagate. However, this study presented no explicit mechanism for how the sedimentary basin actually blocks *Lg*.

This report presents the results of a follow-up study of the Barents Sea *Lg* blockage. We examine the nature of the blockage in more detail, using data from the NORSAR teleseismic array. A preliminary analysis of this data had been presented in an earlier study (Baumgardt, 1990), in which it was argued that the blockage of *Lg* from Novaya Zemlya could not be explained by the effects of anelastic attenuation alone. Moreover, we also present additional data from *Lg* recorded at different arrays to compare and contrast paths which do and do not pass through the Barents Sea, in order to show how the Barents blocks *Lg* propagation.

We have also studied in detail the topographic and geological characteristics of the propagation paths across the Barents Basin, using information from the Soviet geological literature. Two-dimensional ray tracing calculations of *S* waves in a simulated basin structure were done in order to model how *Lg* waves, which are primarily composed of S-wave reverberations in the crust, could be blocked by such a structure. It will be shown that if the granitic layer in the crust is replaced by a lower velocity sedimentary column in a basin, the basin essentially acts as an *Lg* trap, in which the *Lg* waves are captured by the basin and are attenuated by reverberations within the basin. The effects of such sedimentary basin structures, which are quite common throughout the entire Soviet Platform, need to be taken into account, along with anelastic attenuation, in correcting *Lg* amplitudes for propagation path effects in both event identification and yield estimation.

1.2 NORSAR DATA FOR NOVAYA ZEMLYA EXPLOSIONS AND NEARBY PNES

The characteristics of regional waveforms recorded at NORSAR from several nuclear explosions were analyzed. These include Soviet peaceful nuclear explosions (PNEs) on the Kola Peninsula and near the White Sea and five explosions at Novaya Zemlya. The source parameters for these explosions are given in Table 1, and the locations of the explosions and great circle paths from the explosions to NORSAR are shown on the map in Figure 1-1. These events were selected for comparison because the paths from the two PNEs are entirely continental, whereas the path from Novaya Zemlya to NORSAR has a segment which includes the Barents Sea. Thus, comparison of the Lg waves from the PNEs with those from Novaya Zemlya will show directly the effects of the Barents segment on the Lg propagation efficiency.

Although several nuclear explosions have been tested at Novaya Zemlya during the time that the NORSAR array has been operating, almost all the events produced clipped P waveforms at NORSAR because of the large size of the explosions and the efficient propagation paths from Novaya Zemlya to NORSAR. The largest Novaya Zemlya explosions, with body-wave magnitudes in excess of 6.0 which occurred prior to 1976, wrote clipped waveforms at NORSAR throughout the entire time period when Sn and Lg energy is expected. The Novaya Zemlya explosions selected for this study had magnitudes less than 6.0 and were not clipped at the times when Sn and Lg are expected, although the P waves were clipped.

Figure 1-2 shows a record section of the waveforms recorded at the N01A0 channel of NORSAR for the two PNEs and one of Novaya Zemlya explosions. Each waveform has been filtered in the 0.6 to 3.0 Hz band. The arrivals, which have been interpreted as being Pn, Sn, and Lg, are so marked on the waveforms. The two PNEs produced waveforms which resemble typical regional waveforms, with relatively sharp Pn onsets, an emergent arrival corresponding to the Sn

3

TABLE 1

PARAMETERS FOR EVENTS STUDIED AT NORSAR

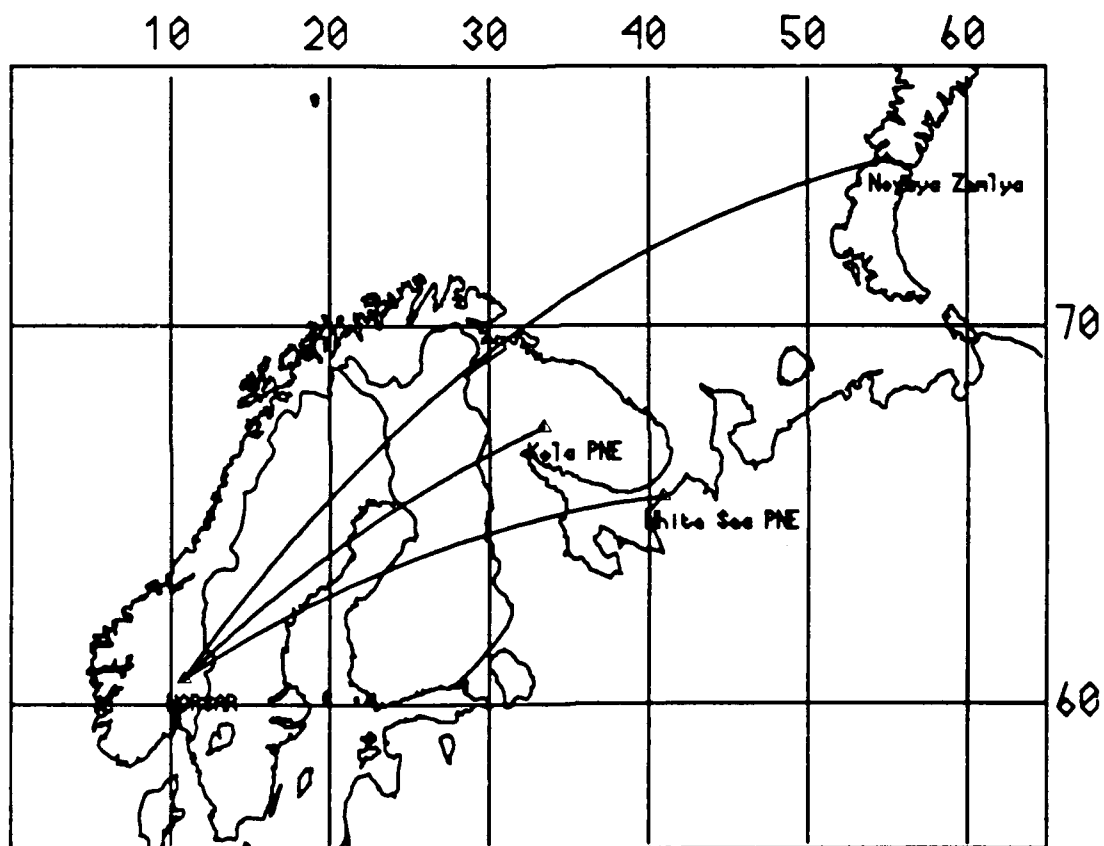| Date	Time	Latitude	Longitude	mb	Region
09/04/72	07-00-03.6	67.69	33.45	4.6	Kola Peninsula
08/10/78	07-59-57.7	73.31	54.70	5.9	Novaya Zemlya
10/11/80	07-09-57.2	73.36	54.82	5.7	Novaya Zemlya
08/18/83	16-09-58.6	73.38	54.87	5.9	Novaya Zemlya
09/25/83	13-09-57.9	73.35	54.38	5.8	Novaya Zemlya
10/25/84	06-29-57.7	73.37	54.96	5.9	Novaya Zemlya
07/18/85	21-14-57.4	65.97	40.86	5.0	White Sea

FIGURE 1-1: Map showing the propagation paths from the Kola Peninsula PNE, the White Sea PNE and the Novaya Zemlya test site from the NORSAR array.
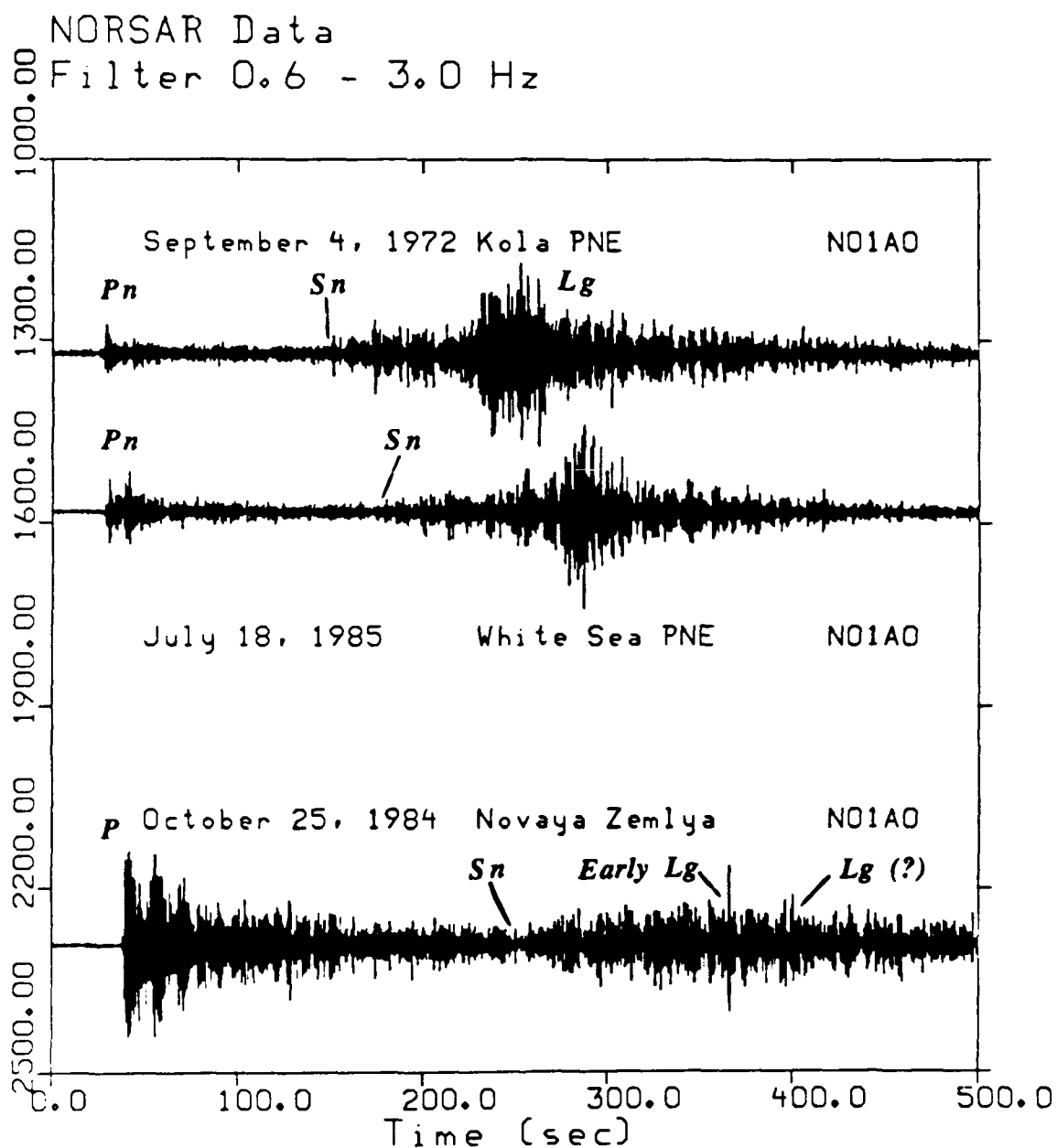
5

FIGURE 1-2: Record section of the waveforms, recorded a the N01A0 subarray sensor at NORSAR, from the Kola Peninsula PNE, the White Sea PNE and the October 25, 1984 Novaya Zemlya nuclear explosion.

6

onset, and strong *Lg* arrivals. The Novaya Zemlya explosion produces a strong *P* signal at NORSAR, an emergent *Sn* onset similar to the one from the PNEs, but no corresponding *Lg* arrival. It should be noted that the *Pn* signal from Novaya Zemlya is clipped, so the actual amplitude of *Pn* relative to *Sn* is actually much greater than that implied in Figure 1-2.

Figure 1-2 clearly shows that *Lg* has been greatly reduced relative to *Pn* for the Novaya Zemlya explosion compared with that of the nearby PNEs. Although some attenuation in *Lg* would be expected due to the increased distance of Novaya Zemlya from NORSAR, compared with the PNEs, the lack of *Lg* from Novaya Zemlya cannot be explained by anelastic attenuation effects alone.

One notable feature of the Novaya Zemlya recording is that there is a strong arrival which appears in the *Sn* coda well ahead of the expected on-time *Lg* arrival. This arrival corresponds in time to the "early *Lg*" phase discussed by Baumgardt (1990), which was also observed for recent Novaya Zemlya explosions recorded at NORESS. This phase was interpreted as being an *Lg* phase because its phase velocity, measured by the frequency-wavenumber (FK) method, was less than 4.0 km/sec. This velocity is lower than expected for *Sn*, but about right for *Lg*. Because the NORESS array is located within the larger NORSAR array, we interpret this phase to be the same "early *Lg*."

The early *Lg*, however, is too early to be the *Lg* which propagates directly from Novaya Zemlya. This phase was interpreted by Baumgardt (1990) to be an *Lg* phase produced by mode conversions of *Sn* at the interface of the Barents Sea and the Kola Peninsula, as shown in Figure 1-3. The point at which the direct *Sn* from Novaya Zemlya intersects the Kola Peninsula, assuming it propagates along the great-circle path, is at a distance of about 13° from NORSAR, as
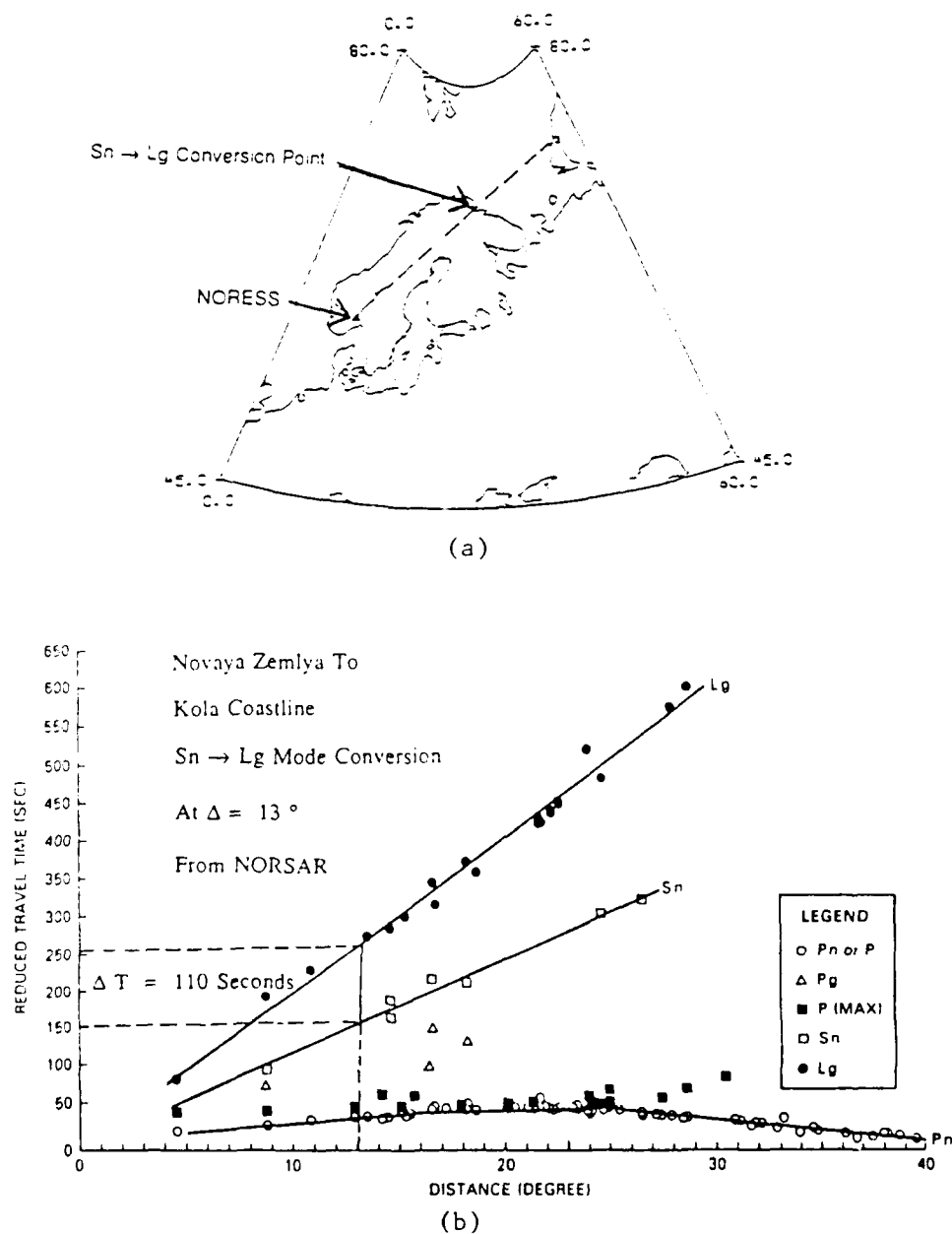
7

FIGURE 1-3: (a) Map showing the location of the proposed *Sn* to *Lg* conversion point at the interface of the Kola Peninsula and the Barents Sea. (b) The relative arrival time of the *Lg* which would follow *Sn* for a mode conversion at 13° from the NORSAR array (modified from Gupta, et al, 1980).

8

shown in Figure 1-3a. If *Lg* originates at that point, due to mode conversion from *Sn*, the converted *Lg* would lag the *Sn* phase by about 110 seconds, using the travel-time curve of Eurasia of Gupta et al (1980), shown in Figure 1-3b. This is about the time delay between the *Sn* onset and the *Sn* - coda arrival in Figure 1-2.

Figure 1-4 shows a plot of the incoherent beams of all five Novaya Zemlya explosions recorded at NORSAR. Incoherent beams, whose computation is described in detail by Baumgardt (1985), are array-stacked log-rms envelope traces. Each trace begins at the *P* onset time and has been shifted by one log-rms unit for display purposes, so the vertical axis only gives relative log-rms amplitudes. The horizontal dashed lines show the mean noise level averaged over two-minutes of noise just ahead of the *P* onset. Each waveform was filtered from 0.6 to 3.0 Hz before the log-rms stack traces were computed.

The first solid vertical line indicates the inferred onset of *Sn*, the vertical dashed line shows the expected arrival time of the *Sn*-to-*Lg* conversion at 110 seconds after the *Sn* phase. A large pulse can be seen on all of the traces, which has a log-rms amplitude above that of the maximum *Sn* amplitude. The second solid vertical line shows the inferred arrival time of the direct *Lg* phase, which should have a group velocity of 3.5 km/sec. This arrival seems to be manifested on each trace by a flattening of the coda level after the early *Lg* onset. This arrival is, in fact, easier to discern on these log-rms incoherent beam traces than on the original seismograms. The signal-to-noise ratio at the time of the expected on-time *Lg* is quite large, although the *Lg* is much less than the *Sn* amplitude.

In summary, the NORSAR data supports the conclusions of Baumgardt (1990) that the propagation of the *Lg* phase from Novaya Zemlya to Norway is blocked and that the shear phases
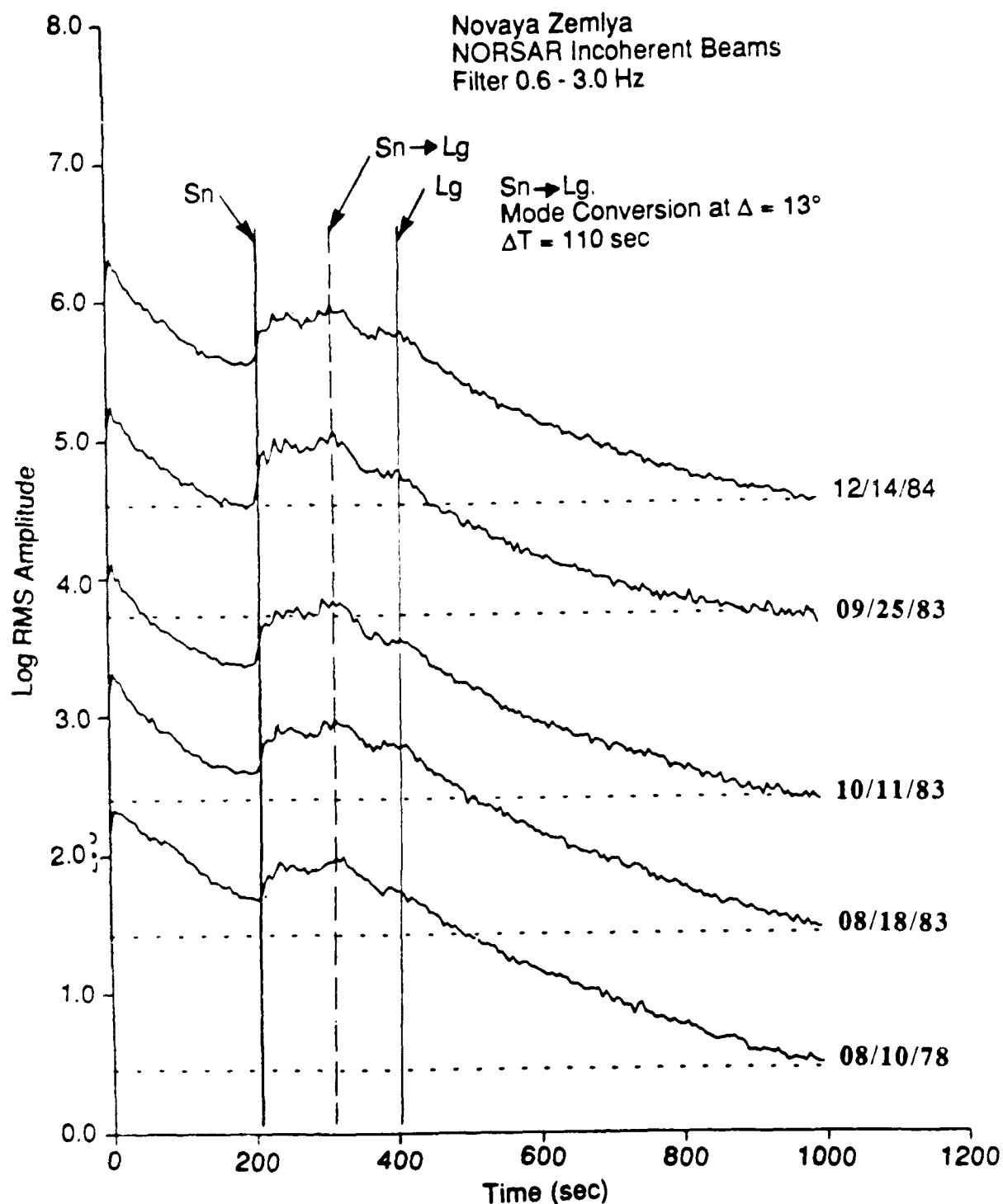
9

FIGURE 1-4: Incoherent beam plots of five Novaya Zemlya nuclear explosions recorded at the NORSAR array. The inferred arrival times of Sn, Lg and the Sn-to-Lg mode conversion from the Kola-Barents interface. Each beam has been shifted by one rms unit for display purposes, so that the vertical axis only refers to relative amplitude levels.

10

from Novaya Zemlya are dominated by the *Sn* phase and an *Sn*-to-*Lg* mode conversion at the Barents Sea-Kola Peninsula interface. A direct *Lg* can also be inferred on the incoherent-beam traces, which is somewhat more apparent on the the NORSAR beams than on the NORESS beams studied by Baumgardt (1990). Although the *Sn* coda at the expected time for *Lg* does have high signal-to-noise ratio, this phase has apparently been much attenuated along the propagation path. Since the only difference between the propagation paths from the PNEs, which produced strong *Lgs* at NORSAR, and Novaya Zemlya is the Barents Sea, it would appear that the Barents Sea segment of the path is responsible for the *Lg* blockage.

1.3 ARCESS, NORESS, AND GRAEFENBURG RECORDINGS OF NOVAYA ZEMLYA EXPLOSIONS

In this section, we present additional analysis of waveforms, recorded at the new ARCESS and NORESS sensors in Norway and at the Graefenburg array in Germany, for nuclear explosions at the Novaya Zemlya test site. This follows up and completes an initial study described by Baumgardt (1990). The event parameters of the Novaya Zemlya explosions which have occurred since ARCESS began recording data are presented in Table 2. The locations of the three arrays and the great-circle propagation paths from Novaya Zemlya to the sites are shown in Figure 1-5.

The waveforms for the three explosions recorded at the ARCESS array center element (FRA0) are shown in Figure 1-6. Baumgardt (1990) showed an incoherent beam for the May 7, 1988 event and indicated that there was no *Lg* recorded at the time expected for an *Lg* with a group velocity of 3.5 km/sec. This fact is reinforced in Figure 1-6, where virtually no energy is present on the ARCESS waveforms for 3.5 km/sec.

11

TABLE 2

PARAMETERS FOR NOVAYA ZEMLYA EVENTS RECORDED AT NORESS AND ARCESS

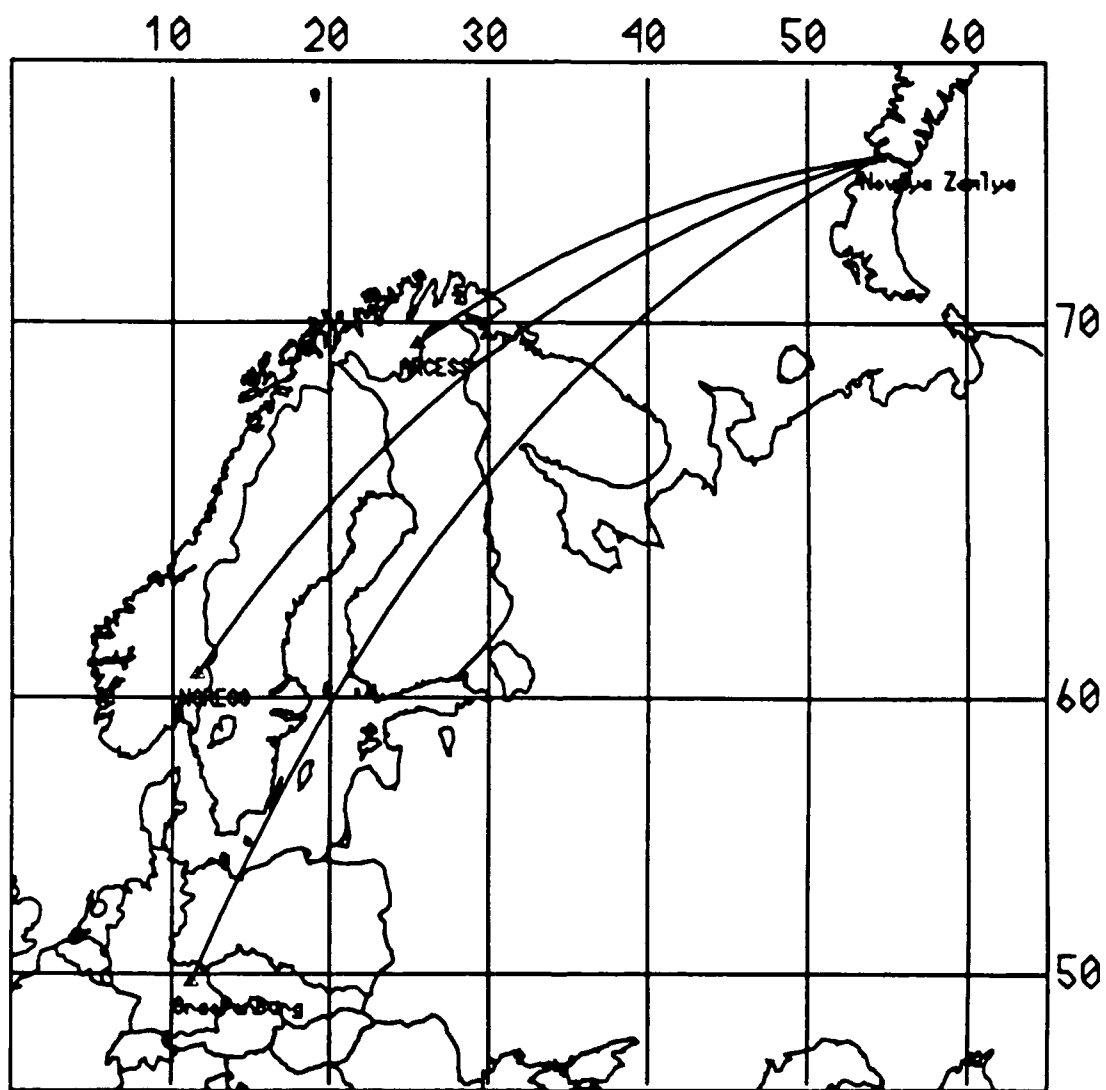| Date	Time	Latitude	Longitude	mb
05/07/88	22-49-58.0	73.35	54.47	5.6
12/04/88	05-19-53.6	73.49	54.18	5.7
10/24/90	14-57-54.7	72.86	54.66	5.4

FIGURE 1-5: Propagation paths from the Novaya Zemlya test site region to the ARCESS, NORESS and Graefenburg arrays.
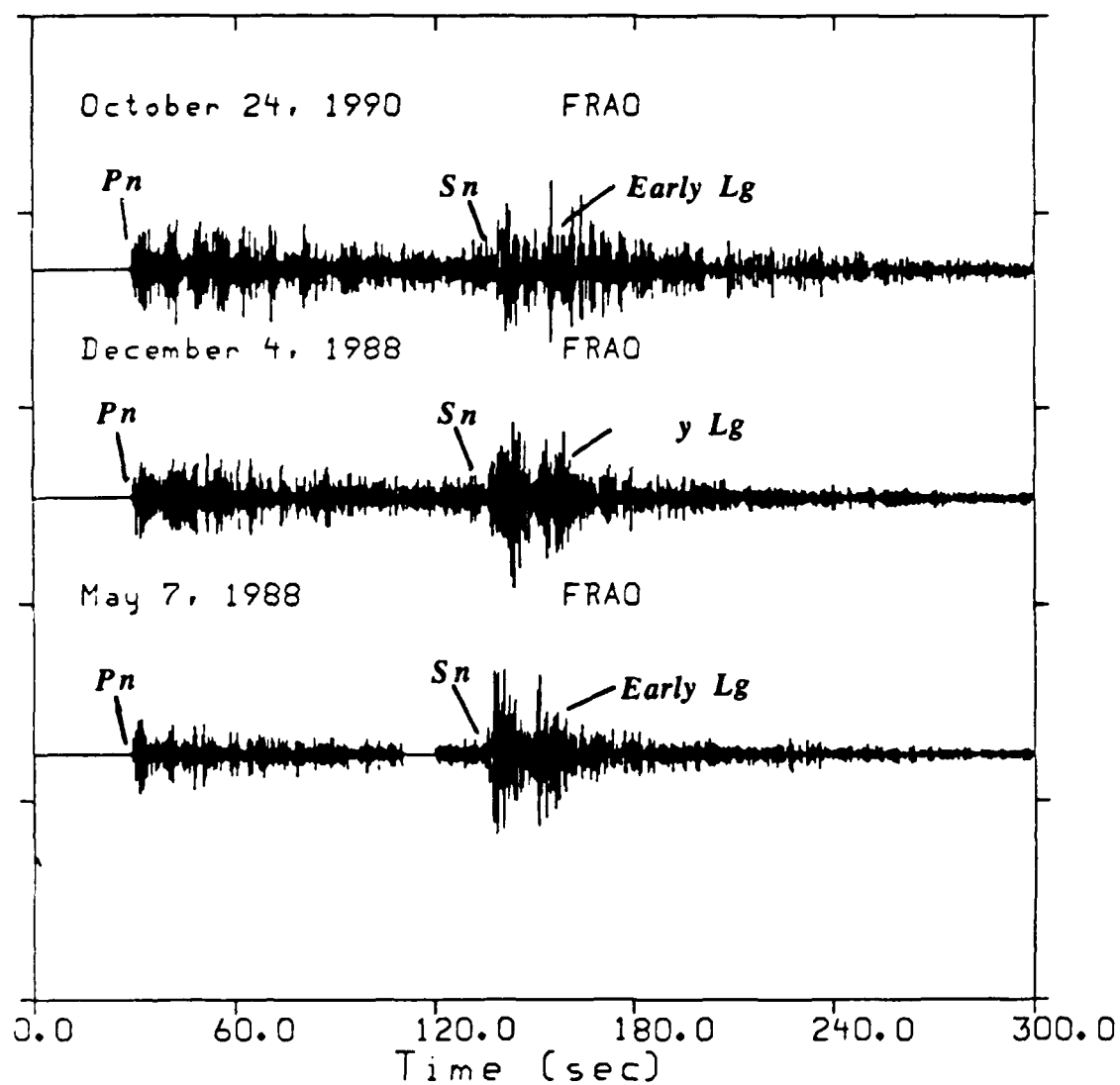
13

FIGURE 1-6: Recordings at the center element (FRA0) of ARCESS from three Novaya Zemlya nuclear explosions.

The results of incoherent beam analysis of these events are shown in Figures 1-7 and 1-8, which show, respectively, the unlogged and logged rms incoherent beams. The beams were computed like the NORSAR beams discussed above by averaging across the array the rms amplitude, in the case of Figure 1-7, and the log-rms amplitude, in Figure 1-8, computed in one second time windows shifted down the trace. The waveforms were pre-filtered from 0.5 to 2.5 Hz prior to computing the beams. The beams have been aligned to the first P onset time, and the horizontal dashed line shows the mean noise level in the segment immediately ahead of the P. Comparison of Figures 1-7 and 1-8 shows that taking the logarithm of the rms amplitude reduces the dynamic range between the largest and smallest amplitudes.

Figures 1-9 and 1-10 show unlogged incoherent beams at ARCESS and NORESS for the December 4, 1988 and the October 24, 1990 events, respectively. The corresponding logged rms incoherent beams are plotted in Figures 1-11 and 1-12. For wavetrains where this dynamic range is large, as in the case of the NORESS recordings of the Novaya Zemlya events shown in Figures 1-9 through 1-12 and for the NORSAR incoherent beams in Figure 1-4, taking the logarithm is useful because of the large difference in amplitude between the P and S wave amplitudes. More details of the Sn codas at NORESS can be discerned on the log-rms plots than on the unlogged plots. In the case of the ARCESS recordings of the same explosions, this amplitude contrast is smaller and the unlogged plots are more informative.

The interesting features visible in the ARCESS recordings of the Novaya Zemlya explosions are that the Sn wave is well recorded, with an impulsive type onset and amplitude which exceeds that of the P wave, and that there is a secondary pulse about 10 to 15 seconds into the Sn coda. This secondary pulse may correspond to the "early Lg" arrival observed at NORSAR and NORESS. Since NORESS and NORSAR are co-located, the "early Lg" phase can be seen in the short period data from both arrays. (Note: It is easiest to see the early Lg at NORESS on the log-rms beam traces in Figures 1-11 and 1-12.) Figures 1-9 through 1-12 compare these

Novaya Zemlya
ARCESS Incoherent Beams
Filter 0.5 - 2.5 Hz.
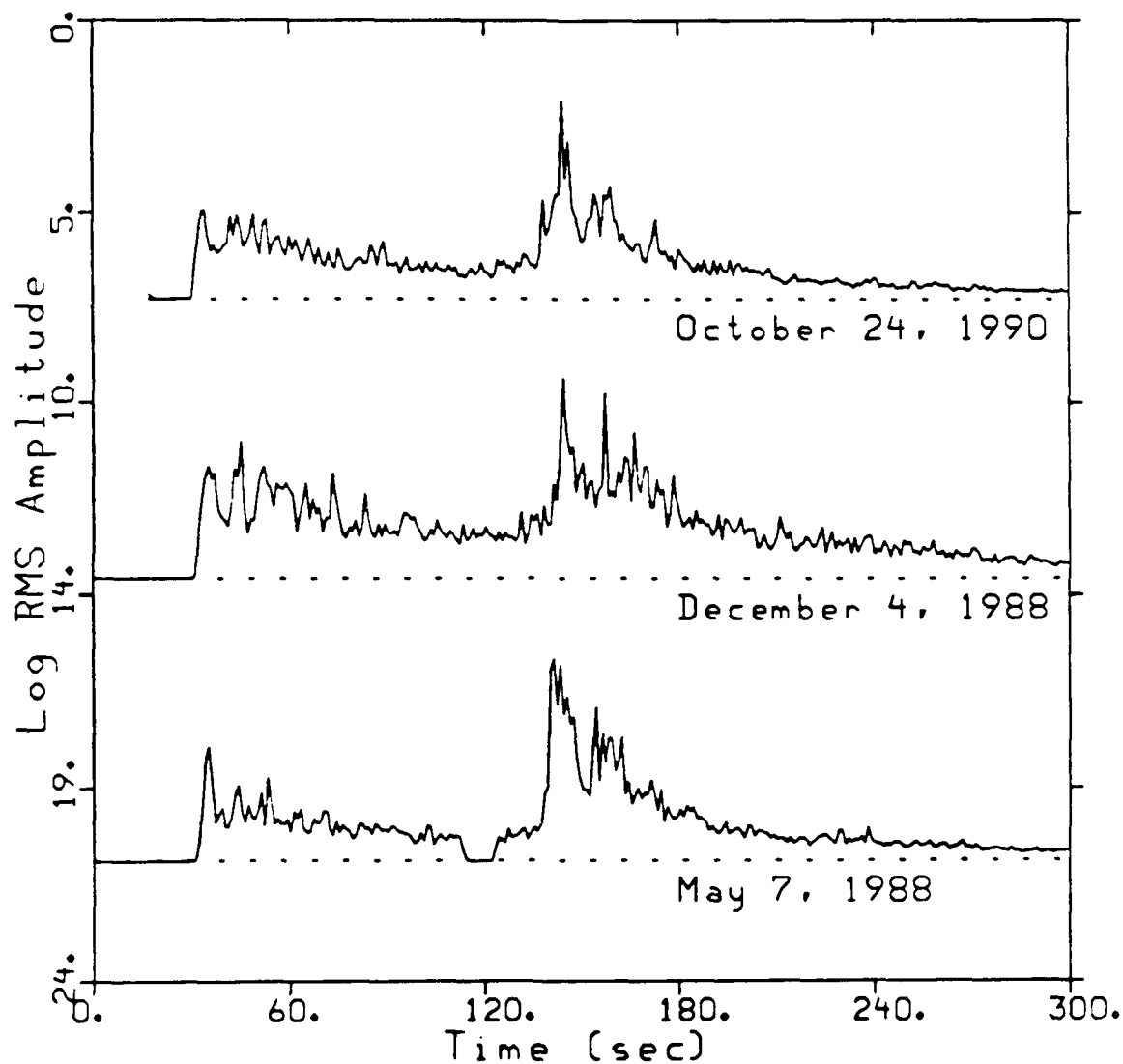
FIGURE 1-7: Unlogged incoherent beams of the same three Novaya Zemlya explosions recorded at the ARCESS array, whose waveforms are shown in Figure 1-6.

16

Novaya Zemlya
ARCESS Incoherent Beams
Filter 0.5 - 2.5 Hz.

FIGURE 1-8: Logged incoherent beams of the same three Novaya Zemlya explosions recorded at the ARCESS array, whose waveforms are shown in Figure 1-6.

Novaya Zemlya
ARCESS and NORESS Incoherent Beams
Filter 0.5 - 2.5 Hz.
December 4, 1988
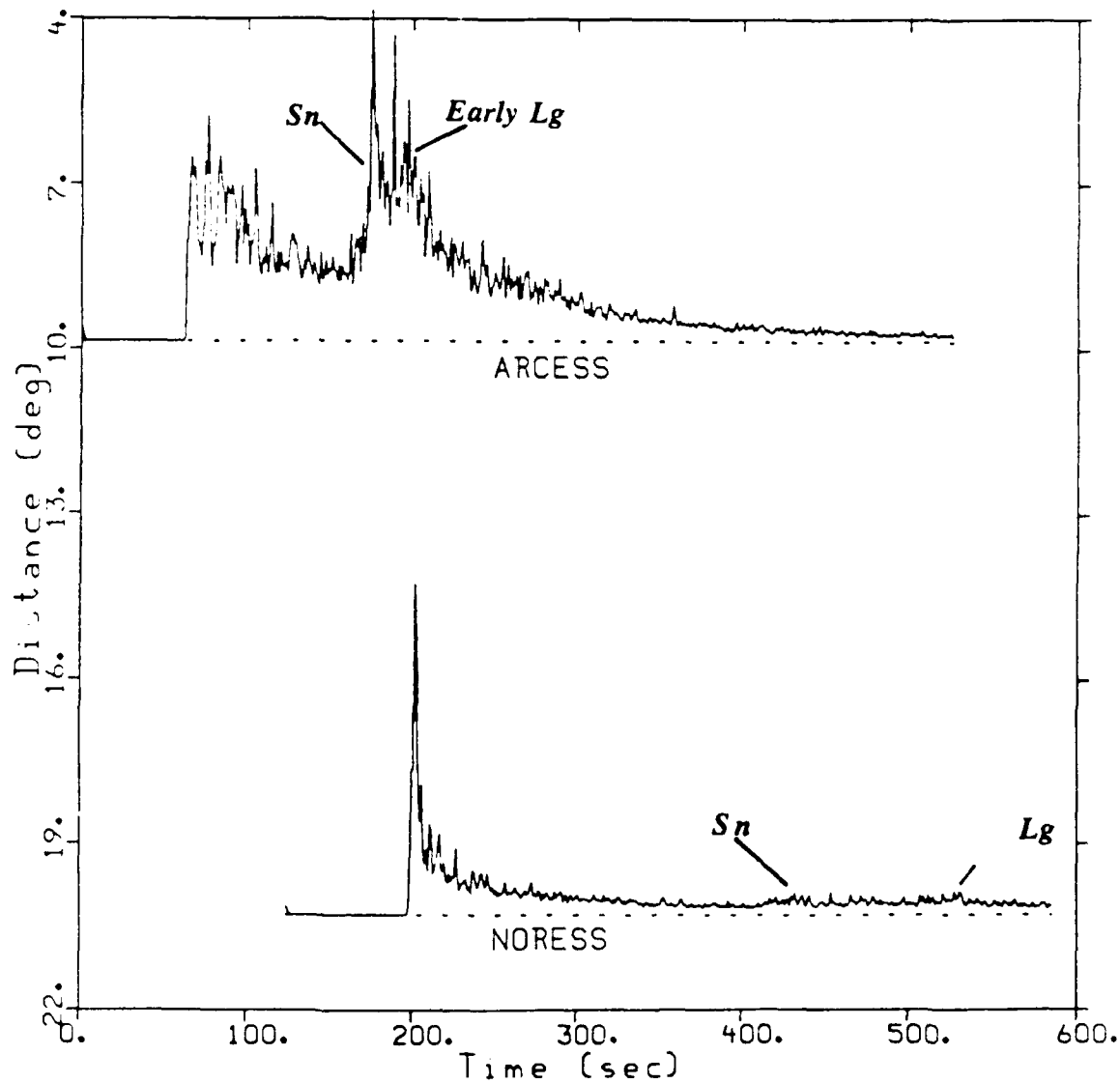
FIGURE 1-9: Comparison of unlogged incoherent beams at ARCESS and NORESS for the December 4, 1988 explosion.

18

Novaya Zemlya
ARCESS and NORESS Incoherent Beams
Filter 0.5 - 2.5 Hz.
October 24, 1990

FIGURE 1-10: Comparison of unlogged incoherent beams at ARCESS and NORESS for the October 24, 1990 explosion.

Novaya Zemlya
ARCESS and NORESS Incoherent Beams
Filter 0.5 - 2.5 Hz.
December 4, 1988
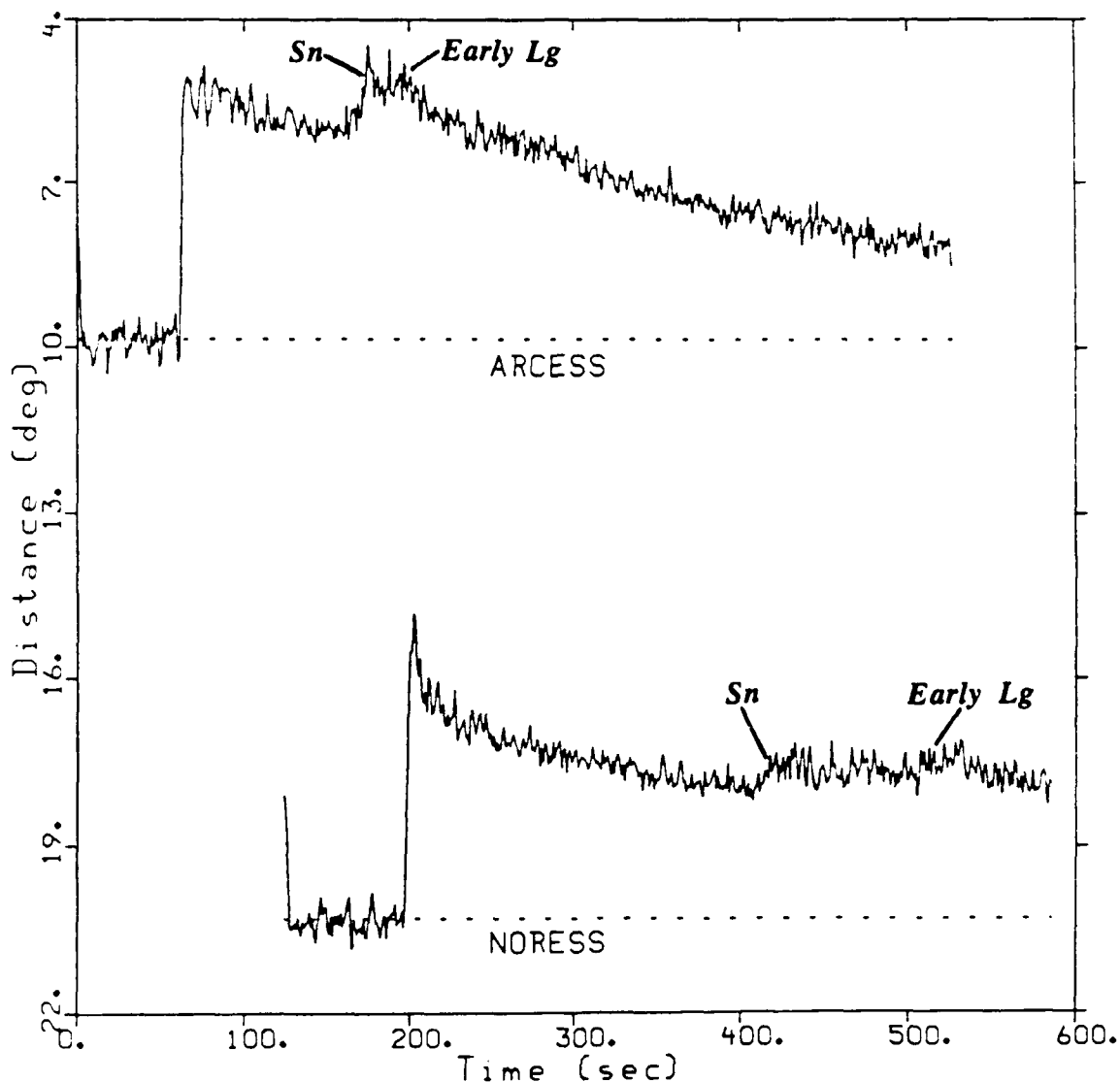
FIGURE 1-11: Comparison of logged incoherent beams at ARCESS and NORESS for the December 4, 1988 explosion.

Novaya Zemlya
ARCESS and NORESS Incoherent Beams
Filter 0.5 - 2.5 Hz.
October 24, 1990
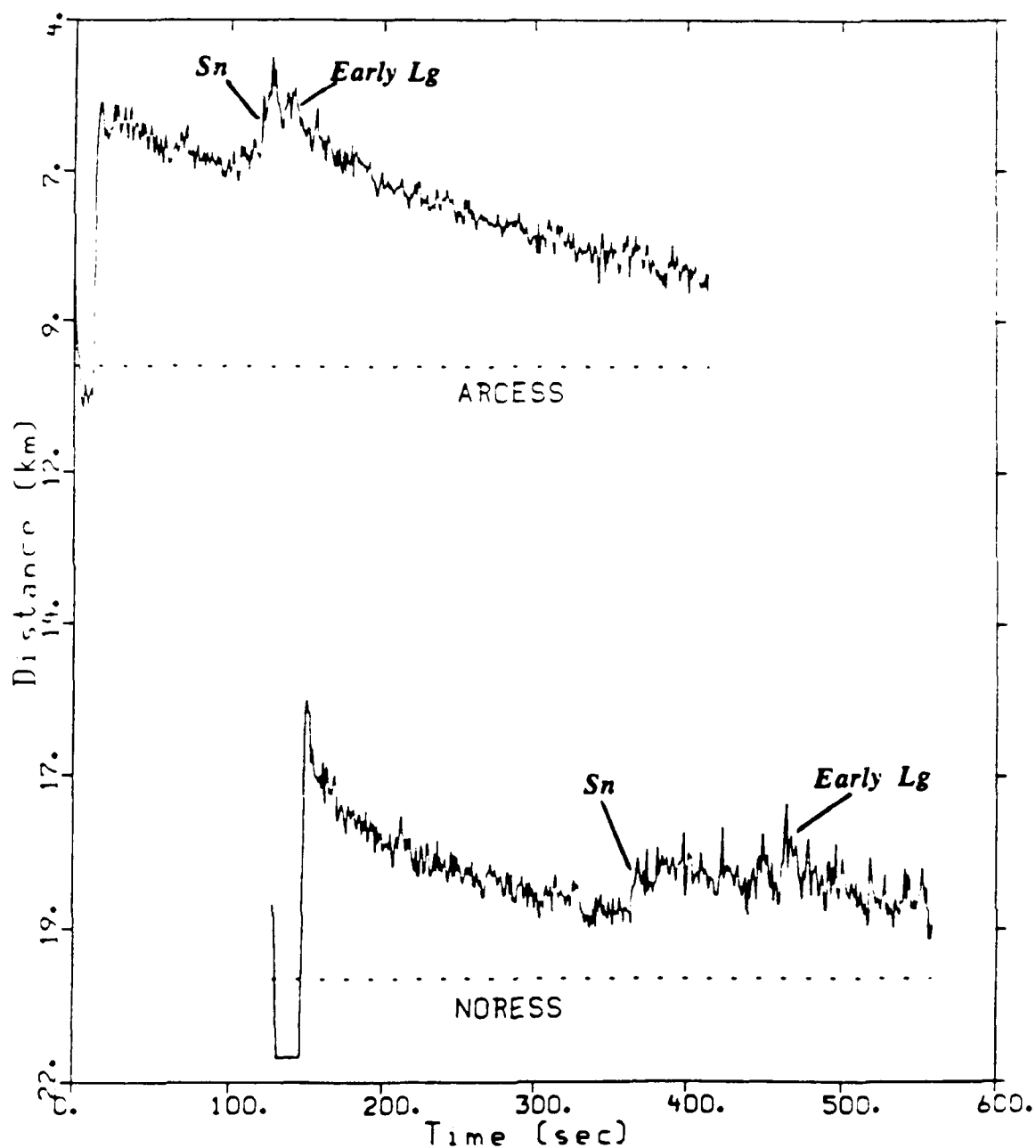
FIGURE 1-12: Comparison of the logged incoherent beams at ARCESS and NORESS for the October 24, 1990 explosion.

secondary coda arrivals. The relative arrival time between the secondary pulse at ARCESS and the "early *Lg*" is about 3.5 km/sec, which suggests these arrivals are, in fact, *Lg* waves.

It has been argued in the previous section and in Baumgardt (1990) that the "early *Lg*" at NORSAR and NORESS comes from an *Sn*-to-*Lg* mode conversion from the interface between the Barents Sea and the Kola Peninsula, based on it's arrival time relative to *Sn*. Whether the secondary pulse in the *Sn* coda at ARCESS is the same arrival depends on whether its arrival time relative to *Sn* agrees with what is expected for the distance of ARCESS from the Barents-Kola interface. This point will be addressed again when the topographic cross-sections are discussed in the next section.

Figure 1-13 shows a plot of the Graefenburg incoherent beams for the Novaya Zemlya explosions. A 0.6 to 3.0 Hz bandpass filter was applied to each waveform prior to computing the incoherent beams. Although the instrument response of the Graefenburg sensors, described by Harjes and Seidl (1978), is different than the Norwegian arrays, these differences are not significant in the narrow 0.6 to 3.0 Hz passband. Thus, the relative excitation of regional phases in this band can be considered without correcting for differences in instrument response.

Baumgardt (1990) compared the incoherent beams of one of the Novaya Zemlya events (May 7, 1988) with the NORESS and ARCESS recordings of the same event and showed that an *Lg* phase with amplitude above the *Sn* amplitude is observed at the Graefenburg sensors. Furthermore, the *Lg* appears to arrive somewhat late, at a group velocity of about 3.3 km/sec instead of the usually observed 3.5 km/sec group-velocity time. The incoherent beams for other Novaya Zemlya events recorded at the Graefenburg array, plotted in Figure 1-13, show the same general feature, although the onset of *Lg* for most of the events is emergent and not as clear as it is for the May 7, 1988 event. The beginning of the *Sn* energy is also quite emergent with no clear
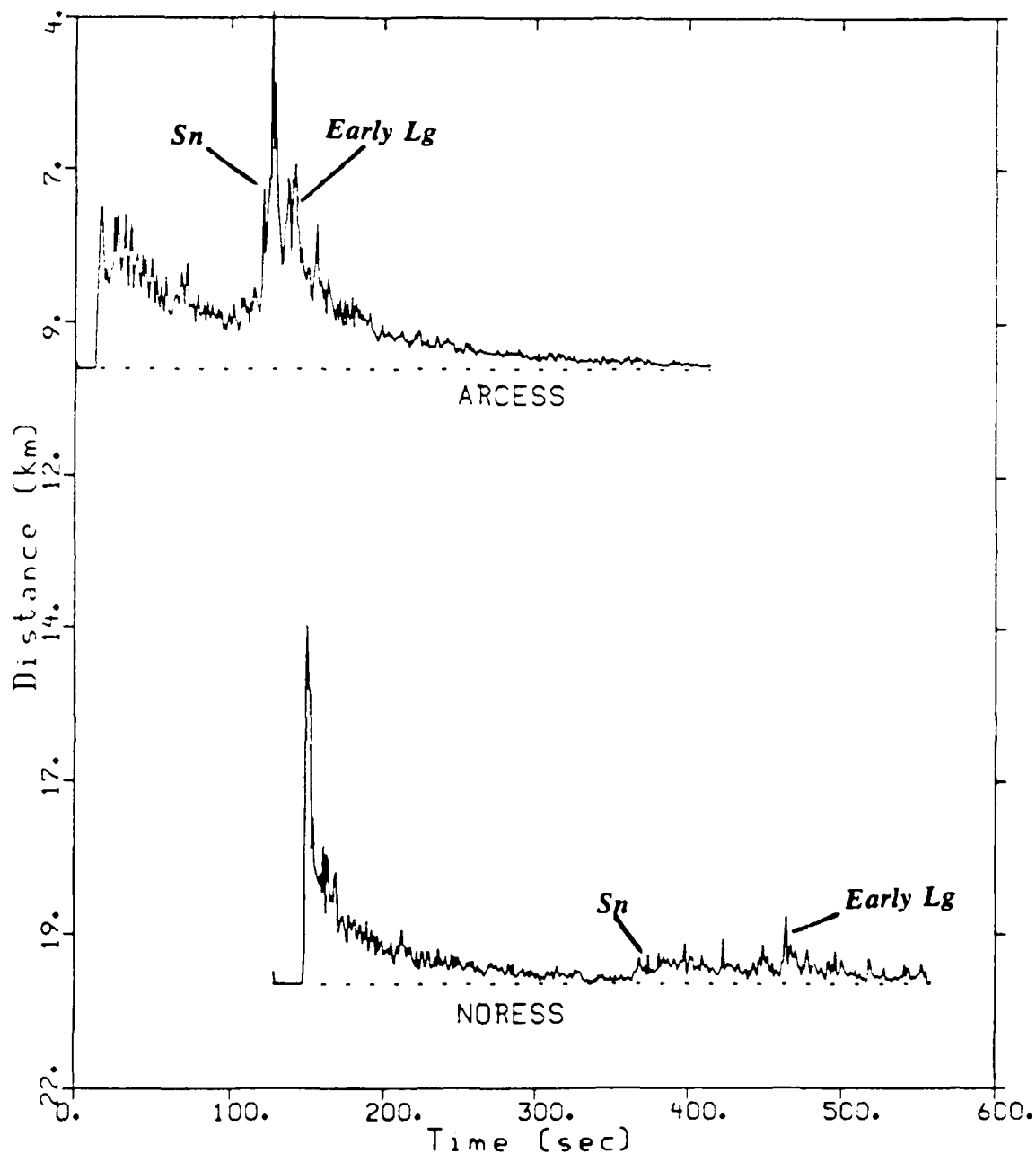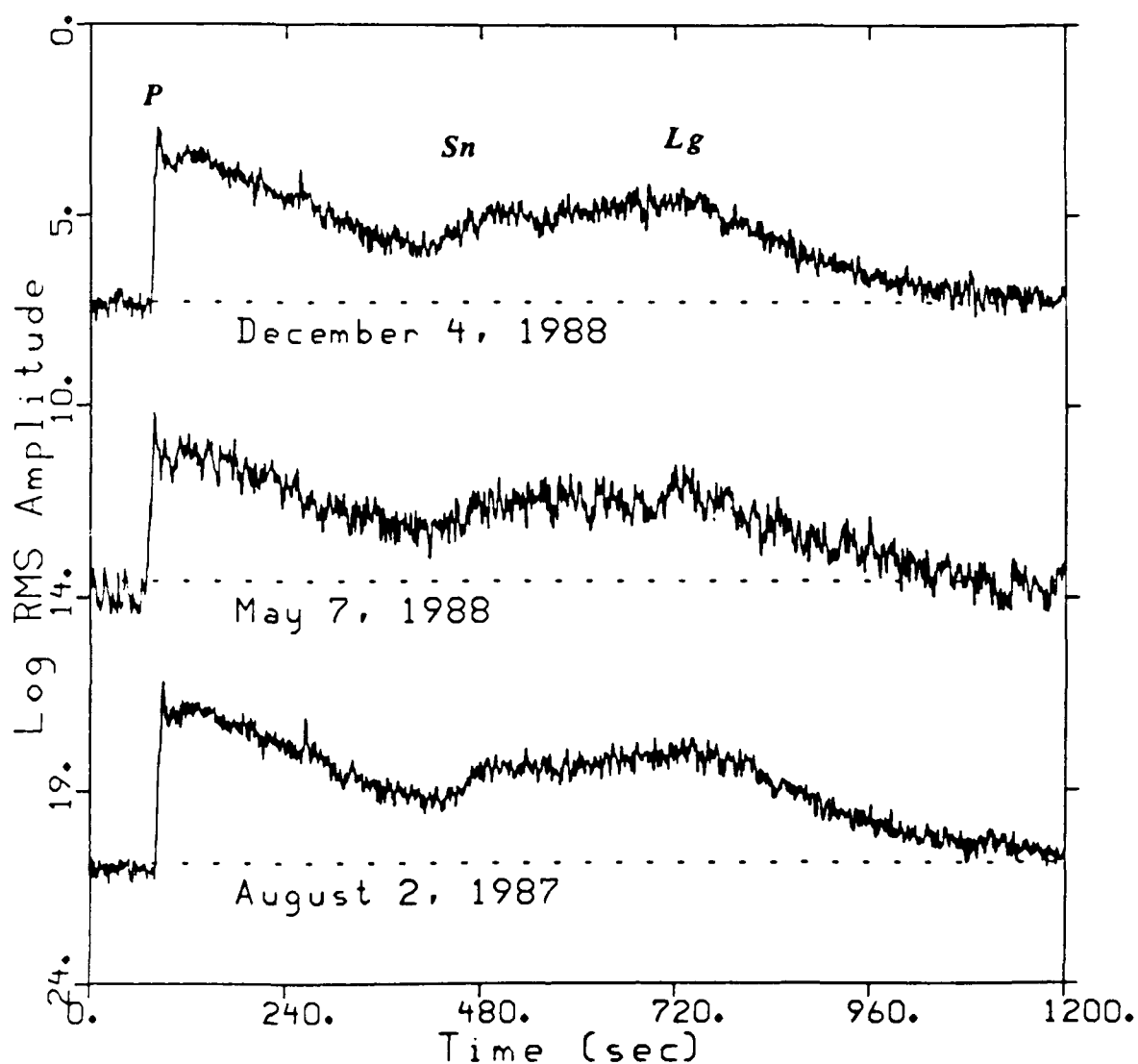
22

FIGURE 1-13: Logged incoherent beams for the Novaya Zemlya explosions recorded at the Graefenburg array.

onset. The *Sn* coda also appears to gradually increase with time to the peak *Lg* amplitude, with only a slight break in the trend which seems to correspond to the *Lg* onset time.

Thus, we conclude that, although *Lg* appears to be blocked to the Norwegian arrays such that the on-time *Lg* has energy less than the maximum *Sn* energy, *Lg* energy of some kind does appear to get through to the Graefenburg array at about the time expected for on-time *Lg*. This implies that the path to Graefenburg from Novaya Zemlya does not pass through the same kind of blocking structure in the Barents Sea as does the paths to the Norwegian arrays. Baumgardt (1990) suggested, based on analysis of a geologic cross-section through the Barents Basin structure, that the sediment thickness variations may not be as great along the Novaya Zemlya-to-Graefenburg path as they are along the path to the Norwegian arrays. However, the intense *Sn* coda and the lack of a clear *Lg* onset at Graefenburg suggests that there is still intense scattering of *Sn* and *Lg* along the Novaya Zemlya - to - Graefenburg path if not outright blockage of *Lg*.

1.4 FREQUENCY-WAVENUMBER POLAR-SCAN ANALYSIS OF ARCESS DATA

As a further check on the identification of the *Sn* and "early *Lg*" waves at ARCESS, continuous frequency-wavenumber (FK) analysis was applied, using the methods described by Baumgardt (1990). Continuous FK analyses of the "early *Lg*" arrivals at NORESS, displayed in Baumgardt (1990) as "FK polar scans," confirmed that these arrivals had apparent phase velocities consistent with those expected for an *Lg* phase. In the present study, we have done the same analysis to the secondary pulse in the *Sn* coda at ARCESS.

Broadband FK spectra (Kvaerna and Doornbos, 1986) were computed in adjacent, two second windows shifted over a time period which encompassed the shear waves. For each FK, the *F*- statistic, apparent velocity, and azimuth of the FK peak were determined and stored. The broadband FK was computed for the 0.7 to 1.3 Hz band in all cases.

The F- statistic, first developed by Shumway (1974) and applied by Blandford (1974) to array data, gives a measure of the significance of the FK peak or the coherence of the signal. According to Blandford (1974), the F- statistic is defined as follows:

$$F = \frac{(N-1)}{N} \frac{\langle (S_i)^2 \rangle}{\langle (S_i^2) \rangle - \frac{1}{N} \langle (S_i)^2 \rangle},$$

where N is the number of channels used in the FK and S_i is the maximum power in the FK for the i'th time window. The numerator in the above expression is essentially the beam power at the velocity and azimuth of the arrival, which is the FK maximum power, and the denominator is the difference in the beam (or FK maximum) power and the average power in each channel. In essence, the F- statistic can be thought of as the ratio of the coherent power to the incoherent power. If the signal is coherent, the FK maximum power will be large and the denominator term will be small and the F value will be very large.

The F value, defined above, statistically follows the F distribution with $N1$ and $N2$ degrees of freedom, under the assumption that (1) the signals are identical on each channel and (2) that the noise is statistically independent, has a normal distribution, and has a stationary auto-correlation function. The numerator number of degrees of freedom, $N1$, is $2BT$, where B is the signal bandwidth and T is the time window length. The denominator number of degrees of freedom term, $N2$, is $(N-1)N1$, where N is the number of channels. With $N = 25$, $T = 2$ seconds, and $B = 0.6$ Hz, since the FK is done in the 0.7 to 1.3 Hz band, this gives $N1 = 2$ and $N2 = 48$. From an F distribution table, this gives an F value of about 5 at the 99% confidence level. This means if the F value of the maximum peak in FK space exceeds 5, the signal can be considered to be coherent at the 99% confidence level.

Generally, we have observed that the background noise at ARCESS and NORESS to have F values of between 3 and 5 in the 0.7 to 1.3 Hz band, which is consistent with the statistical argument above. Most signals have F values of much in excess of 5 to 10, depending on the signal-to-noise ratio. Taking the conservative approach in looking for coherent signals in the Sn coda, we use 30 as the minimum F- statistic for a signal.

Figure 1-14 shows an FK "polar scan" for the first pulse of the Sn wave for the October 24, 1990 event recorded at ARCESS. The FRAO channel waveform for this event, which was recorded by the center short-period sensor at ARCESS, is shown plotted at the top of the display. The bracket on the waveform, indicating the time from 122 to 134 seconds, corresponds to the first Sn wave packet for which the continuous FK analysis was applied. The polar plots at the bottom show the velocity and azimuth of the FK measurements in this time period. The distance out from the center of the polar plots gives the velocity and angle from the vertical (0 to 180) axis gives the azimuth. The expected azimuth of the event is shown by the line. The symbol sizes on the polar plots are proportional to the time into the window (time-proportionate), on the left plot, and the F- statistic (F- proportionate), on the right plot, as shown in the two legends. Only FK results where the F- statistic exceeded 30 are plotted.

Figure 1-14 shows that only two windows exceeded the F- statistic threshold of 30, both with phase velocity greater than 4.5 km/sec, as expected for Sn type energy, and arrives on the azimuth of the event. The most coherent measurement, which had an F- statistic of greater than 60, is for the earliest arrival in the window.
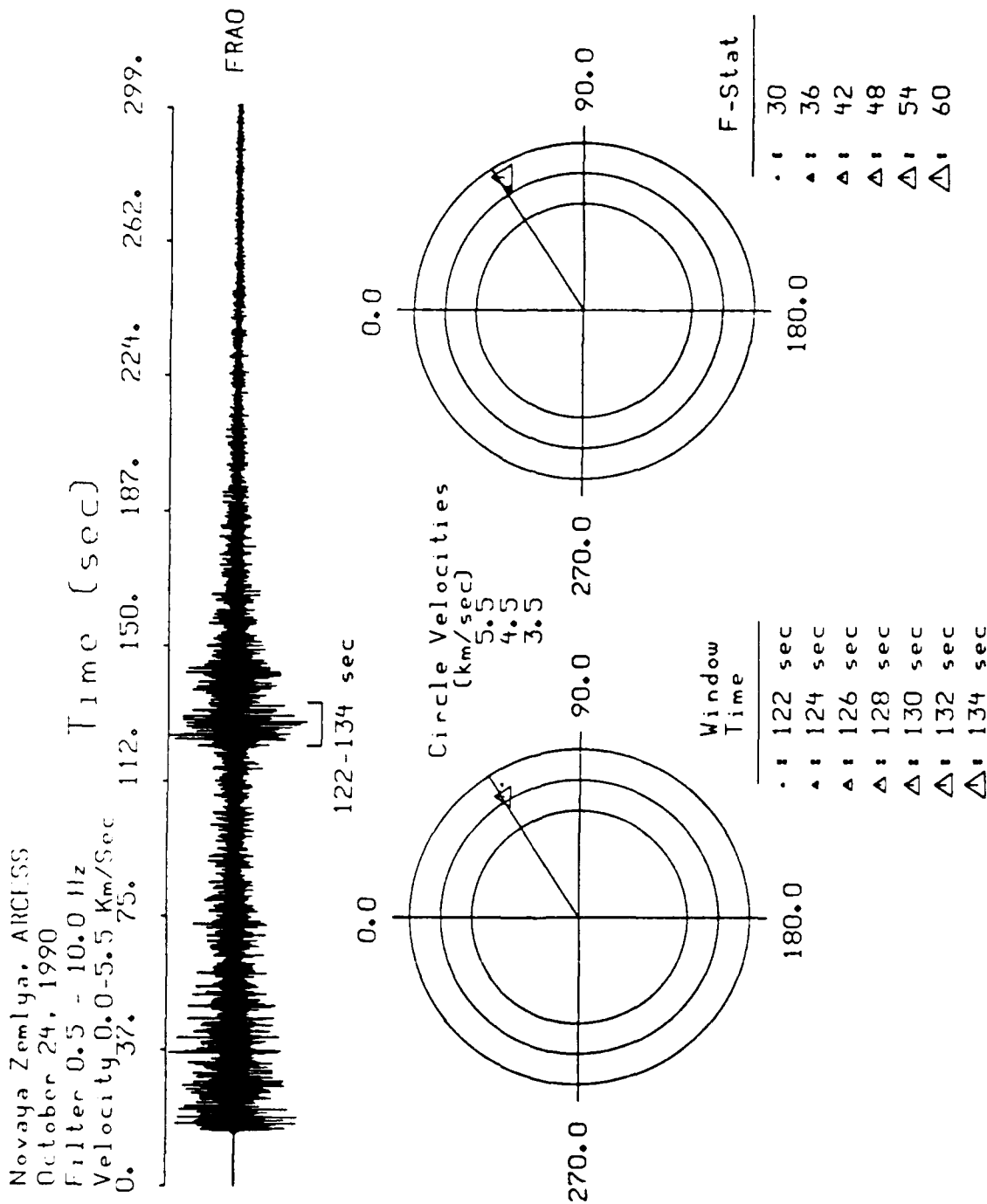
FIGURE 1-14: FK polar scans for the *Sn* wave recorded at the ARCESS array recording of the October 24, 1990 Novaya Zemlya explosion. The trace at the top shows the window in which continuous FK was applied. Polar plots of FK measurements show triangle symbols plotted with polar radius proportional to velocity and with angle from the vertical equal to the azimuth. Symbol size proportional to time into the window (left) and *F*-statistic (right).

Figure 1-15 shows the measurements for the window on the second energy packet, which might be the early *Lg*. In this window, coherent energy can be observed with velocities near 4.0 km/sec, which is the phase velocity expected for *Lg* waves. The most coherent energy arrives essentially on azimuth. These results are consistent with this second energy packet being an *Lg* type mode. However, the energy arrives too early for it to have a group velocity near 3.5 km/sec,which is expected for direct *Lg*.

Figures 1-16 and 1-17 show the same measurements on the December 4, 1988 event. In this case, as before, the most coherent arrivals in the first window in Figure 1-16 come in early and have velocities near 5.0 km/sec, again consistent with this being the first arrival *Sn* wave. The second wave packet in Figure 1-17 has velocities near 4.5 km/sec.

These results show that the most coherent arrivals in the first wave packet have phase velocities between 4.5 and 5.0 km/sec, which is what is expected for *Sn*. Energy in the *Sn* coda and the second wave packet after the *Sn* onset seem to have somewhat lower velocities. Thus, the FK measurements on the second wave packet are generally consistent with this arrival being an *Lg* phase, which arrives early. This separation in phase velocity is not as distinct as it was for the NORESS data, discussed by Baumgardt (1990). These FK results by themselves do not prove unequivocally that the second wave packet at ARCESS is an "early *Lg*" produced by a coherent conversion at the Barents Sea - Kola Peninsula interface. However, given that the distance of ARCESS from the probable conversion point (about 100 km) is much shorter than that of NORESS, we might not expect much difference in the velocity of *Lg* and *Sn*. However, the *Sn* coda does appear to be composed of a mixture of *Sn* and *Lg* type modes, based on the velocities, albeit most of the energy has low coherence. Because this energy comes in at times much earlier than that expected for on-time *Lg*, all this early *Lg* type energy may come from scattering of *Sn*.
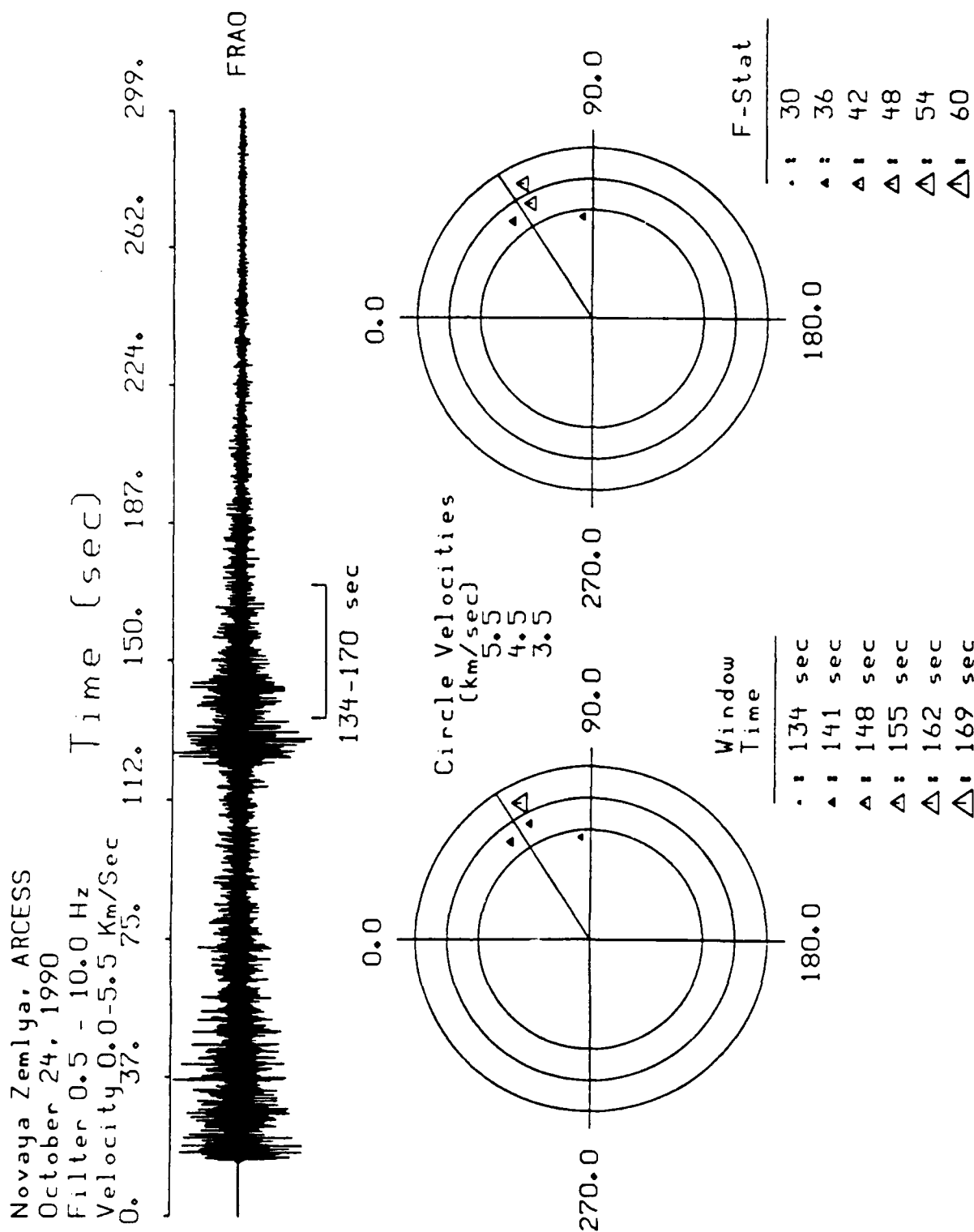
FIGURE 1-15: FK polar scan for *Sn* coda window for the October 24, 1990 Novaya Zemlya explosion.
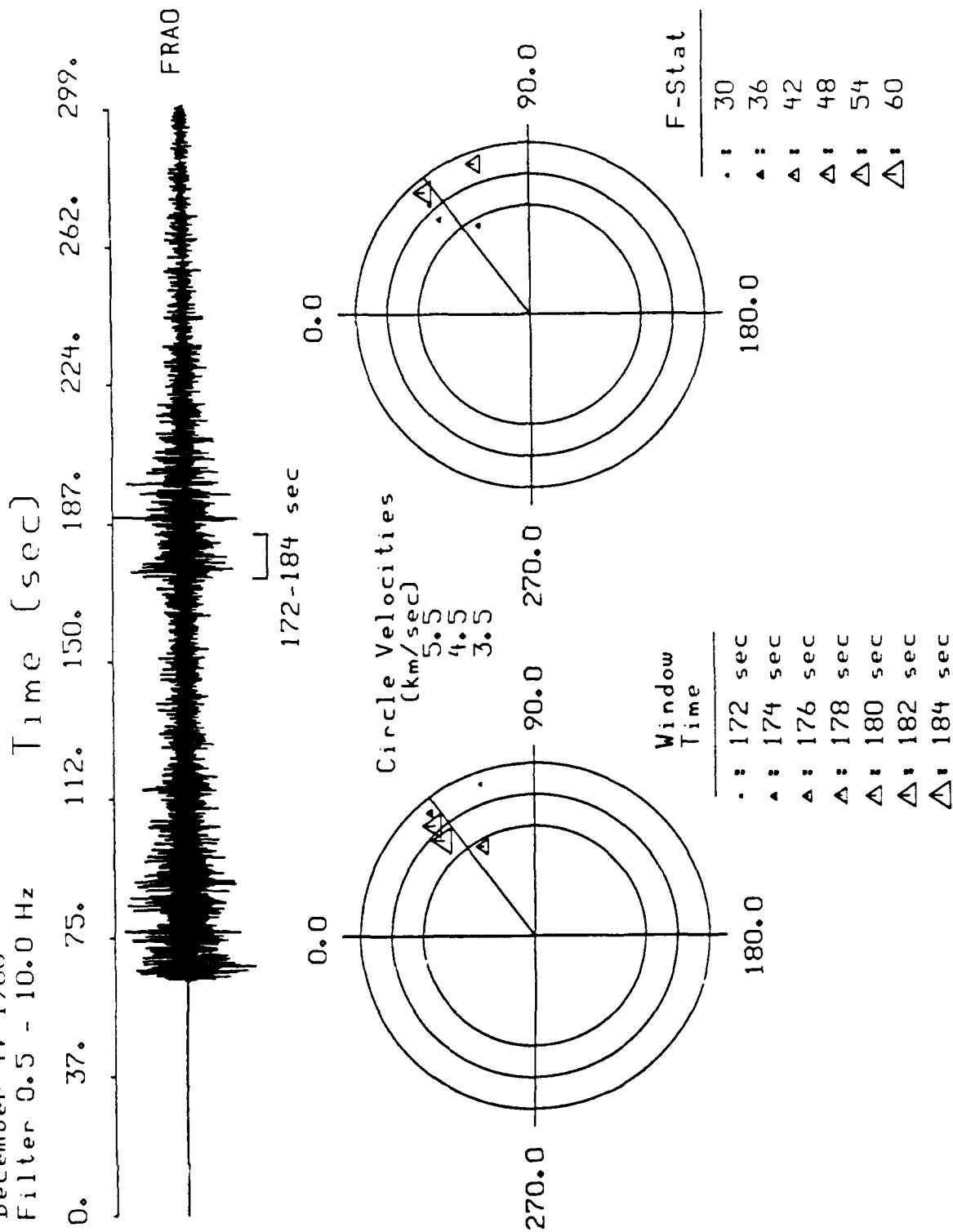
FIGURE 1-16: FK polar scan for the *Sn* window for the December 4, 1988 Novaya Zemlya explosion.
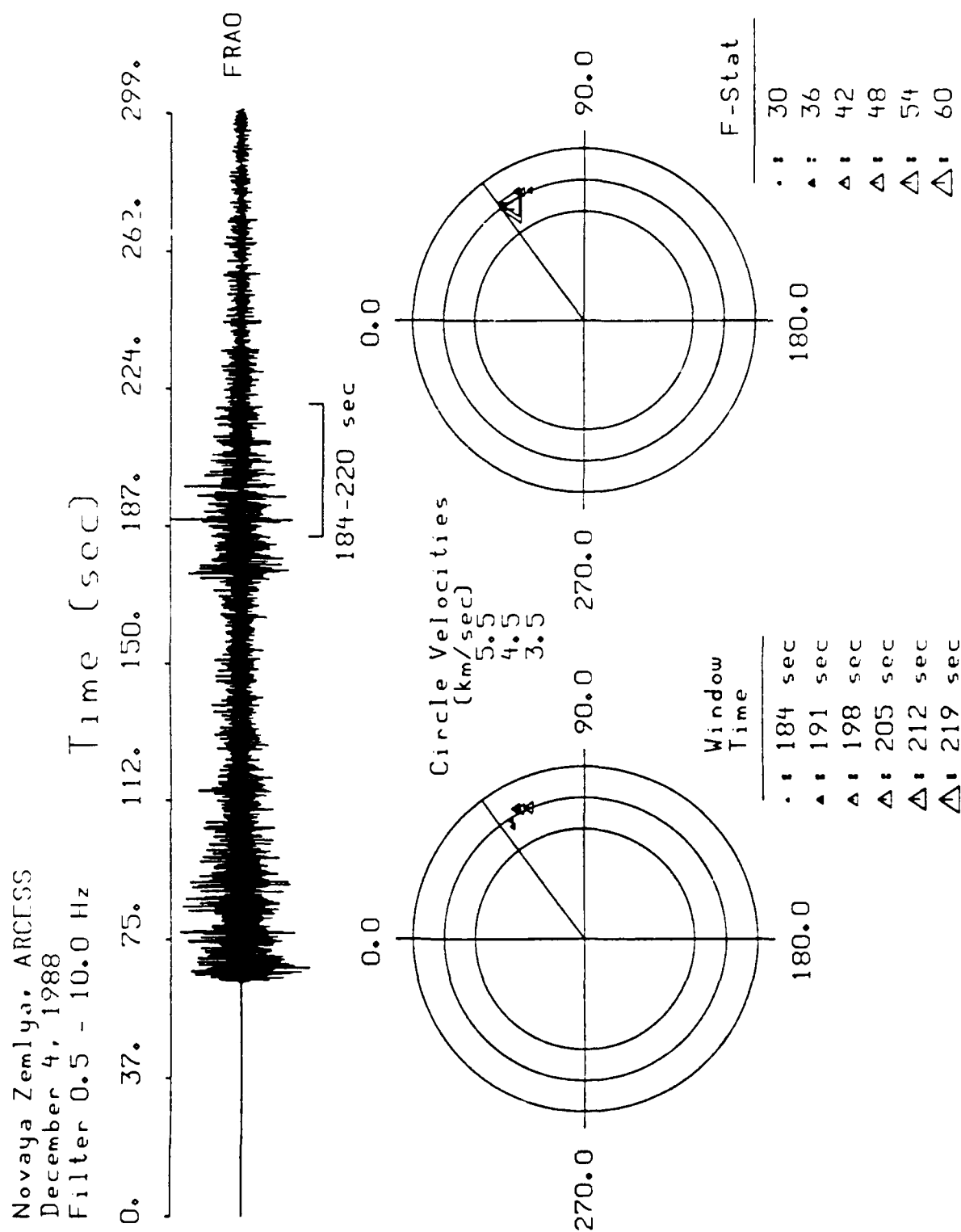
FIGURE 1-17: FK polar scan for *Sn* window for the December 4, 1988 Novaya Zemlya explosion.

31

1.5 COMPARISON OF ARCESS - NOVAYA ZEMLYA AND NORSAR - KOLA EXPLOSIONS - EVIDENCE FOR LG BLOCKAGE

As a final, striking illustration of the Lg blockage in the Barents Sea, we compare the recordings of a Novaya Zemlya explosion, recorded at ARCESS, and the Kola Peninsula explosion, recorded at NORSAR. These two events were recorded by two different sensors at two very different times. However, they are interesting to compare because they give a direct indication of the effect of the Barents Basin on Lg propagation.

Figure 1-18 compares the great-circle propagation paths for Lg from these two events to the two arrays. The two great circle propagation paths are nearly the same distance and, in fact, are nearly parallel. However, the Barents Sea constitutes most of the propagation path from Novaya Zemlya to ARCESS. The path from the Kola Peninsula to NORSAR does cross the northern tip of the Gulf of Bothnia, but most of the path is continental.

Figure 1-19 shows the waveforms for the two signals, plotted as a record section. The top trace is the ARCESS FRA0 recording of the December 4, 1988 Novaya Zemlya event and the bottom trace is the center NORSAR NO1A0 recording of the September 4, 1972 PNE on the Kola Peninsula. The NORSAR waveforms were sampled at 20 samples/second, whereas the ARCESS waveforms were sampled at 40 samples/second, and they have different short-period instrument responses, as discussed above. However, because both waveforms have been filtered in the 0.6 to 3.0 Hz frequency band, these differences in instrument characteristics should not affect in a major way the relative amplitudes of the regional phases. The Kola explosion had a magnitude of 4.6 (Table 1) whereas the Novaya Zemlya explosion had a much larger magnitude of 5.7. Because of this difference in magnitude and instrument response, the NORSAR trace amplitudes were scaled by a factor of three relative to those of the ARCESS Novaya Zemlya explosion so that their Pn wave amplitudes were nearly the same.
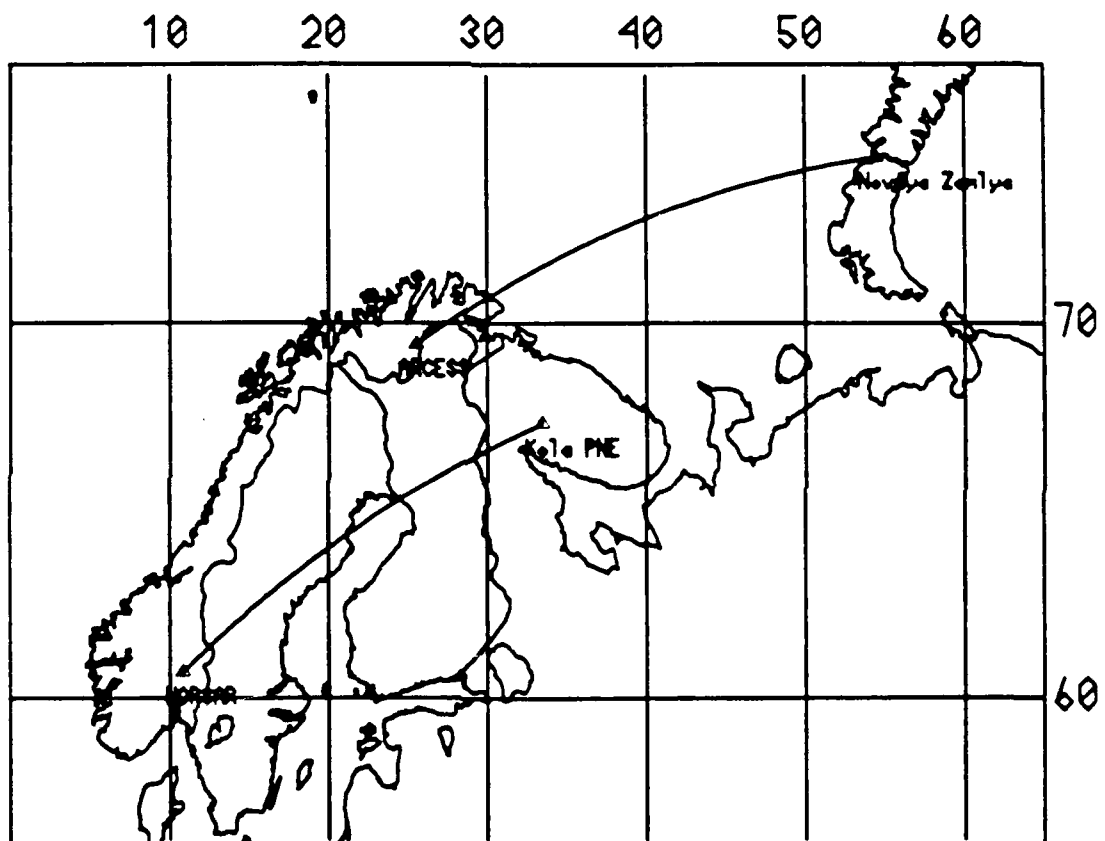
FIGURE 1-18: Map showing comparison of the propagation path from the Kola PNE to NORSAR and the Novaya Zemlya region to ARCESS. Both paths are nearly parallel and have similar distance.
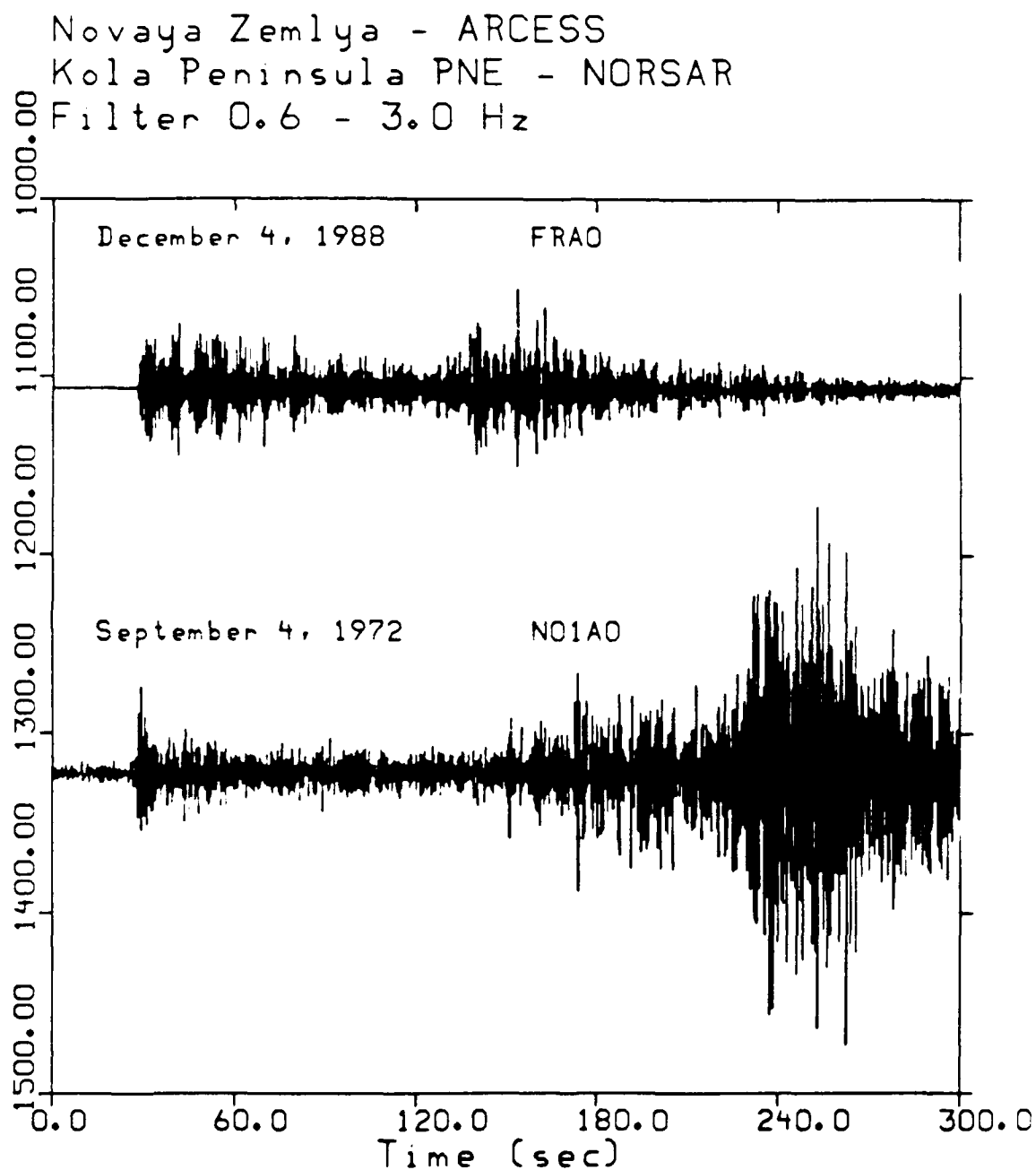
FIGURE 1-19: Comparison of the ARCESS FRA0 trace of the October 24, 1990 explosion with the NORSAR N01A0 recording of the September 4, 1972 Kola Peninsula explosion.

34

Comparison of the two waveforms in Figure 1-19 shows that the relative *Pn* and *Sn* amplitudes are about the same. However, the most striking difference is that the Kola PNE produced a strong *Lg* signal at NORSAR, whereas no such signal was recorded by ARCESS from the Novaya Zemlya explosion. Moreover, the *Pn* coda levels appear to be higher, compared with the maximum *Pn* amplitude, on the ARCESS seismogram than on the NORSAR seismogram.

This comparison shows that the disappearance of *Lg* at ARCESS is unusual for Scandinavia, given the excellent propagation conditions of most events in the region, and confirms that the Barents Sea is a major block to *Lg* propagation. Furthermore, the increased coda levels for the ARCESS recordings of the Novaya Zemlya explosions indicates that there may be significant scattering from the structure along with the blockage of *Lg* propagation. In the next section, we consider in more detail the geology of the region and offer an explanation for the blockage and scattering of *Lg* in this structure.

1.6 GEOLOGICAL EXPLANATION FOR THE BARENTS SEA LG BLOCKAGE

Explanations for Lg Blockage

A number of suggestions have been made for the causes of *Lg* blockage in the Barents Sea. As summarized by Baumgardt (1990), they include:

(1) Variations in crustal thickness.

(2) Scattering from tectonic boundaries.

(3) Strong anelastic attenuation in upper-crustal sediments.

(4) Lack of an upper-crustal "granitic layer."

The first explanation was first posed by Ruzaikin et al (1977) in order to explain the inefficient propagation of *Lg* in the Tibetan Plateau. The region was known to have unusually thick (up to 70 km) crust due to the convergent type tectonics of the region. Kennett et al (1985) also suggested that *Lg* propagation across the Norwegian Sea might be blocked by a region of crustal thickening beneath a graben structure. The second explanation has been invoked by a number of investigators who have used the efficiency of *Lg* propagation as a method for mapping tectonic boundaries (e.g., Kadinsky-Cade et al, 1981; Ni and Barazangi, 1983). Baumgardt (1985, 1990) has provided evidence for *Lg* scattering in the Ural Mountains, which is believed to be a collisional suture zone and appears to partially block the propagation of *Lg* waves from the Semipalatinsk test site in eastern Kazakh to the ARCESS array. Mitchell and Hwang (1987) have suggested that the attenuation of *Lg* may be strongly affected by low Q sediments, which are known to be present in the Barents Basin (Chan and Mitchell, 1985). Finally, the "missing granitic layer" explanation originates from the idea that such a layer is essential to provide the waveguide for *Lg* propagation, which is only observed in continental regions. Piwinskii (1981) has explained the poor propagation of *Lg* in the Caspian Sea region of the Soviet Union in terms of an implied "missing granitic layer," which has been reported in the Soviet geophysical literature for the Caspian Sea sedimentary basin.

Geology of the Barents Sedimentary Basin

The geological and tectonic structure of the Barents Sea region has been of great interest because of its economic importance. Clark and Rachlin (1990) have given a detailed description of the region, gleaned from publications in the Soviet geological literature. They report one geologic map, originally published by Gramberg (1988) and shown in Clarke and Rachlin (1990) and Baumgardt (1990).

Baumgardt (1990) has pointed out that any of the *Lg* blockage explanations could be invoked to explain the *Lg* blockage in this region. The basin is characterized by crustal thickness variations, sediment accumulations as great as 15 km, and regions of "missing granitic layer," which are the stippled regions in Figure 1- 20. Clark and Rachlin (1990) report that this structure is based on lows in magnetic anomalies, due to the missing granitic layer, and gravity highs caused by the elevation of the Moho. Seismic studies have reported that the granitic layer, characterized by *P*-wave velocities on the order of 6.0 to 6.5 km/sec, has been replaced by lower velocity sediments, with velocities of 4.0 to 4.5 km/sec. The parallel lines on the map indicate regions where there is a complete lack of sediments. These include the coastlines of the island of Novaya Zemlya and the Kola Peninsula.

Figure 1-20 shows that all three propagation paths pass through the region of missing granitic layer and crustal thinning. The paths to ARCESS and NORESS pass through the middle of the eastern Barents Basin, whereas the path to Graefenburg passes through the southeastern part of the basin. Baumgardt (1990) has suggested that the extreme lateral heterogeneity of the sediment thicknesses in the region, where the depths to basement vary from 0 km at Novaya Zemlya, 15 km in the basin itself, and 0 km again on the Kola Peninsula over a distance of about 600 km, may be a partial cause of the *Lg* blockage in the basin. These variations may cause the *Lg* waveguide to breakdown, and scattering may be enhanced by the presence of large, lateral variations in crustal velocity. The greatest effects are felt by the *Lg* waves which propagate toward ARCESS and NORESS through the middle of the basin. The lateral heterogeneity may be less extreme along the path from Novaya Zemlya to Graefenburg, which passes more through the southeastern end of the basin.
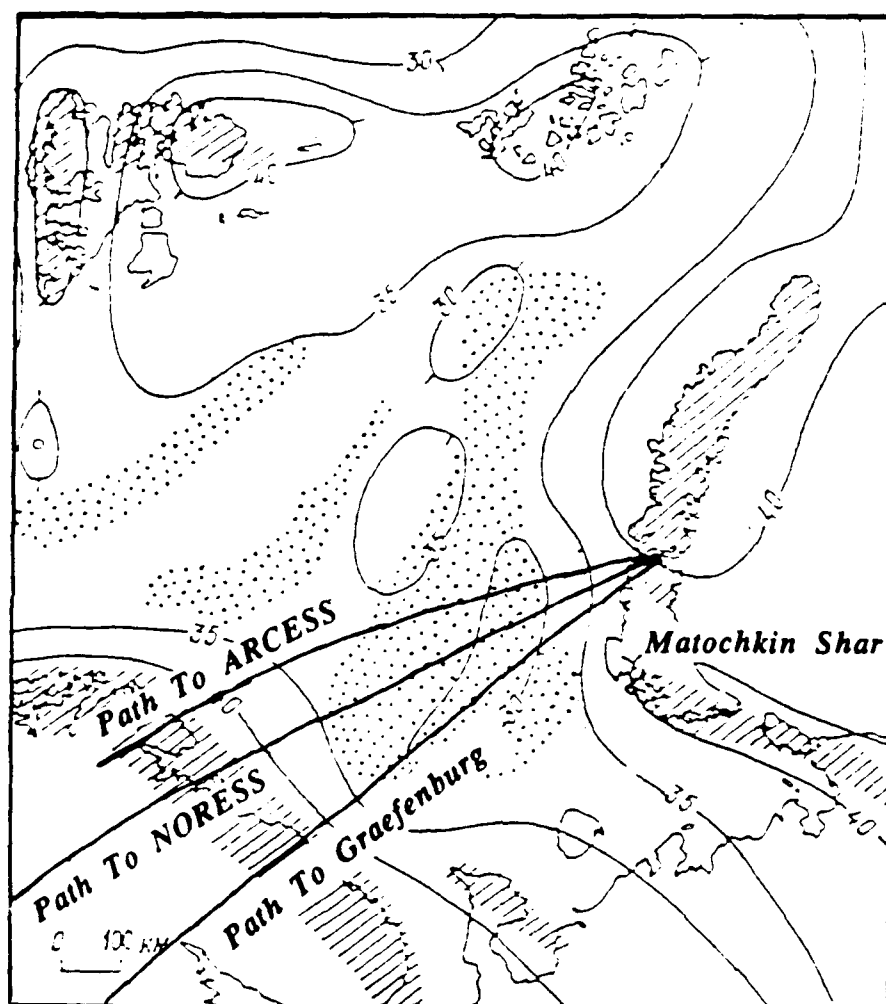
FIGURE 1-20: Map showing propagation paths from the Novaya Zemlya region across the geologic structures in the Barents Sea region (after Gramberg, 1988).

Crustal Cross-Sections

In order to more closely examine the possible propagation path effects, approximate crustal cross-sections for the great-circle propagation paths from Novaya Zemlya to the Norwegian arrays and the Graefenburg array were generated. A 5' by 5' digital topographic database, ETOPO5, was used to generate the topographic cross-section for the great circle path from a source to a receiver. The great circle path was computed through the ETOPO5 database grid, and the elevation for points along the great circle which fall between grid points was computed by interpolation. The crustal depth was then inferred from the topographic cross-section by assuming that the topographic variations were compensated by the Airy isostatic compensation model.

Figures 1-21, 1-22, and 1-23 show the inferred crustal cross-sections for the three paths, Novaya Zemlya to ARCESS, NORESS, and Graefenburg, respectively. The top plots in each figure are the elevations, in meters, obtained for the great circle path from Novaya Zemlya to the receiver extending out to a maximum of 2500, 3,000 and 4,500 km from the array. The horizontal axis shows the distance from the array, with the array located at 0 km on the left edge of the plot. The triangles on each plot, labelled "Novaya Zemlya," give the location of the northern test site, in a region called Matochkin Shar. The vertical elevation scale on each plot is the same, ranging from 400 m below sea level to 2000 m above sea level. The bottom plots give the inferred crustal cross-section. Also shown on the bottom plots is the inferred depth of the sediments in the part of the basin traversed by the path. The sediment thickness estimates are very approximate, since the studies of Gramberg (1988) and Clarke and Rachlin (1990) do not give complete lithographic maps of the sediments in the basin. They were primarily inferred from Figure 1-20, which shows the regions where there are no sediments, and the NW-SE cross-section through the southern Barents Basin shown in Gramberg (1988) and reproduced by Clarke and Rachlin (1990) and Baumgardt (1990).

39

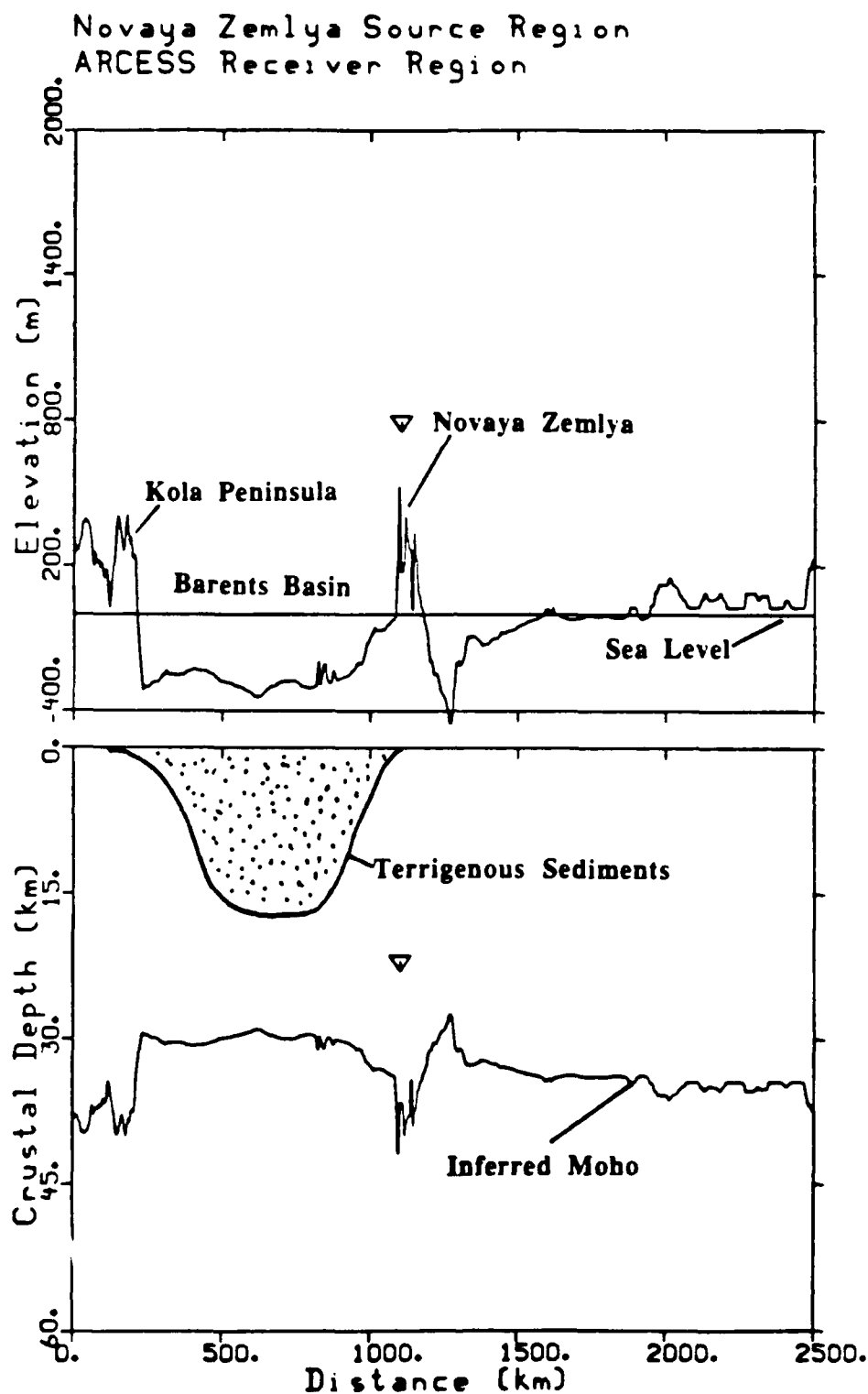**FIGURE 1-21:** Crustal cross-sections for the path from Novaya Zemlya to ARCESS. Top: Elevation cross-section, from ETOPO5. Bottom: Inferred depth of sediments, from Clarke and Rachlin (1990) and Moho depth for 100% compensation of surface topography.
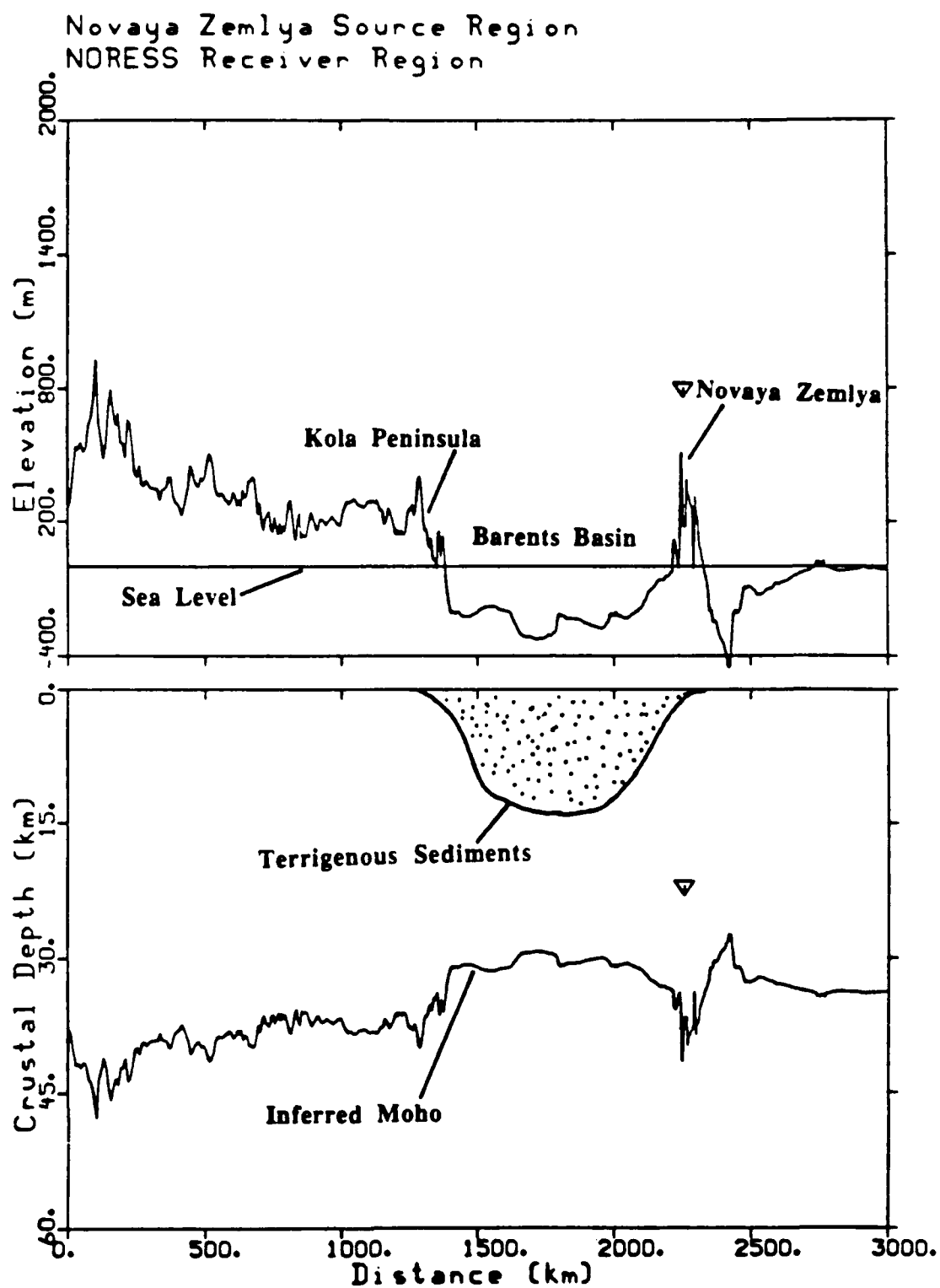
FIGURE 1-22: Crustal cross-section for the path from Novaya Zemlya to NORESS.

41
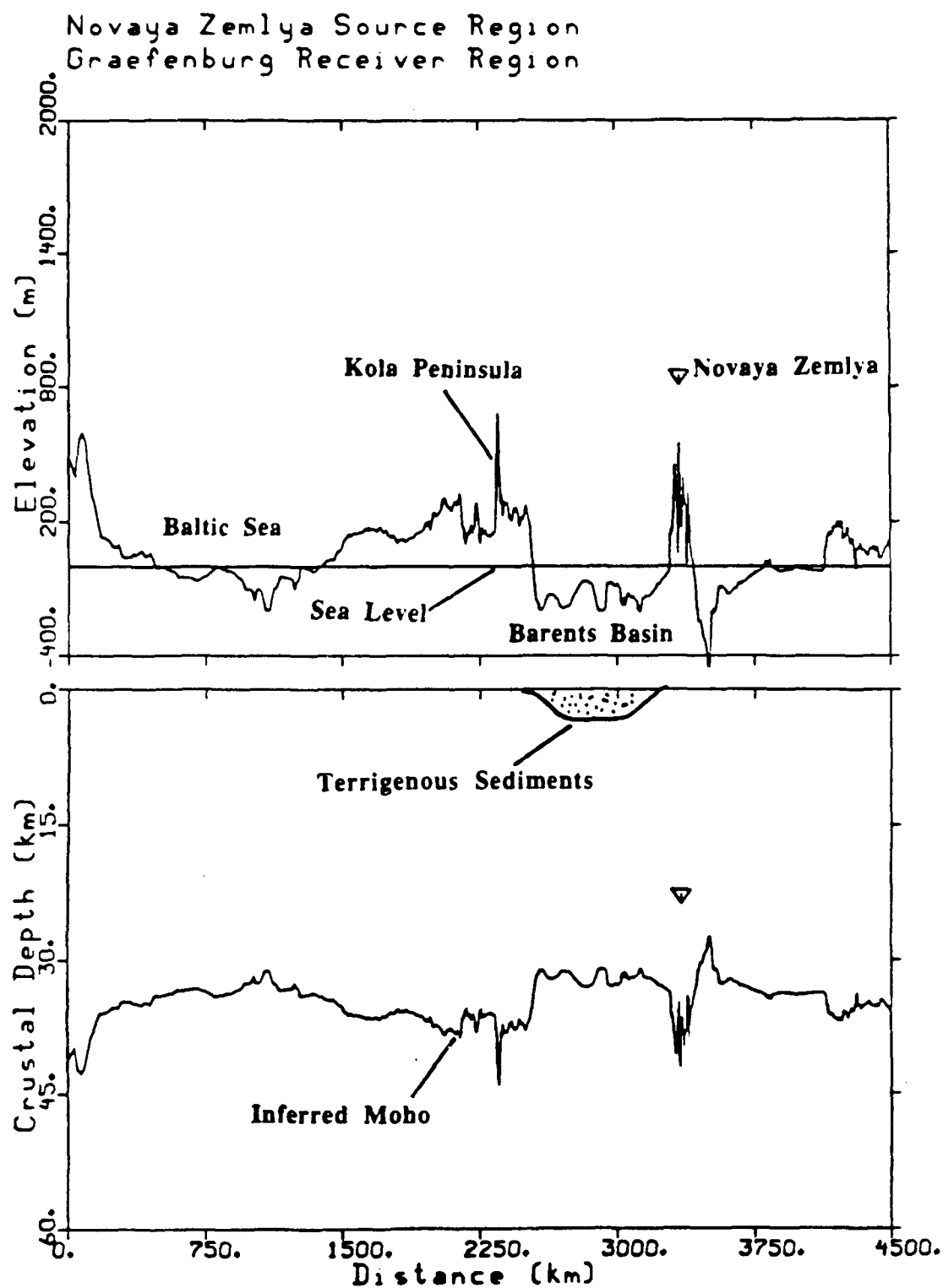
FIGURE 1-23: Crustal cross-section for the path from Novaya Zemlya to Graefenburg.

42

All three plots show that Novaya Zemlya is an island which stands about 500 m above sea level. The explosions occur in a region called the Matochkin Shar, which is located behind a tall ridge. In the case of the paths to ARCESS and NORESS in Figures 1-21 and 1-22, the elevation falls quickly to the south of the ridge into the Barents Basin, which has a gradual slope to its deepest depth of below 300 m beneath sea level. For the path to Graefenburg in Figure 1-23, the depth and width of the Barents Sea is not quite as large as it is for the ARCESS and NORESS paths, although the sea bottom seems to be somewhat undulatory. For all three paths, a very sharp increase in elevation marks the interface between the Southern Barents Basin and the Kola Peninsula.

The inferred Moho depths, shown on the bottom plots, assumed a crustal density of 2.67 g/cm^3, a mantle density of 3.27 g/cm^3, and an average crustal thickness, for sea level, of 40 km. The surface elevation was assumed to be completely compensated to obtain a change of Moho depth from 40 km to 30 km below the Basin, as has been reported in the Soviet literature based on seismic and gravity data and shown in Figure 1-20. The crustal depth variations were not smoothed so that the roughness of the Moho near 1100 km distance is purely a manifestation of the elevation variations of Novaya Zemlya and is probably not real.

For the paths to ARCESS and NORESS, sediment thicknesses of greater than 15 km are indicated in the same part of the structure where there is a 10 km elevation in the Moho depth. This reflects the general view of the basin portrayed in the Soviet geological literature, according to Clarke and Rachlin (1990). The terrigenous sediments replace the granitic layer, which is present beneath Novaya Zemlya and the Kola Peninsula. Based on seismic profiles of the Basin, the sediment compressional velocities range from 3.9 to 5.5 km/sec in the sediments in contrast to the 6.0 to 6.5 km/sec velocities in the granitic layer, which would correspond to shear wave velocity contrasts of 2.2 to 3.17 km/sec for the sediments and 3.46 to 3.75 km/sec for the granitic rocks. This contrast in velocities produces strong impedance contrasts at the boundaries of the Basin and

43

thus, seismic energy which propagates into the Basin may be captured and attenuated by repeated reverberations within the Basin.

Figure 1-21 shows that the distance of ARCESS from the Barents-Kola interface is about 250 km. We argued earlier that the Sn phase might convert to Lg at this interface, producing the "early Lg" at ARCESS. Assuming a group velocity of 4.5 km/sec for Sn and 3.5 km/sec for Lg, this would imply that the Sn-to-Lg conversion should arrive about 15 seconds after the onset of Sn. This is consistent with the time interval of the second wave packet, or "early Lg," which can be observed at ARCESS (See Figures 1-6 and 1-14 through 1-17). Figure 1-22 shows that the distance of this interface from NORESS is about 1400 km, or about 13°, which implies that the mode converted Lg should lag Sn by 110 seconds, as shown in Figure 1-3. This is again consistent with the observations at both NORESS and NORSAR.

The cross-section from Novaya Zemlya to Graefenburg in Figure 1-23 shows a thinner sedimentary layer than for the paths to ARCESS and NORESS. This inference is based on the Barents Sea cross-section of Gramberg (1988), which shows substantially reduced sediment thicknesses and the presence of a granitic layer to depths of 15 km in the southeastern part of the Basin, the region crossed by the great-circle path to Graefenburg. The rest of the path to Graefenburg crosses the elevated regions of the Kola Peninsula, Scandinavia, and the depressed region of the Baltic Sea. However, the crust beneath the Baltic Sea is continental with no major sediment accumulations, like those found in the Barents Sea.

Based on this analysis of crustal cross-sections for the Lg propagation paths from Novaya Zemlya to the ARCESS, NORESS, and Graefenburg arrays, we conclude that the main cause of the Lg blockage in the Barents Sea, for the paths to the Norwegian stations, is the presence of thick sediment accumulations in the sedimentary basin beneath the southern part of the Barents Sea. The 15 km of low-velocity sediments, which replace the granitic layer in the region of the

44

ARCESS/NORESS paths, traps all the seismic energy which propagates in the continental granitic layer. Since *Lg* is commonly believed to be composed of shear modes which propagate along the granitic layer waveguide, the presence of a deep sedimentary basin will substantially disrupt this waveguide by trapping and scattering the various shear modes which compose the *Lg* wavetrain. Because the sediment thicknesses are significantly less and the basin, in general, is shallower along the Novaya Zemlya to Graefenburg path, there is less blockage of *Lg* along this path, as has been observed.

Although *Lg* is better observed at Graefenburg than at either ARCESS and NORESS, in spite of much longer propagation path to Graefenburg, a significant amount of coda energy, both after *P* and after *Sn*, is still apparent. The coda may be generated by scattering of the crustal guided phases, primarily *Sn* and *Lg*, from the geological and topographic heterogeneities along the path. For example, Figure 1-23 shows that the Kola Peninsula stands high along the path to Graefenburg and this structure can scatter both *Sn* and *Lg* energy which gets through the Barents Basin. Both shear modes, *Sn* and *Lg*, can interconvert to each other as well as forward scatter into *Pn* and *P* modes, thus building up the pre-*Sn* coda. Figure 1-13 shows that the *Sn* coda builds up after the onset of *Sn*, and that "early *Lg*" energy, produced by scattering at the Kola Peninsula interface, may be present at Graefenburg. Thus, the *Lg* recorded by Graefenburg, although not completely blocked, has still probably undergone considerable scattering from the various lateral heterogeneities along the path.

It should be noted that we expect that *Lg* should be better observed from Novaya Zemlya at two other regional arrays, FINESA and GERESS, because the propagation paths across the Barents Sea to these two arrays are essentially the same as those to the Graefenburg array. In a preliminary report about *Lg* waves recorded at the regional arrays, Ringdal (1990) shows a plot (Figure 7.1.6) of recordings at the FINESA and GERESS arrays of the October 24, 1990 explosion along with the ARCESS and NORESS recordings that we have studied. A small pulse

can be seen in the later part of the *Sn* coda at FINESA at the time expected for *Lg*, which is small, but at least larger than what is observed at ARCESS and NORESS. The recording at the GERESS array is very similar to what we observe at Graefenburg, in which these two arrays are located close to each other. As expected, on-time *Lg* seems to be better recorded at FINESA and GERESS than at ARCESS and NORESS.

Ray Tracing Calculations

In trying to explain the blockage of *Lg* in the Barents Sea, it is necessary to account for the observation that *Lg* waves are blocked, but *Sn* waves seem to propagate freely through the region. Baumgardt (1990) has argued that *Lg* primarily propagates in the upper crust and is sensitive to lateral heterogeneities in the upper crust. For this reason, variations in the depth of the Moho should not affect *Lg*. Thus, whatever blocks *Lg* must exist in the upper crust. Since *Sn* primarily propagates as a diving wave in the upper mantle, it is not affected by the upper crustal effect and is not blocked.

Two-dimensional ray tracing was done to better elucidate the affects of a sedimentary basin on the propagation of *Sn* and *Lg*. We use the method of Kennett (1986) where the interaction of *Lg* with structural boundaries is modeled by tracing *S* type rays through the two-dimensional structure. The phase velocity of the wave is the horizontal component of shear wave velocity in the upper layer of the velocity model, which is controlled by the shear wave velocity in the layer and the takeoff angle of the ray from the source. We assume that the phase velocity is about 4.5 to 5.0 km/sec for *Sn* and 4.0 to 4.5 for *Lg*. The group velocity is the distance that the wave traverses divided by the travel time. Group velocities are about 4.5 km/sec for *Sn* and 3.5 km/sec for *Lg* waves.

A sedimentary basin, similar to the Barents Basin, is modeled as an inverted trapezoidal structure, whose top width is 5000 km and bottom width is 2000 km. The basin is assumed to be filled with sediments reaching a maximum depth of 15 km. The shear-wave velocities inside the basin are assumed to be 2.6 km/sec at the top which gradually increase to about 3.46 km/sec at the bottom and sides of the basin. Assuming a Poisson solid, these velocities correspond to compressional velocities of 4.5 km/sec in the sediments and 6.0 km/sec at the sides of the basin. The velocities in between are interpolated by cubic splines. The velocities outside the basin in the granitic layer are assumed to be 3.46 km/sec. The rest of the model is assumed to be a normal, continental type structure, with two layers in the crust overlaying the mantle. The details of this model are given in Table 3.

In the ray tracing calculations, the source is assumed to be located on the left side of the structure, about 500 km from the upper corner of the basin, and the rays travel from left to right. The receiver is assumed to be located somewhere on the right hand side of the structure outside of the basin. This approximates the situation of the Novaya Zemlya to ARCESS path. The ray-tracing calculations were made using RAY81 (Cerveny et al, 1977).

Figure 1-24 (a) and (b) contrasts the propagation of an Lg type ray in a structure without and with the sedimentary basin, respectively. As shown in Figure 1-24 (a), simple shear wave reverberation in the granitic layer of the laterally homogeneous structure produces the combination of phase and group velocity expected for Lg. Shear waves which propagate into the lower crust below 15 km, with phase velocity of 4.0 km/sec, would have a group velocity of 3.73 km/sec (see Figure 1-27 (a)), which is faster than is expected for Lg. Although other combinations of reverberations may produce velocities close those expected for Lg, shear wave reverberations in the granitic layer of the crust have phase and group velocities most consistent with those expected for Lg.

TABLE 3

CRUSTAL MODEL FOR TWO-DIMENSIONAL RAYTRACING

Laterally Homogeneous Model

Depth Range (km)	Velocity Range (km/sec)
0 - 15	3.46 - 3.75
15 - 45	3.75 - 4.04
45 - 100	4.68 - 4.85

Laterally Heterogeneous Model

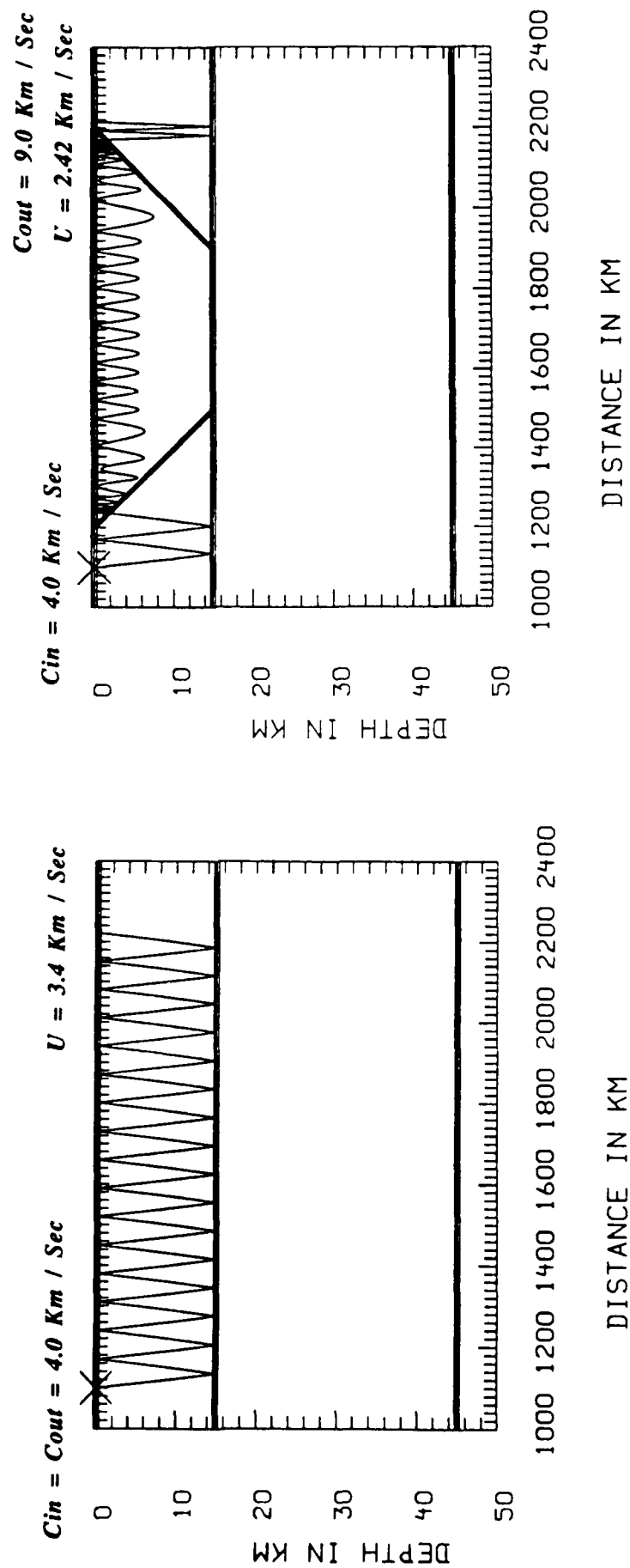| Depth (km)	Velocity (km/ sec)														
	Horizontal Distance (x 1000 km)														
	1.0	1.1	1.2	1.3	1.4	1.5	1.6	1.7	1.8	1.9	2.0	2.1	2.2	2.3	2.4
0.0	3.58	3.58	2.60	2.60	2.60	2.60	2.60	2.60	2.60	2.60	2.60	2.60	2.60	3.58	3.58
5.0	3.63	3.63	3.63	2.60	2.60	2.60	2.60	2.60	2.60	2.60	2.60	2.60	3.63	3.63	3.63
10.0	3.70	3.70	3.70	3.70	2.89	3.18	3.18	3.18	3.18	3.18	2.89	3.70	3.70	3.70	3.70
15.0	3.75	3.75	3.75	3.75	3.75	3.46	3.46	3.46	3.46	3.75	3.75	3.75	3.75	3.75	3.75

FIGURE 1-24: Ray tracing plots for simulated *Lg* waves. (a) Laterally homogeneous crust. (b) Laterally heterogeneous crust with sedimentary basin. Phase and group velocity are c and U, respectively.

Figure 1-24 (b) shows that the presence of the sedimentary basin in the structure severely disrupts the pattern of propagation of the reverberations in the granitic layer. One effect is that the waves which propagate into the basin are bent upward by the velocity contrast between the granitic velocities outside the basin and the slower, sedimentary velocities inside the basin. Another is that the rays become trapped in the upper layers of the structure. The waves are then guided by the slower velocities in the upper part of the basin structure until they arrive at the other side of the basin. After they emerge back into the homogeneous structure, they have been considerably slowed down. In this case, the group velocity would be reduced almost by half. Furthermore, the original phase velocity has been greatly altered because of the dipping interfaces between the basin structure and the surrounding homogeneous structure. For the model in Figure 1-24(b), the S wave reverberations, which start out with Lg phase velocities, have been converted to rays with phase velocities near 9 km/sec. These phases may become Sn type modes or convert to P waves. Thus, this mechanism might explain how Lg waves scatter into P and Sn coda waves.

As shown in Figure 1-24, the effect of the basin structure on Lg is that it is captured in the upper layers and that "on-time" Lg is essentially delayed to much later times. Because of the repeated reverberations in the upper layers and the likely lower Q in these layers, the original Lg waves would be severely dissipated. Whether the Lg is completely dissipated or not depends on the dimensions of the basin through which the Lg waves must propagate. The most likely result would be that the Lg modes, instead of arriving as a distinct arrival, would be spread out into long coda with amplitudes which diminish with time. This example shows that it is lateral heterogeneity in the upper crust that is required to block the propagation of Lg, and that effects in the lower crust or at the Moho would have little effect on Lg, assuming is is primarily composed of shear wave reverberations in the upper crust.

Two examples of Sn type propagation are shown in Figure 1-25, which models Sn as diving wave in the lower crust and upper mantle. No attempt has been made to model decreased
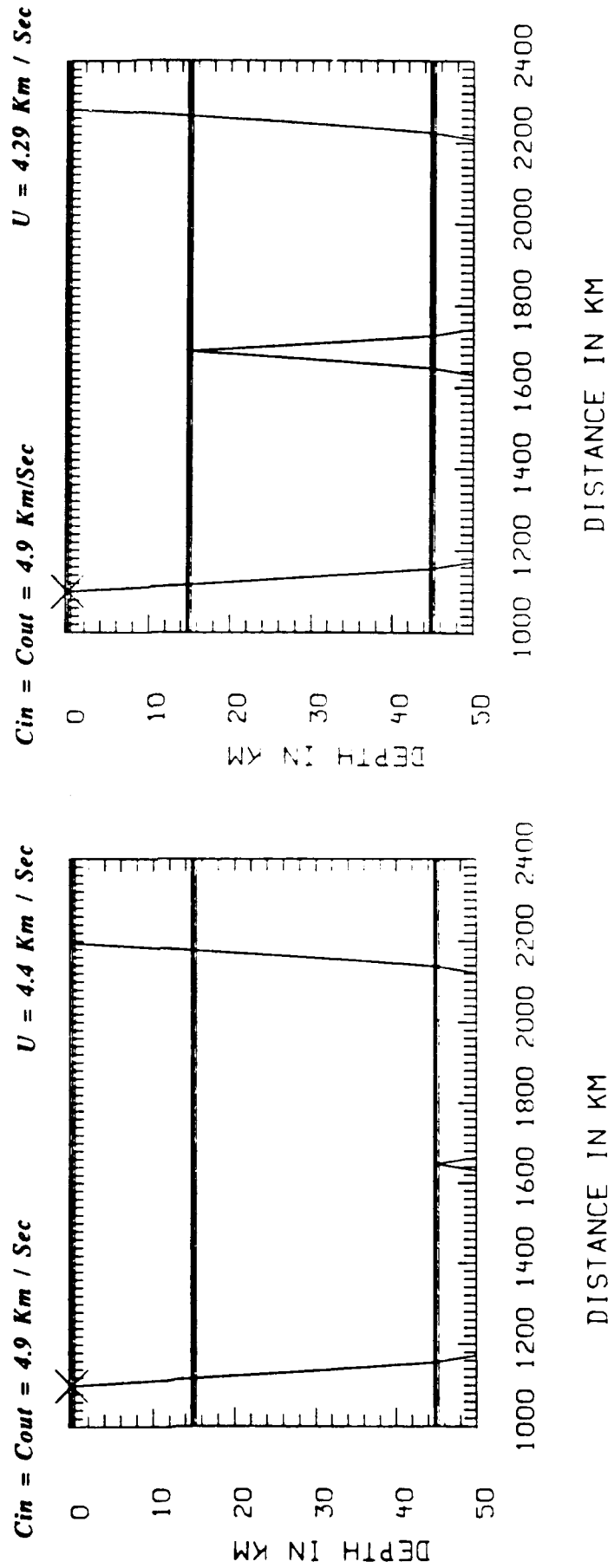
50

FIGURE 1-25: Ray tracing plots for simulated *Sn* waves. (a) Diving waves in the mantle. (b) Lower crustal reverberations.

51

depth of the Moho, which has been observed in the Barents Basin. However, Figure 1-25 makes clear that *Sn* would not be greatly affected by such an effect, since it is mainly controlled by the structure of the upper mantle, although Moho depth variations may change the group velocities of *Sn* modes which bounce off the bottom of the Moho. Also, the *Sn* wave would propagate below the sedimentary basin and be totally unaffected by it.

Figure 1-26 shows another type of *Sn* propagation which might be affected by the presence of the basin. Shear-wave reverberations which involve the entire crust would produce group velocities of about 4.1 km/sec which are on the lower end of the range expected for *Sn*. As shown in Figure 1-26 (b), this mode would propagate into the basin structure. However, because of the high phase velocities of these *Sn* modes and steeper angles of incidence, they are not captured by the basin and essentially propagate through the structure with virtually no effects.

1.7   CONCLUSIONS AND RECOMMENDATIONS

The main objective of this study has been to further analyze and explain the poor propagation of *Lg* from Novaya Zemlya to the Norwegian arrays, which was first pointed out by Baumgardt (1990). This poor *Lg* excitation is not an expected feature of regional propagation in Scandinavia, since strong *Lg* is observed for other paths at comparable distances. Most of the evidence points to the Barents sedimentary basin as the cause of the *Lg* blockage from Novaya Zemlya. We have presented a model which explains *Lg* blockage by the sedimentary basin capturing and delaying the *Lg* modes and their amplitudes being reduced by repeated reverberations and scattering within the basin.
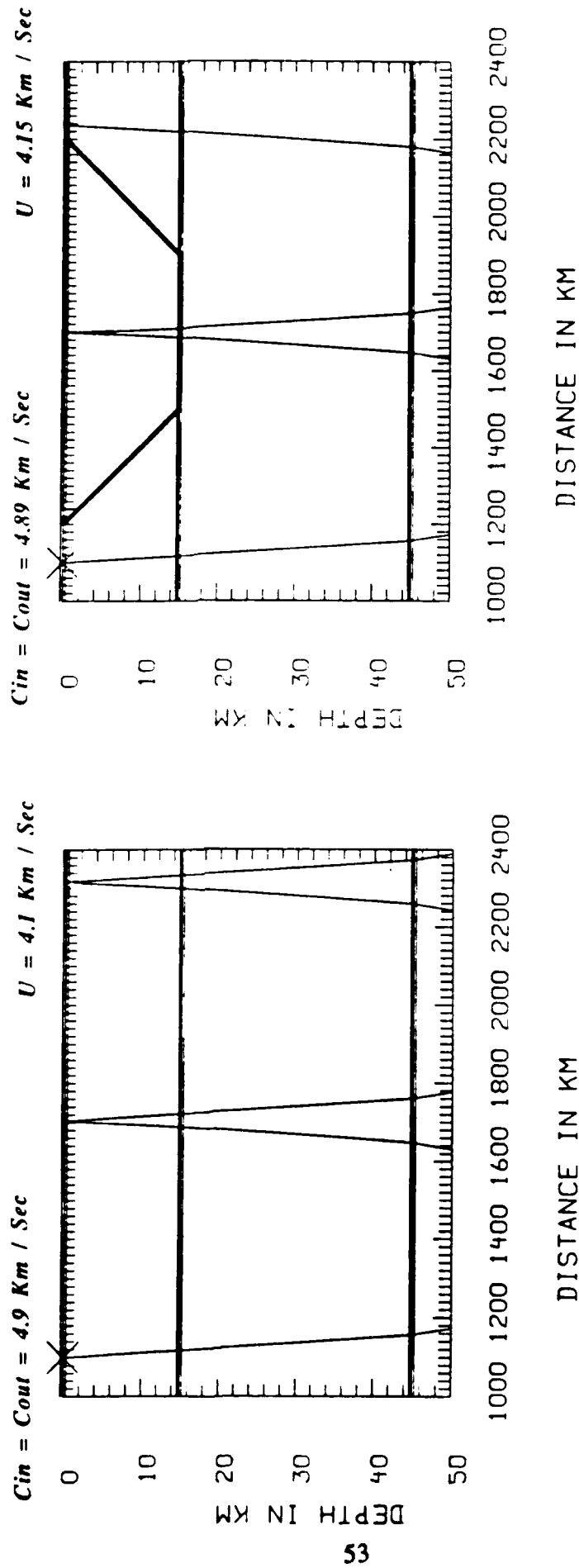
FIGURE 1-26: Ray tracing plots for simulated *Sn* waves which might pass through the sedimentary basin. (a) No sedimentary basin. (b) Sedimentary basin present.

The ray tracing study only gives a first order representation of the propagation of *Lg* through the sedimentary basin. Only the primary rays, i.e., shear waves which reverberate in the crustal granitic layer, were included in the ray tracing. Actual *Lg* waves consist of many such rays, and undoubtedly some may follow paths which do not pass through the heterogeneous structure. A true modeling of *Lg* should include all possible rays, which would probably show that some of the *Lg* energy can propagate through the heterogeneous structure. The incoherent beam analysis of the Novaya Zemlya events has, in fact, shown that the coda shapes flatten at the expected time of the onset of on-time *Lg* so that *Lg* is not completely blocked. However, the ray plots of the primary rays represent the paths traversed by most of the *Lg* energy, and they will clearly be diverted by the sedimentary basin along the path.

Another assumption made in the interpretation of the Barents Sea *Lg* blockage is that *Lg* propagates primarily along the great-circle path from the source to receiver. Our FK analyses of *Lg* waves at the regional arrays, both in this study and in Baumgardt (1990), showed most of the energy in the *Sn* wave train arrives at the array on the expected azimuth of the event, indicating that this energy follows the great-circle path. However, the FK analysis of weak *Lg* arrivals at NORESS by Baumgardt (1990) showed that much of the late *Lg* arrivals (i.e., *Lg* coda waves) were coming in off azimuth, mainly more to the east than the expected azimuth of Novaya Zemlya relative to NORESS. This result indicates that *Lg* energy has been diverted around (multi-pathed) to the east, possibly by the sedimentary basin itself, and arrives late because of the longer propagation paths. This would further reduce the energy of the on-time *Lg* arrivals, which would be delayed and spread out in time in the *Lg* coda. Such an analysis has not yet been done for the presumed ARCESS *Lg* arrivals, primarily because they were so weak.

Finally, the question of the utility of *Lg* for yield estimation and event identification at Novaya Zemlya must be addressed. These studies indicate that *Lg* yield estimation at Novaya

54

Zemlya may be limited with the Scandinavian arrays. The blockage and scattering of *Lg* would definitely make absolute yield estimation impossible, unless corrections could be determined for the amount of amplitude reduction due to the blockage. Corrections may be derived from empirical studies, such as those described in the next section, but more studies would be required. Modeling may give some estimates of the amount of energy lost by *Lg* at a sedimentary basin, but precise knowledge of the model parameters would be required. These parameters would have to be known three-dimensionally, because of the observation of extreme multi-pathing in the region. Moreover, techniques for synthesizing *Lg* in three-dimensional media have not yet been developed and would probably be difficult given current processing resources.

Although absolute *Lg* yield estimation may not be possible, *Lg* could provide precise relative yield estimates, since *Lg* type energy can be observed at the Scandinavian arrays from the test site with high signal-to-noise ratio, largely because of the close proximity of the sensors to Novaya Zemlya. Stronger *Lg* waves have been observed at the Graefenburg array, and the preliminary results of Ringdal (1990) indicate that stronger *Lg* waves are seen at the GERESS, located near Graefenburg, and the FINESA array. Assuming all events are located at the same test site and calibration shots with known yields are available, the observed *Lg* waves, including possibly the "early *Lg*" waves, may provide the same kind of relative yield estimation stability that has been observed for other test sites in the Soviet Union (Hansen et al, 1990).

However, the caveat which must be considered is that all the *Lg* waves from Novaya Zemlya are considerably scattered, including those observed at Graefenburg array. There is some preliminary indication that the relative amplitude of "early *Lg*" compared to the *P* coda at both ARCESS and NORESS may depend on the precise location of the explosions along the Matochkin Shar. This may indicate that even small perturbations in the propagation path, due to differences in location of the explosions, may cause significant variations in the nature of the scattering of *Lg* that cause observable amplitude variations.

With respect to event identification, this study has shown that amplitude ratio discriminants, like the P-to-Lg ratio, would clearly identify the Novaya Zemlya explosions as "explosion." However, this ratio would be much greater than may be observed from other explosions over the same distance, but without Lg being blocked. Thus, in the case of Novaya Zemlya, path effects would greatly obscure any source effects that might be used for discrimination. As the results of the next study will show, other explosions can generate much greater Lg energy, compared to the P wave energy, than those at Novaya Zemlya.

2.0 SEDIMENTARY BASIN STRUCTURES AND THE BLOCKAGE AND SCATTERING OF LONG-RANGE LG WAVES FROM NUCLEAR EXPLOSIONS IN THE SOVIET CRATON

2.1 INTRODUCTION

Complete knowledge of the efficiency of *Lg* propagation across the entire continental craton of the Soviet Union is required to make effective use of the phase for yield estimation and discrimination. The results of the Novaya Zemlya study of the last section have shown how *Lg* waves are blocked by laterally heterogeneous structures like the Barents Sea sedimentary basin. The question we address in this section is whether other blockages of this type occur in other parts of the Soviet Union.

The earliest view of how *Lg* propagation can be blocked is the presence of 100 km or more of oceanic crust along the propagation path (Ewing et al, 1957). This seemed to be supported by the fact that *Lg* wave propagation is not observed in oceanic basins. Other investigators (Ruzaikan et al, 1977; Kadinsky-Cade et al, 1981; Ni and Barazangi, 1983; Kennett et al, 1985) have suggested that *Lg* blockages in the continents result from lateral heterogeneities throughout the entire crustal structure. The inefficient or lack of *Lg* propagation in southern Eurasia has largely been attributed to extreme variations in crustal thickness and high anelastic attenuation. However, in the previous section, it was shown how *Lg* amplitudes are affected by the geological heterogeneity along the propagation path and that sedimentary basins can capture and block *Lg* propagation. Knowledge about the presence of such structures along the propagation path and how they affect *Lg* is essential whenever *Lg* amplitude measurements are used for discrimination or yield estimation purposes.

Most previous studies have concentrated on the propagation of *Lg* in the southern parts of the Soviet Union, in the region of Tibet, Pamirs, and Hindu Kush. Fewer studies of *Lg* propagation have been done in the northern and western parts of the Soviet Union because of the lack of station coverage in this region. However, it has been found (e.g., Bath, 1954; Baumgardt, 1985) that *Lg* waves propagate to great distances from Eurasian events to Scandinavian seismic stations, which suggests that propagation in this region may be very efficient.

In this section, the long-range propagation of *Lg* to the Scandinavian arrays from events in the Soviet Union is examined. This data is interpreted using the geological cross-section method applied in the previous section to the interpretation of *Lg* blockage from Novaya Zemlya. This study will again show that geological heterogeneity, particularly the replacement of the granitic layer by lower velocity sediments in continental sedimentary basins, is the primary feature responsible for the partial or complete blockage of long-range propagation of *Lg* in the platform regions of the Soviet Union.

The results of this study provides a means for knowing whether or not *Lg* amplitudes have been reduced beyond that expected from anelastic attenuation. Because *Lg* primarily propagates in the upper layers of the crust and because *Lg* blockages are mainly caused by upper crustal geological heterogeneities, it may not be necessary to know the entire crustal structure in a region to determine *Lg* propagation efficiency. All that may be required is knowledge of variations in the upper crust, which can be obtained from surface and subsurface geological studies, and other geophysical information, such as deep seismic sounding velocity profiles. Ultimately, it may be possible to devise methods for correcting *Lg* amplitude measurements for the effects of known geological blockages, based on information obtained from geological and geophysical studies, in addition to corrections for anelastic attenuation determined from seismological studies.

58

2.2   APPROACH

Source-Receiver Propagation Paths

To study the effects of geological heterogeneity on *Lg* propagation, the geological characteristics of the propagation paths from the presumed nuclear explosions, mostly peaceful nuclear explosions (PNEs) in the Soviet Union, to NORSAR, NORESS, and ARCESS have been examined in detail. The events analyzed in two previous studies (Baumgardt, 1985b; Baumgardt, 1987) have been re-examined. The epicenter parameters of the events are given in Table 4.

Figure 2-1 shows a summary geologic/tectonic map of the Soviet Union, derived from Watson (1976), which shows the propagation paths for the *Lg* waves which have been studied. Most of the central and northern areas of the Soviet Union have been classified tectonically as a combination of Precambrian shield, in the west, Phanerozoic platform in the main part of the craton, exclusive of the Urals, including the Soviet Platform west of the Urals and the Siberian Platform east of the Urals, and Phanerozoic orogenic belts, which encompasses most Ural mountain block. As shown in Figure 2-1, there are several sedimentary basins which are traversed by the paths, most of which are located in the southern regions and around the Ural mountains.

For the purposes of geological characterization, each of the source receiver paths have been grouped in 10 categories, with designations and abbreviations given in Table 4 and the paths are labeled with the abbreviations in Figure 2-1. These include the following:

59

TABLE 4

Event Parameters for Specific Source-Receiver Paths in the Soviet Craton

| Event Label	Date	Time	Latitude	Longitude	mb	Δ (°)
Northern Russian Platform - NORSAR (NRP-N)						
3A	10/04/71	10-00-00.0	61.61N	47.11E	5.1	17.4
Southern Russian Platform - NORSAR (SRP-N)						
5A	07/09/72	07-00-00.0	49.78N	35.40	4.8	17.7
Northern Urals - NORSAR (NU-N)						
2A	07/10/71	17-00-00.0	64.16N	55.18E	5.1	20.5
14A	08/29/74	09-59-55.0	67.23N	62.11E	5.2	22.8
6	08/11/84	18-59-57.8	65.08N	55.28E	5.3	20.3
Siberian Platform - NORSAR (SP-N)						
3	10/04/79	16-00-00.0	60.68N	71.50E	5.4	28.7
7	08/25/84	19-00-00.0	61.89N	72.09E	5.4	28.5
Tazovski-Gyda Peninsula - NORSAR (TGP-N)						
13A	08/14/74	15-00-00.0	68.91N	75.90E	5.5	27.5
East of the Caspian Sea - NORSAR (ECS-N)						
1A	12/23/70	07-00-57.3	43.83N	54.85E	6.6	31.1
Astrakhan	10/08/80	06-00-00.0	46.70N	48.21E	5.2	25.8
Southeast of Southern Urals - NORSAR (SEU-N)						
4A	10/22/71	05-00-00.0	51.56N	54.53E	5.2	25.5
8A	11/24/72	09-59-57.8	51.84N	64.15E	5.2	30.1
12A	09/30/73	05-00-00.0	51.60N	54.58E	5.2	25.6
West of Semipalatinsk - NORSAR (WE-N)						
10A	08/28/73	03-00-00.0	50.55N	68.40E	5.2	33.0
11A	09/19/73	03-00-00.0	45.64N	67.85E	5.2	36.1
Eastern Kazahk- ARCESS (EK-A)						
Semipalatinsk	02/13/88	03-05-05.9	49.95N	78.91	6.1	31.0
Eastern Kazahk -NORSAR (EK-N)						
Semipalatinsk	04/25/85	00-57-06.5	49.92N	78.97	5.9	38.1
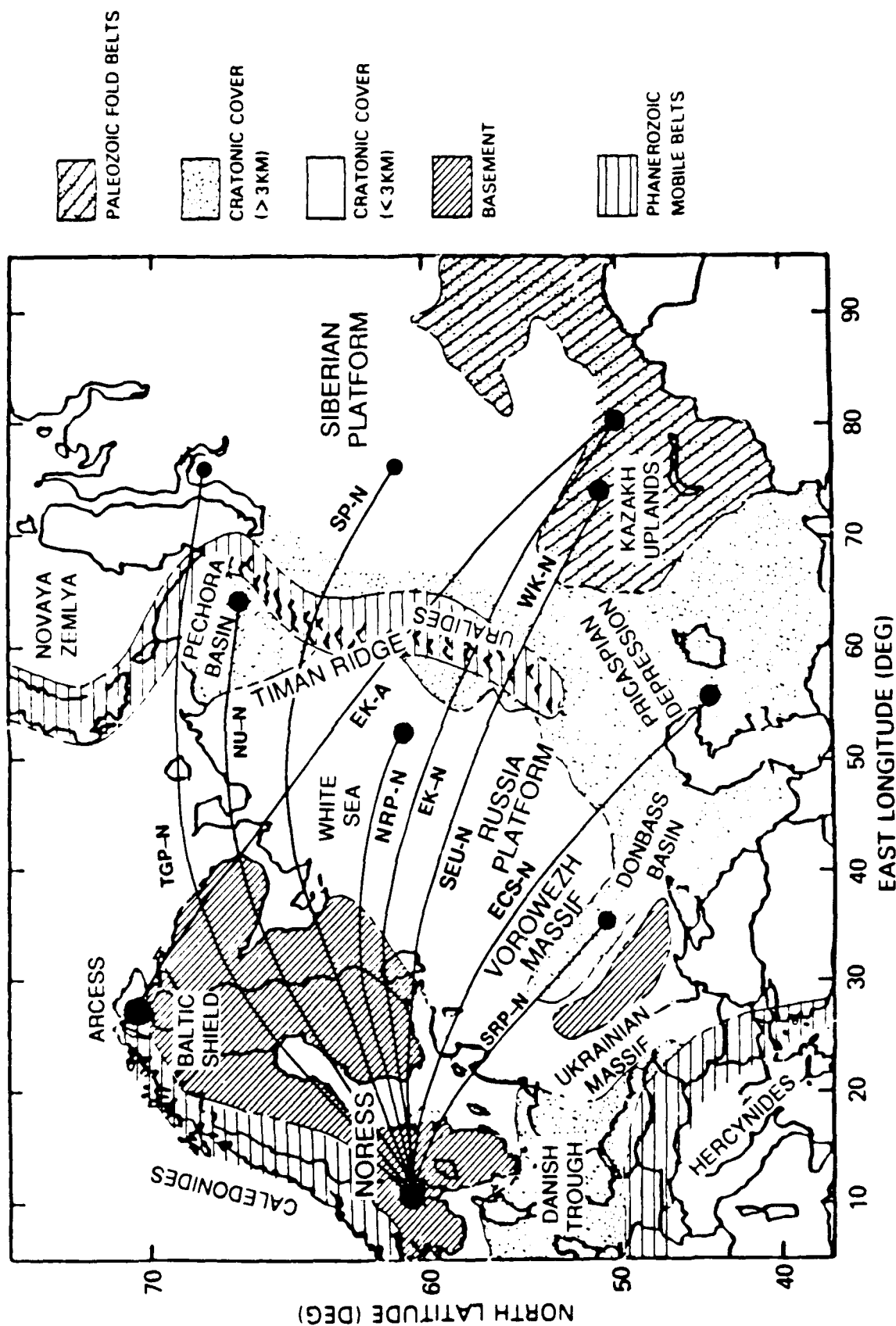
FIGURE 2-1: Propagation paths from explosions in the Soviet Union to NORSAR, NORESS and ARCESS plotted on base map after Watson (1976).

61

(i)   Northern Russian platform PNE recorded at NORSAR (NRP-N) - This
        path runs from one PNE in the north to NORSAR. The path crosses the
        most stable platform region of the Soviet Union and does not cross any
        major heterogeneous structure. The White Sea PNE, studied in the
        previous section, would also fall under this category.

(ii)   Southern Russian Platform PNE recorded at NORSAR (SRP-N) - This path
        runs from one PNE in the south to NORSAR. The PNE occurred in the
        Donbass sedimentary basin and the Lg crossed the western boundary of this
        basin with the Russian Platform.

(iii)   Northern Urals PNEs recorded at NORSAR (NU-N) - This category
        includes several events which occurred in the northern part of the Soviet
        Union in the vicinity of the Ural Mountains. The three events given in
        Table 1 all occurred in a sedimentary basin called the Timan-Pechora Basin.

(iv)   Siberian Platform PNEs recorded at NORSAR (SP-N) - The paths from
        these two events pass across the Ural Mountains and the southern tip of the
        Timan-Pechora Basin.

(v)   Tazovski-Gyda Peninsula PNE recorded at NORSAR (TGP-N) - This is a
        PNE which actually occurred on the Siberian platform but whose Lg waves
        pass north of the Timan-Pechora Basin and across the Kara and Barents
        Seas.

(vi)   East of the Caspian Sea PNE recorded at NORSAR (ECS-N) - The Lg
        propagation path crosses the northern part of the Caspian and the Precaspian
        sedimentary basin. Also included in this category is an event which
        occurred in the Astrakhan region, north of the Caspian, whose Lg
        propagation path is almost the same as that from the PNE east of the
        Caspian Sea, except that it does not cross the Sea itself.

(vii)   PNEs South and Southeast of the Southern Urals recorded at NORSAR
        (SU-N, SEU-N) - This includes a group of PNEs which have occurred in
        the region of the southern Urals. For those PNEs located on the
        southeastern side of the Urals, the Lg waves would have crossed the Ural
        Mountains.

(viii) West of Semipalatinsk PNEs to NORSAR (WK-N) - This explosion
        actually occurred in the western Kazakh uplands, hence the label WK. The
        Lg path to NORSAR crosses the Kazakh uplands, the southern Ural
        Mountains, and the sedimentary basins on either side of the Urals before
        passing into the Russian Platform.

(viv)   Eastern Kazakh explosions to NORSAR/NORESS (EK-N) - This category
        includes all the Soviet tests at the Semipalatinsk site which have been

62

recorded at NORSAR and NORESS. The *Lg* paths of these events cross the southern part of the Ural Mountains.

(x)   Eastern Kazakh explosions to ARCESS (EK-A) - This category includes Soviet tests at the Semipalatinsk site which have occurred since about 1988, when the ARCESS array began operating. The *Lg* paths to ARCESS cross the middle part of the Ural Mountains.

For all the events located at the sites shown on the map in Figure 2-1, short-period *Lg* waves have been recorded at some level although the frequency content of the *Lg* waves decrease with increasing distance.

In this section, the coda shapes of the explosions have been analyzed using the incoherent beam analysis described in the previous section. In all cases, a window length of five seconds was used in the averaging the log-rms amplitudes on each channel before stacking across the array. The waveforms were pre-filtered with a 0.6 to 3.0 Hz Butterworth recursive bandpass filter prior to computing the incoherent beams.

Crustal Cross-Sections

Crustal cross-sections were generated using the methods described in the previous section. The surface-elevation cross-sections were obtained from the ETOPO5 database. The Moho depth was inferred from the elevations, assuming an Airy isostatic model with 80% compensation. The crustal density was assumed to be 2.67 g/cm^3, the mantle density was assumed to be 3.27 g/cm^3, and the average crustal thickness, for sea level, was assumed to be 30 km. (Note: This differs from the Barents Sea model where an average crustal thickness of 40 km was assumed and 100% compensation in order to obtain the type of crustal thickness variations reported in the Soviet literature.)

The upper-crustal sediment thicknesses for the propagation paths were obtained from isopach maps published by the USGS (Alverson et al, 1967). The great-circle paths were traced by hand across the maps which had contours indicating depths to deformed basement rocks. In the stable, platform regions, the ages of these rocks are late Precambrian (post Riphaen), including the Timan-Pechora and Moscow basins, and the basins in the vicinity of the Ural Mountains. For the basins in the Caspian Sea region, the deformed basement is Paleozoic in age. For each great-circle path, depths to the basement were recorded as a function of distance along the path and plotted as cross-sections.

Ideally, this type of analysis should be done by comparing the *Lg* excitation for propagation paths which cross different kinds of geologic structures, but have about the same epicentral distance so as to remove the effects of distance attenuation. Although the paths in this study cover most of the western platform regions of the Soviet Union, they vary considerably in distance since a single receiver for many sources has been analyzed. Because of the variable distances of *Lg* propagation, the possible effects of geological blockages of *Lg* can be evaluated in three ways.

First, the *Lg* level relative to the preceding *Sn* phase can be analyzed, as was done by Kvaerna and Mykkeltveit (1985) in their analysis of *Lg* propagation at closer distances to NORSAR. This assumes that the *Sn* and *Lg* attenuate at more or less the same rate with distance. Whether or not this is true depends on the nature of the propagation path. It has generally been assumed that *Sn* attenuates in the upper mantle (e.g., Kadinsky-Cade et al, 1981) and that this attenuation is more severe if there is a well developed aesthenospheric layer. However, refraction studies for the upper mantle in the platform and shield regions of the Soviet Union (Masse and Alexander, 1974) indicate that the aesthenospheric layer may be absent or not well developed. *Lg* does not feel the effects of aesthenospheric attenuation, although it may be more sensitive to crustal attenuation and scattering than *Sn*. Thus, because anelastic attenuation should be small in the crust

and upper mantle beneath the western Soviet Union, *Sn* and *Lg* amplitudes should decay at about the same rate with distance, and large changes in the relative amplitudes of *Sn* and *Lg* would be due to localized blockages.

Second, the *Lg* excitation can be compared to the coda level after *Pn* and *Sn*, to determine if reduced *Lg* levels correlate with increased coda levels. Such a correlation may indicate that *Lg* is attenuated by forward scattering.

Finally, an estimate can be made of the absolute *Lg* level and the distance decay of the *Lg* amplitude can be compared with what is expected for a standard *Lg* distance-distance attenuation model.

In this study we will use the first two methods, where we examine in detail the relative *Sn*, *Lg*, and coda levels, in a qualitative manner, and look for how the characteristics of the propagation path may be affecting these variations. The basic assumption made is that the *Lg* waves propagate along great-circle paths from source to receiver. FK analyses of *Lg* azimuths in Baumgardt (1990) and elsewhere suggest that, for the first arrival *Lg*, this is a reasonably good assumption. The fact that *Lg*, when observed, usually has a group velocity near 3.5 km/sec indicates that the main *Lg* phase propagation is very close to the great-circle path. *Lg* can be multi-pathed and propagated along different paths than the great-circle path. Much of the *Lg* coda may be made up of later arriving multi-pathed shear waves. However, we assume that such deviations are not significant, at least for the *Lg* which has a group velocity close to 3.5 km/sec, and that the great-circle crustal cross-section represents most of the propagation-path effects that the *Lg* experiences.

2.3 GEOLOGICAL INTERPRETATION OF LG PROPAGATION EFFICIENCY

In this subsection, the *Lg* excitation and propagation efficiency for each of the regions will be interpreted in terms of the crustal cross-sections for each of the great-circle propagation paths. The organization of this section will be to present, for each source receiver path, the incoherent beam analysis of the *Lg* excitation and then the crustal cross-section. In order to facilitate the comparison of crustal cross-sections for different regions, each cross-section has been standardized to a maximum distance of 4500 km, a maximum elevation of 2000 m, and a maximum crustal depth of 40 km. Each cross-section was made for a specific source-receiver path, and the date of the explosion and the path description is given at the top of each figure. However, more than one event may be described by a particular cross-section. The location of the event is indicated on each profile by a black triangle. If the distance to the event is less than the maximum distance, the cross-section has been extended beyond the distance of the event to 4500 km. Thus, the distances, depths, and scales of the different geologic features on each plot can be directly compared.

Russian Platform PNEs (NP-N, SP-N)

Figure 2-2 shows the great circle paths for the two PNEs which occurred in the Russian Platform region and whose *Lg* propagation paths to NORSAR traverse only the Russian Platform and the Baltic shield.
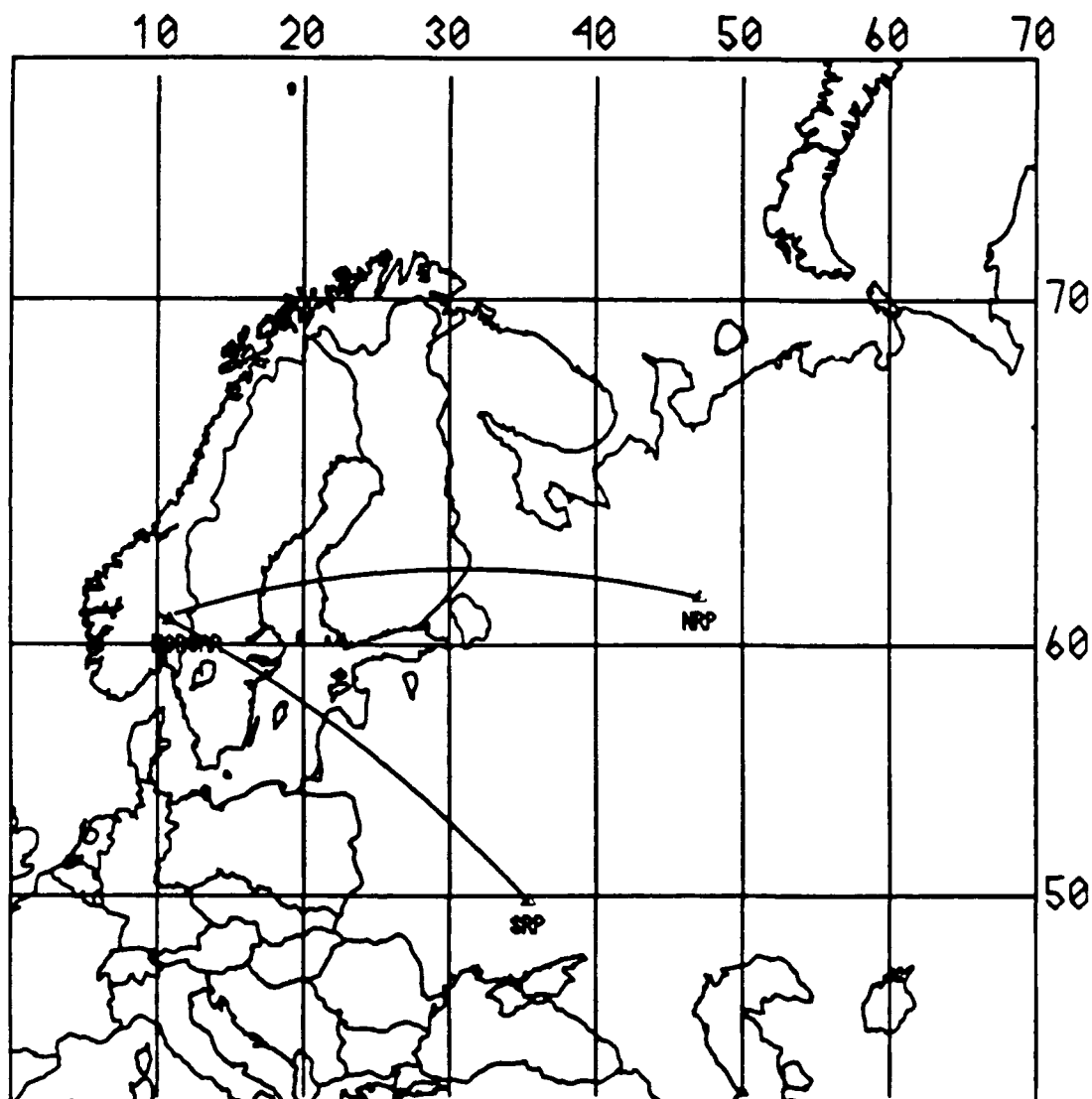
FIGURE 2-2: Propagation paths from the two Russian Platform PNEs to NORSAR.

Figure 2-3 shows the incoherent beam for the 10/04/71 PNE (NP-N), which occurred in the northern part of the Platform. In this figure, the phases which we have identified as P, Sn, and Lg are indicated. Because the PNE is beyond the cross-over distance for Pn and teleseismic P, the first phase, on which all the waveforms were aligned prior to forming the incoherent beam, is teleseismic P, although Pn is probably contained in the immediate coda. The first shear phase is probably direct S, although the coda has been labelled as Sn. Generally, Sn is identified as the energy which arrives in the coda with group velocity near 4.6 km/sec. Lg arrivals have group velocities near 3.5 km/sec.

It is interesting to note in this plot, and in all the succeeding plots, that the P and Sn codas are very different. The P coda decays very rapidly with time whereas the Sn coda is flat up to the arrival time of Lg. Other authors have also observed this sustained Sn coda level at other distances (Barazangi et al, 1977; Chinn et al, 1980; Kennett, 1985) which has been interpreted as resulting from scattering due to interconversions between Sn and Lg. In the previous section and in Baumgardt (1990), conversion of Sn-to-Lg at a single discrete interface may produce wave-packet-like arrivals in the Sn coda like those observed for Novaya Zemlya events. The flat type Sn codas, like that from the Northern Russian Platform PNE Figure 2-3, might be an indication of continuous conversion of Sn-to-Lg from more distributed lateral heterogeneities along the path.

Figure 2-4 shows the crustal cross-section for this path. The event occurred in the Moscow Basin, which contains Paleozoic clastics and carbonates that reach a thickness of 3 to 4 km. The basin gradually thins to the west into the Baltic shield. The elevation cross-section shows that there is some variation in topography on the platform and into Scandinavia which may cause weak scattering. Most of this path outside the Basin, including the Gulf of Bothnia segment, is Precambrian shield, with essentially granitic upper crust that probably lacks significant lateral heterogeneity. There are no major perturbations in the crustal thickness.
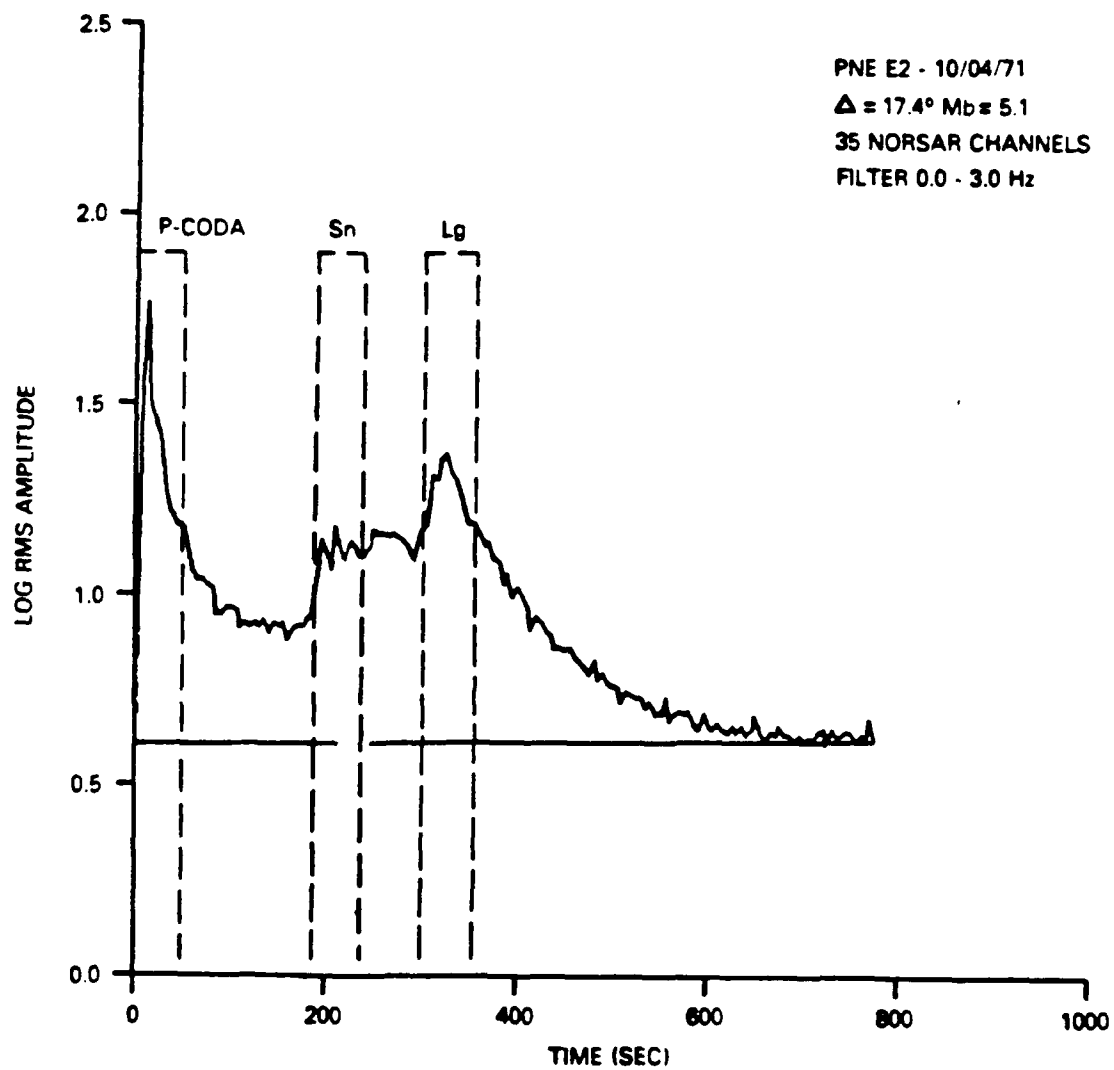
68

FIGURE 2-3: Incoherent beam for the Northern Russian Platform (NRP) PNE, as recorded at NORSAR.

69

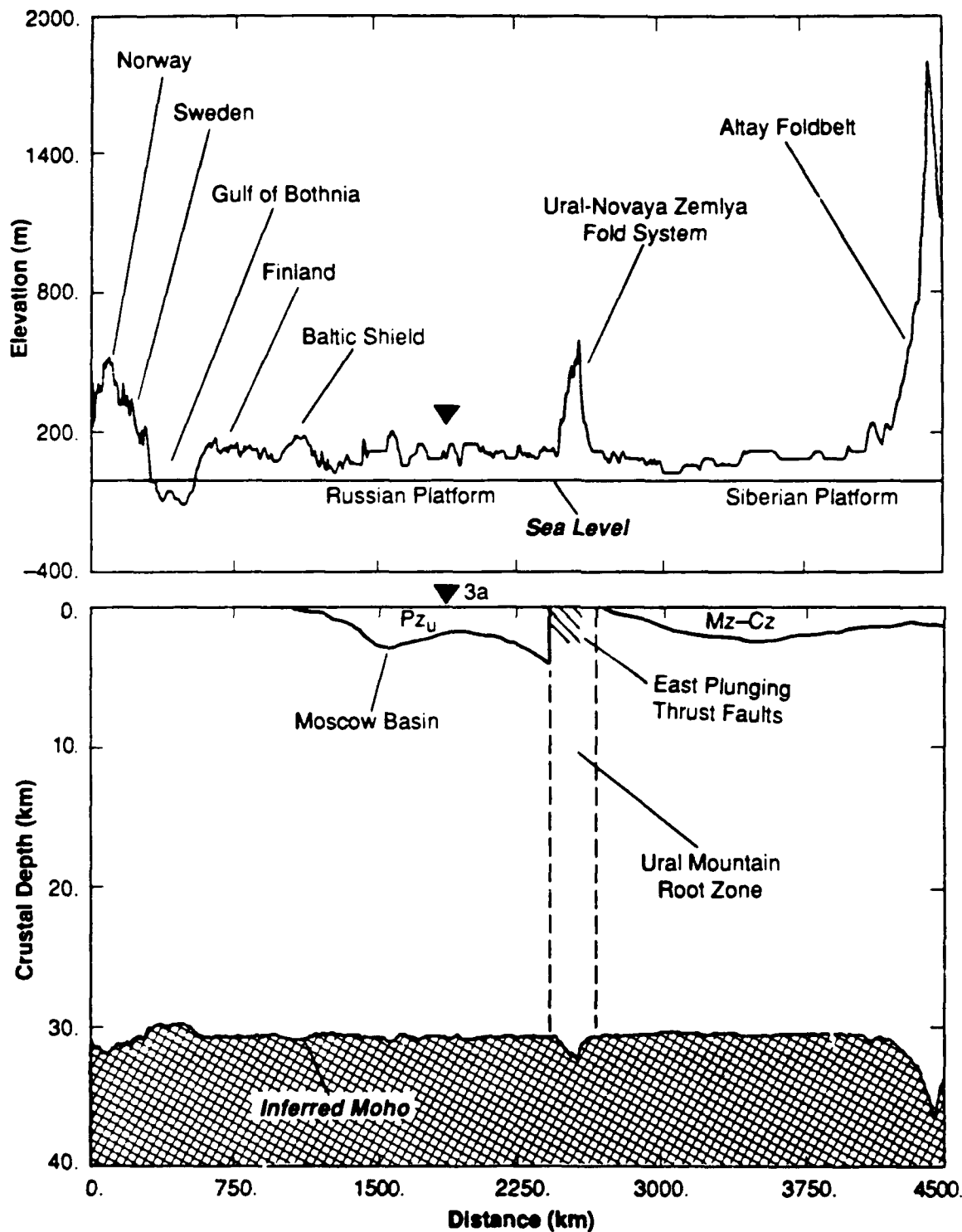# Russian Platform
10/04/71

FIGURE 2-4: Crustal cross-section for the Northern Russian Platform PNE.

70

Figure 2-3 shows that *Lg* excitation exceeds that of *Sn* and the propagation of *Lg* along this path is efficient. There is no significant coda excitation, except for the flat *Sn* coda, which may originate from scattering of *Sn*-to-*Lg* and *Lg*-to-*Sn*. However, this scattering is not strong enough to significantly attenuate *Lg* or *Sn*. Apparently, the gradual thinning of the Moscow Basin to the west does not pose a significant block to *Lg*.

Figure 2-5 shows the incoherent beam for the Southern Russian Platform PNE. This event has a very similar coda to that of the Northern Platform, with the *Lg* excitation being quite strong.

The crustal cross-section for this path, shown in Figure 2-6, is similar to that of the Northern Platform PNE, except for some of the details of the sedimentary basin. This explosion occurred in the middle of NW-SE trending Dnieper Trough, labeled the Donbass Basin in Figure 2-1, which contains Paleozoic carbonates, clastics, and shallow evaporites, including Devonian age salt domes. The post-Paleozoic sediments do not exceed 3 to 5 km, as in the Northern Platform path, although Precambrian (Riphaen) clastic deposits may reach depths as great as 9 km.

As in the case of the Northern Platform PNE, the gradual thinning of the post-Paleozoic sediments in the Baltic Basin to the west into the Baltic shield does not block *Lg* propagation. Both of these examples suggest efficient *Lg* propagation out of gradually thinning sedimentary basins.

Northern Urals PNEs (NU-N, TFP-N)

The map in Figure 2-7 shows the locations and great-circle paths for a group of PNEs located in the northern part of the Russian Platform west of the Urals (NU-N) and one event (TFP-N), which occurred on the Gyda Peninsula to the east of the Urals. The NORSAR incoherent beams for these events are presented as a record section in Figure 2-8. The two Russian Platform
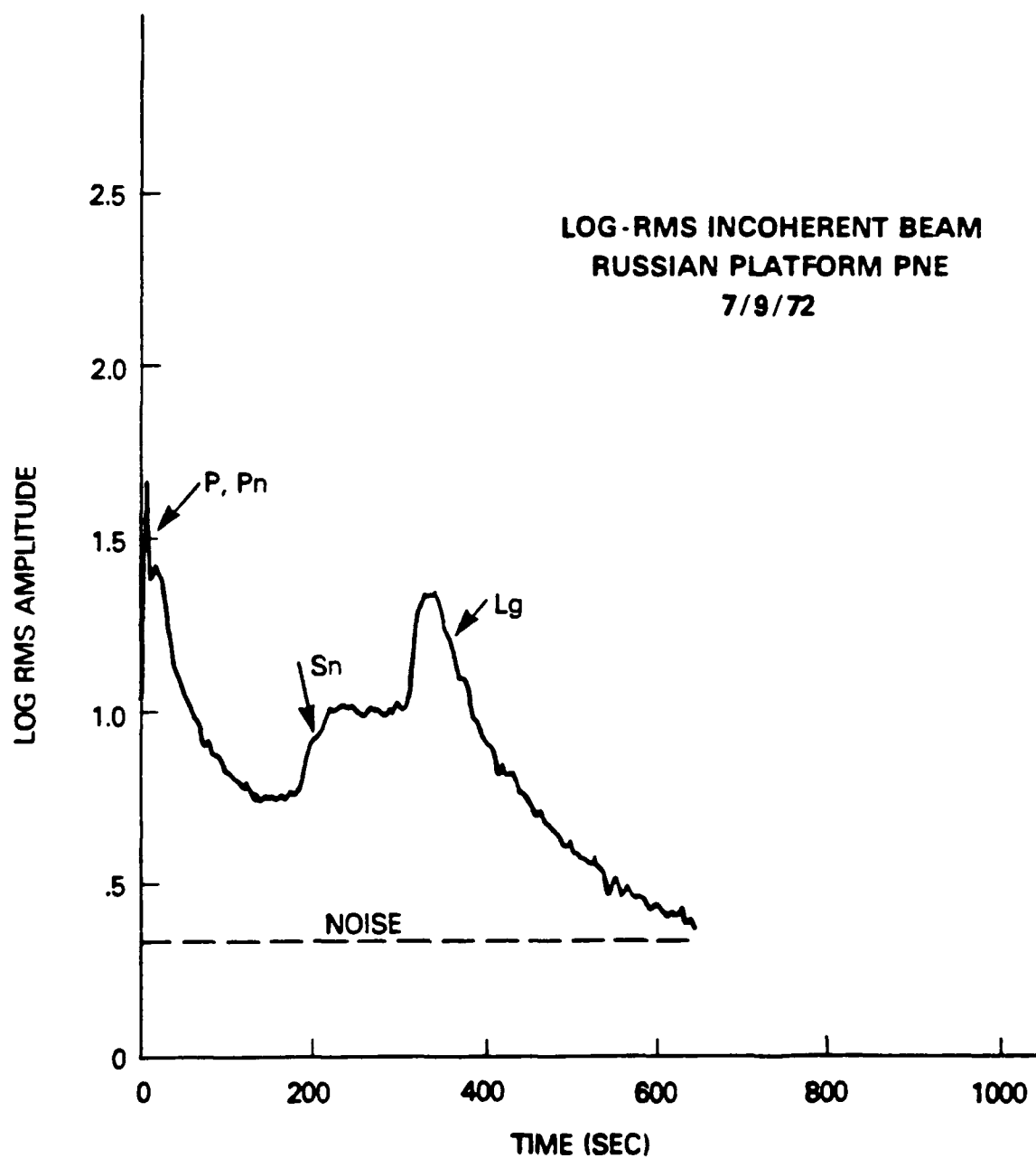
FIGURE 2-5: Incoherent beam for the Southern Russian Platform (SRP) PNE, as recorded at NORSAR.
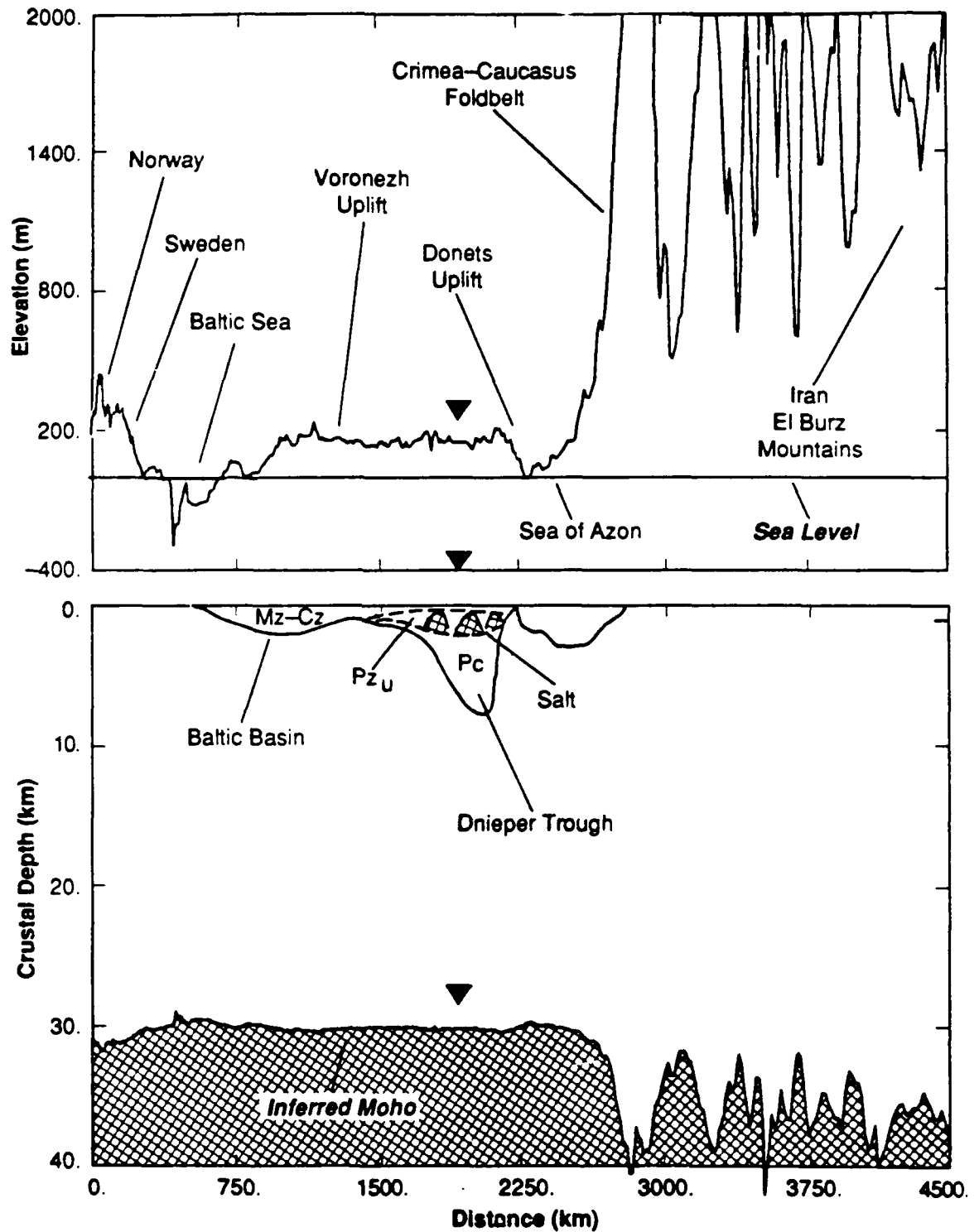
72

Russian Platform
07/09/72

FIGURE 2-6: Crustal cross-section for the Southern Russian Platform PNE.
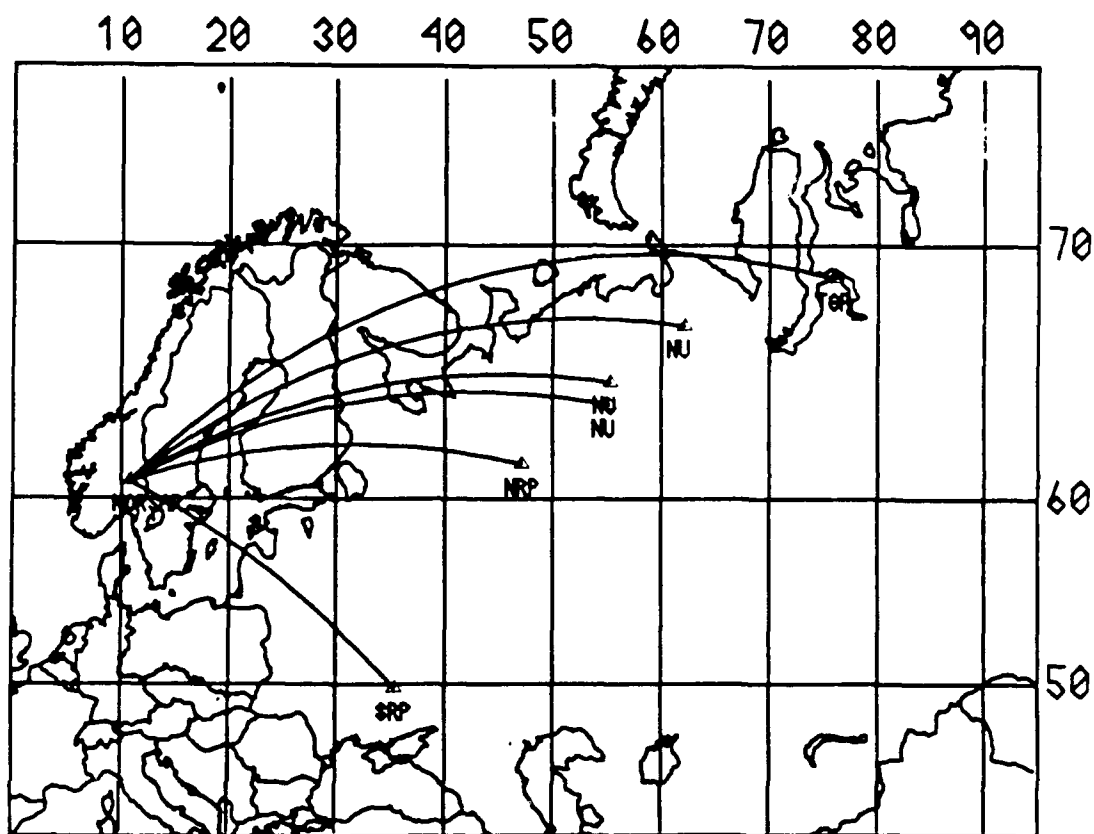
73

FIGURE 2-7: Propagation paths to NORSAR from several events in the Russian Platform and in the Northern Urals (NU).
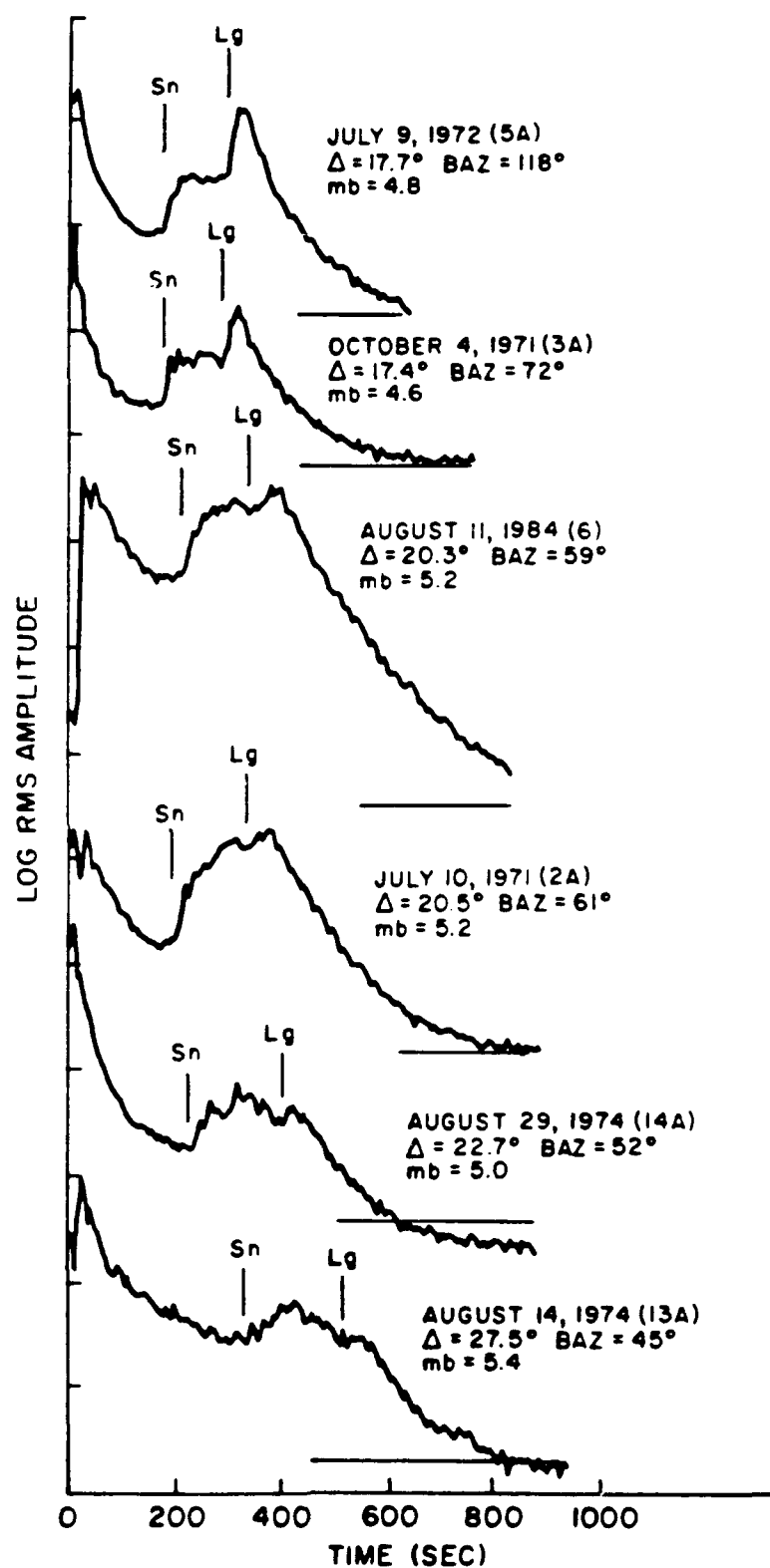
FIGURE 2-8: Record section of incoherent beams from the events whose locations are plotted in Figure 2-7.

events, Events 5A (SRP) and 3A (NRP) are included for comparison as examples of efficient Lg propagation.

The most striking difference between the three Northern Ural (NU) events, 6, 2A, and 14A, and the two Russian Platform (RP) events is that the NU events have much enhanced Sn codas and reduced Lg levels. The Sn codas are interesting in that they begin as a sharp onset, as in the case of the two Platform events, but then the levels increase with time rather than staying flat. In fact, the Sn codas appear to reach a peak at about 50 to 100 seconds before the onset of Lg. This peak is most apparent for Event 14A. The Lg onset is much less sharp, relative to the preceding Sn coda, for Events 6 and 2A, but is still greater than the maximum Sn amplitude. However, for the more distant Events 14A and 13A, the Lg amplitude is less than that of the maximum Sn amplitude. For Event 13A, Lg is only barely visible as a slight increase in the Sn coda level.

The low Lg levels from Events 14A and 13A are not due to distance attenuation, even though these events are at greater distances from NORSAR than the other events. Lg levels in excess of the Sn levels have been observed at greater distances than those of Events 14A and 13A (22.7° and 27.5°, respectively). Examples include Graefenburg recordings of Novaya Zemlya events, shown in the first section of this report and by Baumgardt (1990), and Kazakh events recorded at NORESS and NORSAR, shown later in this report and by Baumgardt (1985) and Baumgardt (1990).

The Lg waves from the NU Events (6, 2A, and 14A) and the TFP Event (13A) have been at least partially blocked along their paths to NORSAR. To investigate the causes of the blockages, Figures 2-9 and 2-10 show the events plotted on geologic maps of the region. The three events, 6, 2A, and 14A, occurred in a petroliferous sedimentary basin called the Timan-Pechora Basin. The basin is a triangular structure bounded on the east by the Ural Mountains, on the east and
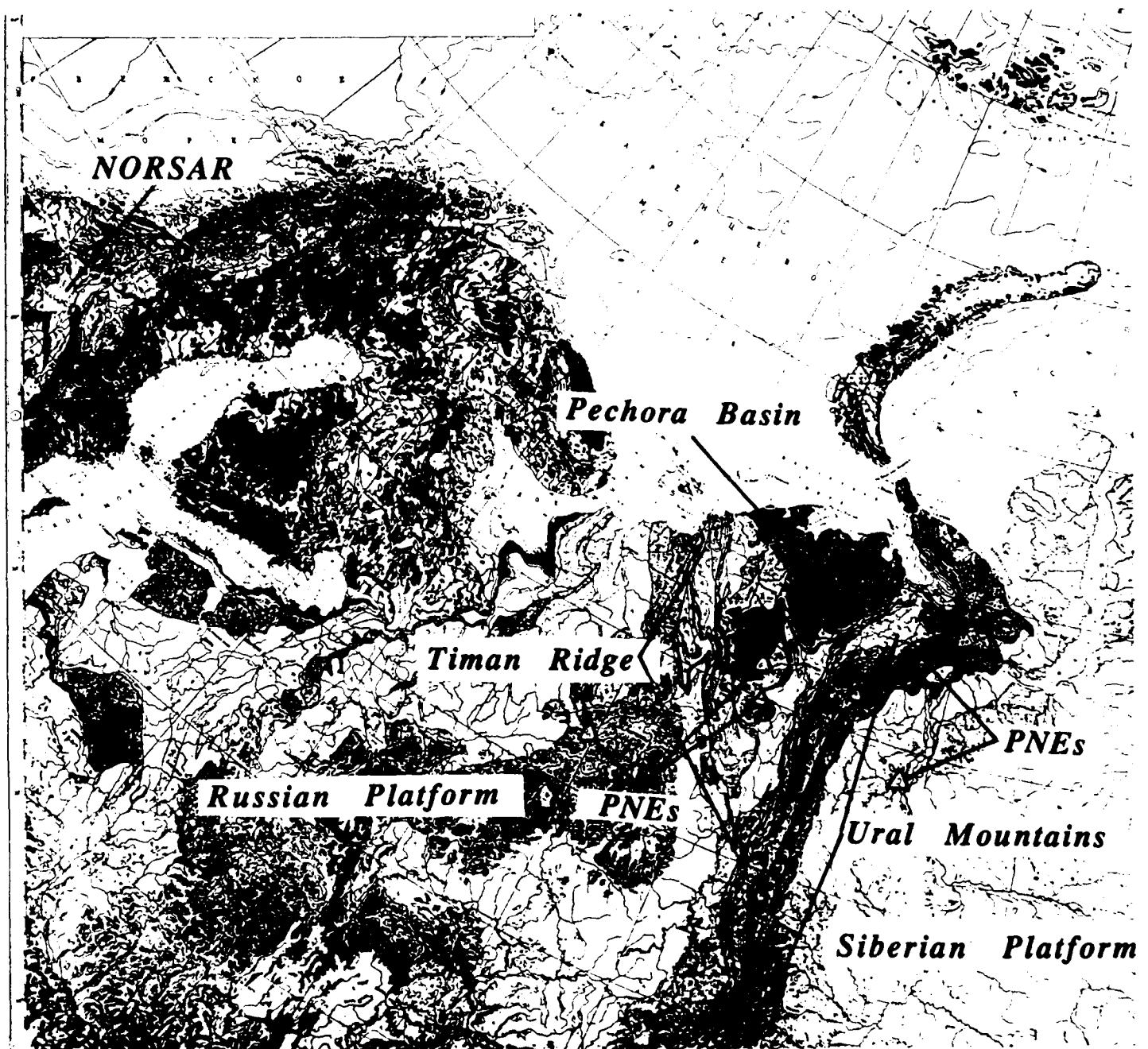
76

FIGURE 2-9: Geologic map of the Northern Ural region, including the Timan-Pechora Synaclese.
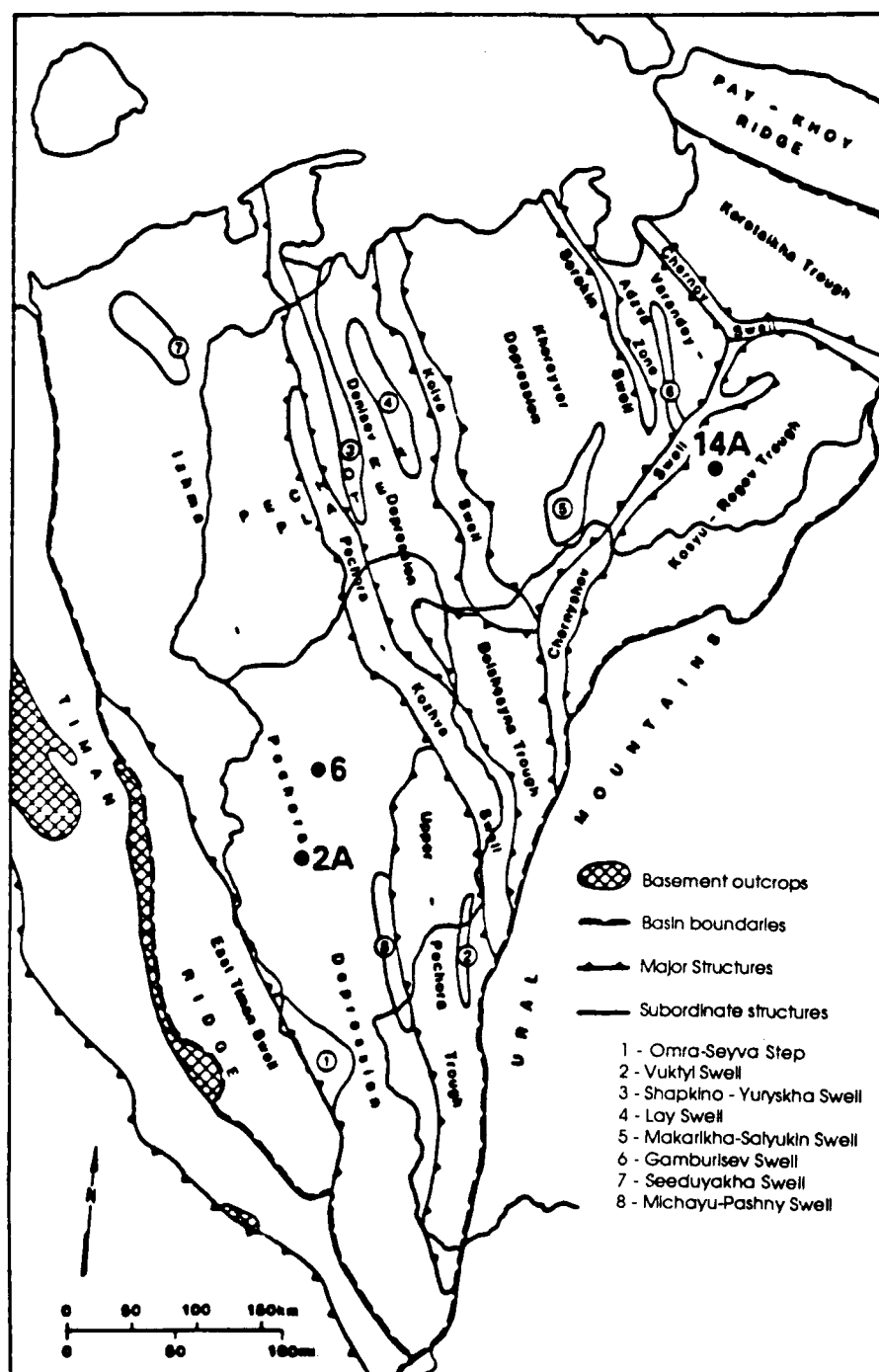
FIGURE 2-10: Map of the Timan-Pechora Synaclese, showing locations of three of the PNE shown in Figure 2-8.

78

south by the Timan ridge, and on the north by the Pechora and Barents Seas. The basin is filled with sediments with depths of 10 to 12 km above the basement. The basement rocks are exposed on the Timan ridge and in the Urals.

Figure 2-10 shows that Events 6 and 2A occurred in the Izhma-Pechora Basin, which contains 1000 m of Permian and Triassic clastics, carbonates, and evaporites and 700 m of lower Cretaceous age clastic coal-bearing sequences, with argillaceous limestone and oil shale (green and blue colors in Figure 2-9). Event 14A occurred to the northeast in the Kosyu-Rogov Trough.

The crustal cross-section in Figure 2-11 is for the most distant event in the Timan Pechora Basin, 14A, indicated by the solid arrow, although it also applies to the other two events as well. This cross-section shows that the post-Paleozoic sediments reach a maximum thickness of near 8 to 9 km, according to the USGS maps, although the Russian literature indicates that the depth to basement may be as great as 12 km in the center of the Basin (Jack Rachlin, USGS, personal communication). Events 6 and 2A were located near the center of the Basin in Figure 2-11.

The Lg waves from all three of these events would have had to pass out of the thick sediments of the Pechora Basin, whose sediments are probably low Q, through a region where there are no sediments, the Timan ridge, and then back into another closed basin, the Moscow Basin, before finally emerging at the sharp coastline of the Kola Peninsula. The Lg blockage may be caused by the enclosed basins, the sediment pinchouts at the Timan ridge, and the sharp topographic interfaces of the Kola Peninsula and Scandinavia. The sharp interfaces and pinchouts at the edges of the Pechora Basin and Moscow Basin may cause the Lg waves to be back-scattered and trapped in the basins, and then attenuated by repeated reverberation in the low Q sediments. Scattering from these features is probably responsible for the enhanced Sn codas levels.
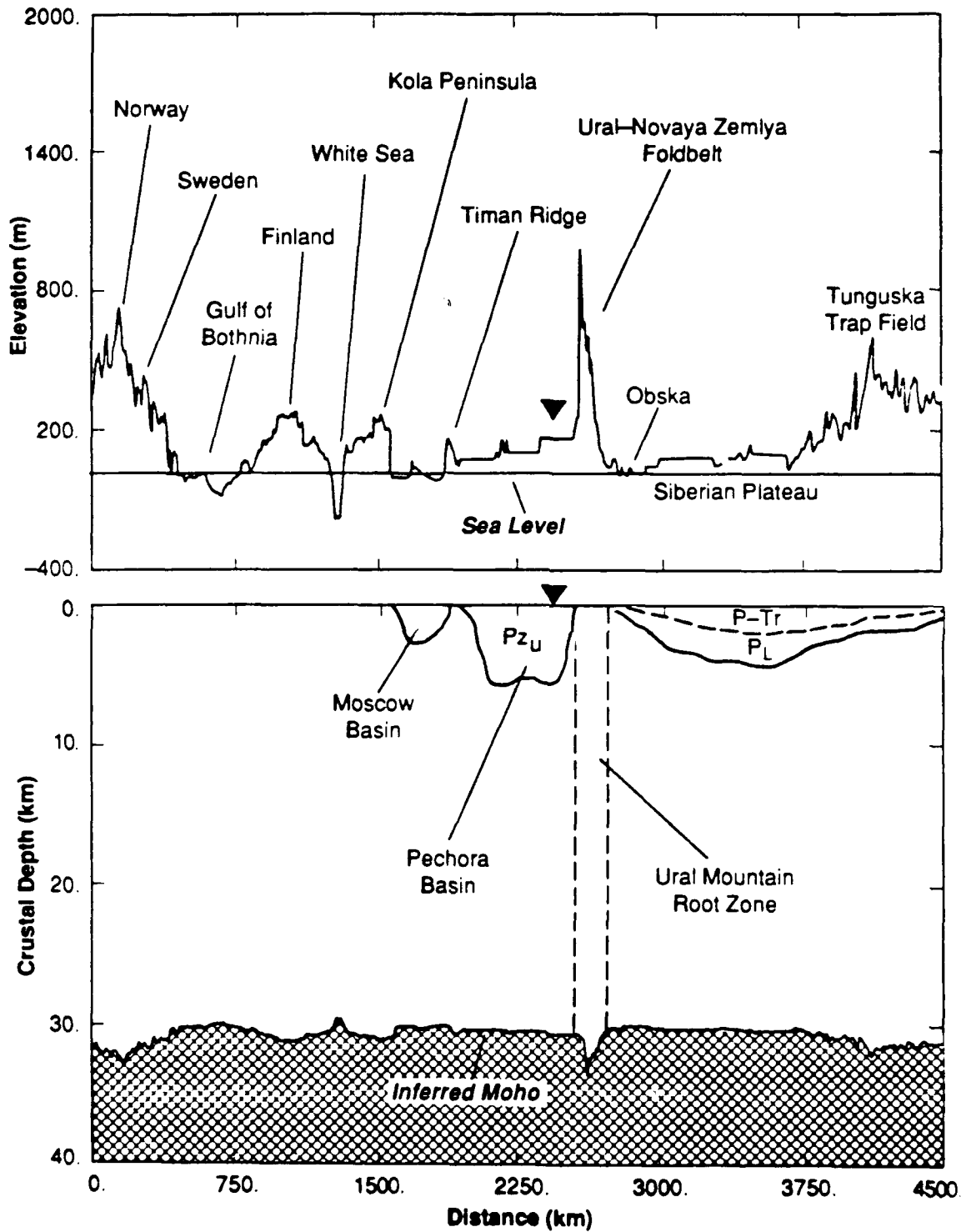
Northern Urals
08/29/74

FIGURE 2-11: Crustal cross-section for the Northern Ural PNEs (NU) which occurred in the Timan-Pechora Synaclese.

80

The crustal cross-section for PNE 13A, which occurred on the Tazovski-Gyda Peninsula, is shown in Figure 2-12. This path passes completely to the north of the Pechora Basin, but passes through the Kara and Barents Sea basins. The details of the sediments beneath these basins were not given in the USGS atlas, but were approximately inferred based on the review of Clarke and Rachlin (1990). Sediment depths as great as 5 km are suggested in these completely enclosed basins, but these are uncertain. Clarke and Rachlin (1990) indicated thicknesses of this order for the eastern part of the Barents Basin, but sediment thickness estimates for the Kara Sea were not available to the study. The path through the Barents Sea is about the same as the Novaya Zemlya-to-Graefenburg path, discussed in the previous section and by Baumgardt (1990). However, the Lg waves appear to be more attenuated for this path than for the Novaya Zemlya-to-Graefenburg path, possibly because the Gyda-to-NORSAR path passes through both the Kara and Barents Basins. However, this interpretation must be considered tentative until more detailed sediment-thickness information, particularly about the Kara Sea, can be obtained.

Comparison of Russian and Siberian Platform (SP-N) Events - The Ural Mountain Effect

Figure 2-13 shows the locations of a group of events around the Ural Mountains, Event 6 in the Pechora Basin, discussed above, Event 3A in the Russian Platform and Events 2, 3, and 7, which occurred on the Siberian Platform. These events provide an interesting opportunity to directly examine the effect of Lg propagation across the Ural Mountains. Figure 2-14 compares the events located west of the Ural Mountains with those to the east. For Events 7 and 3, which are well to the other side of the Urals, the Lg amplitudes are reduced well below the Sn levels compared with Event 3A. The Lg of Event 6 may have been partly blocked by the Pechora Basin. Event 2, which occurred west of the Urals, also appears to have a partially blocked Lg. Also, Events 3 and 7 appear to have much enhanced P coda levels compared to the events to the east of the Urals.

Tazovski–Gyda
08/14/74

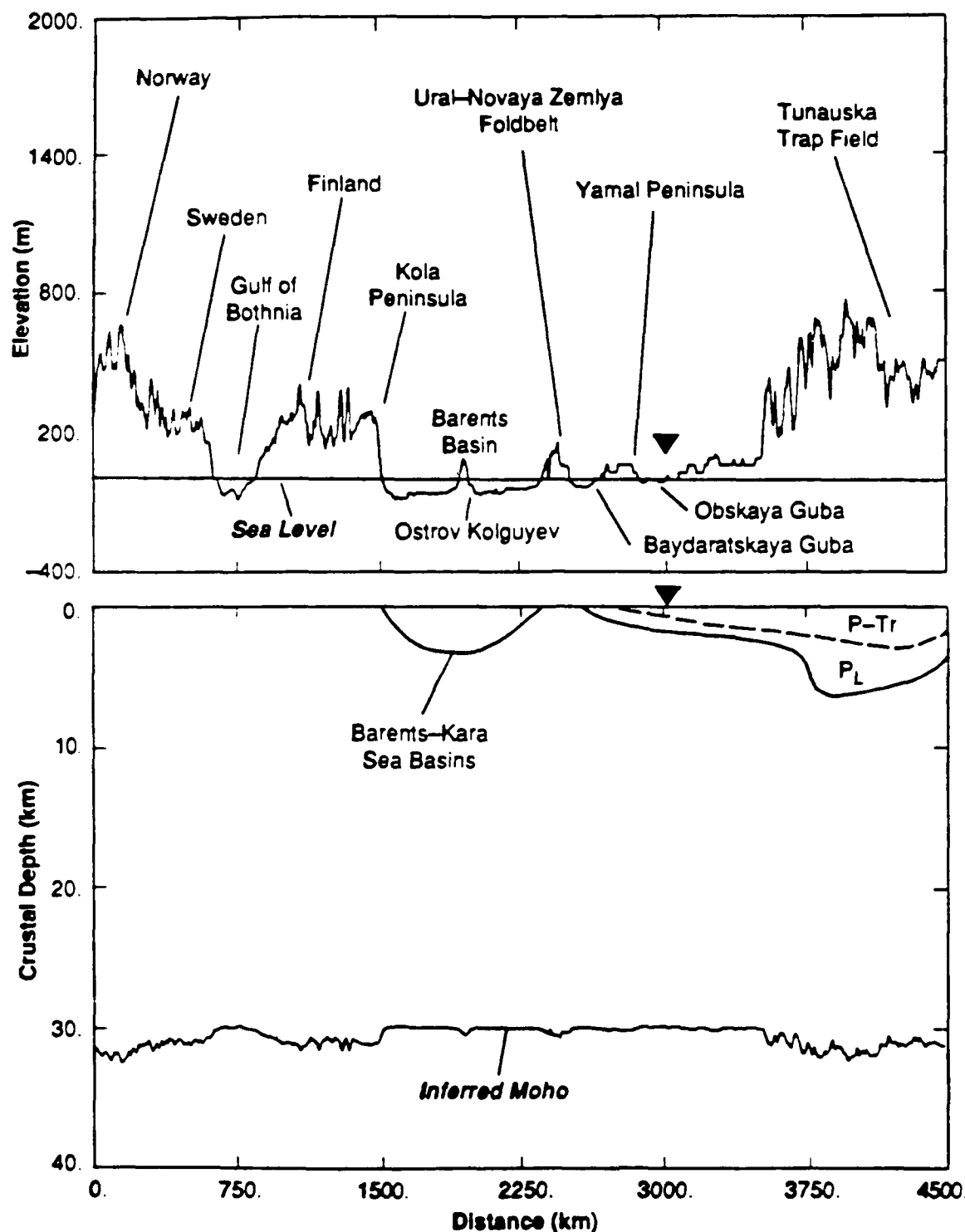FIGURE 2-12: Crustal cross-section for the Tazovski-Gyda region PNE to NORSAR. This path passed north of the Timan-Pechora Synaclese, but passed through the Kara and Barents Sea.
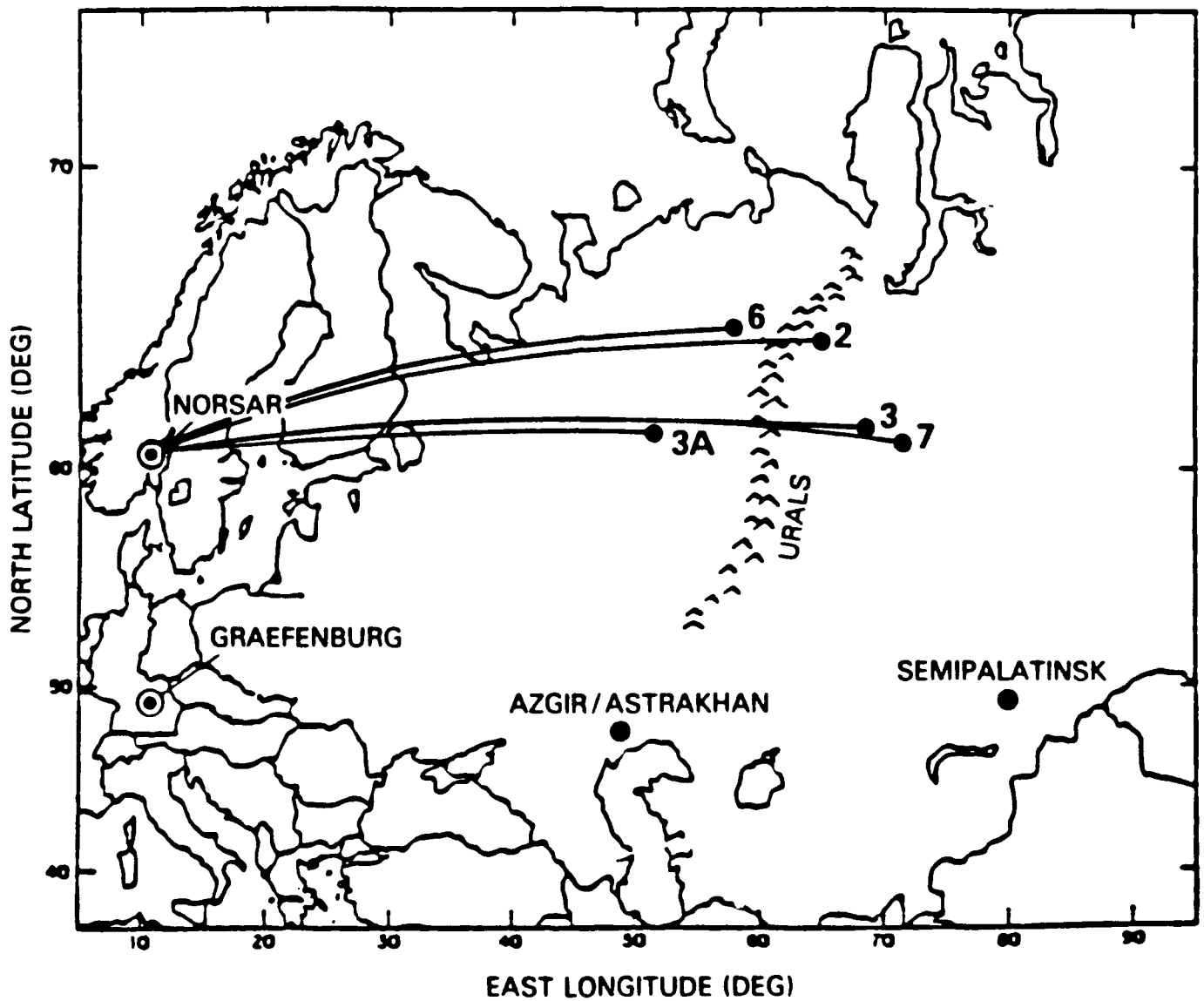
FIGURE 2-13: Propagation paths for five events located near the central part of the Ural Mountains.
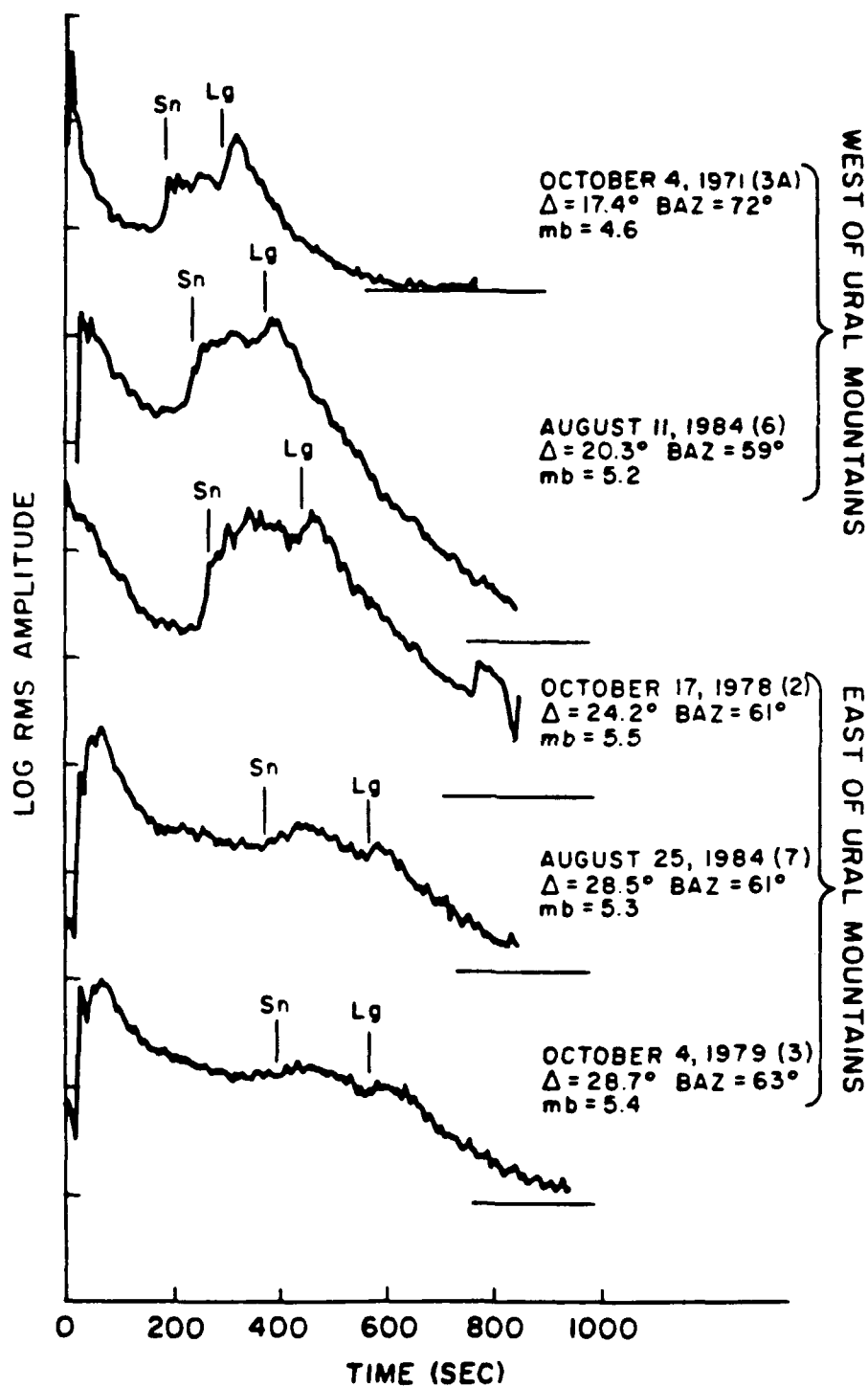
FIGURE 2-14: Record section of the incoherent beams recorded at NORSAR for the five events shown in Figure 2-13.

Figure 2-15 shows the crustal cross-section from Events 7 and 3 to NORSAR. The plot shows that the *Lg* waves from Events 3 and 7 must cross at least three barriers: the Ural Mountains, the Pechora Basin, and the Timan Ridge. The completely enclosed Moscow Basin also lies along the path, but this part of the Basin only contains 2 to 3 km of sediments. These three barriers may be the block to *Lg* from Events 3 and 7.

Why Event 2 has such a strong *Lg*, even though it must pass through the same barriers, is not clear. One possible explanation is that the event may be mislocated and was actually located to the west of the Urals. Its coda shape in Figure 2-14 does have a strong resemblance to that of Event 6, which was located west of the Urals, although it's *P*-to-*Sn* and *Lg* times seems to be greater than that for Event 6, which implies that it occurred at a greater distance. Another possibility is that the *Lg* waves from Events 3 and 7 must also traverse 700 to 800 km the Mesozoic and Cenozoic clastic and carbonate (including coal-bearing) sediments beneath the West Siberian Platform at the flanks of the Urals, which may cause increased attenuation of *Lg*, whereas Event 2 occurred right at the edge of this basin.

Caspian Sea PNEs (ECS-N)

Figure 2-16 shows the great-circle paths for the two events in the Caspian Sea (1A, Astrakhan) and an event located southeast of the Urals (4A). *Lg* has been known for some time to propagate inefficiently across the Caspian Sea region (e.g., Kadinski-Cade et al, 1981; Piwinskii, 1981). The observations from the two Caspian events, 1A and the Astrakhan Event, are in complete agreement with these earlier observations, as shown in Figures 2-17 and 2-18.

85

Siberian Platform
08/25/84
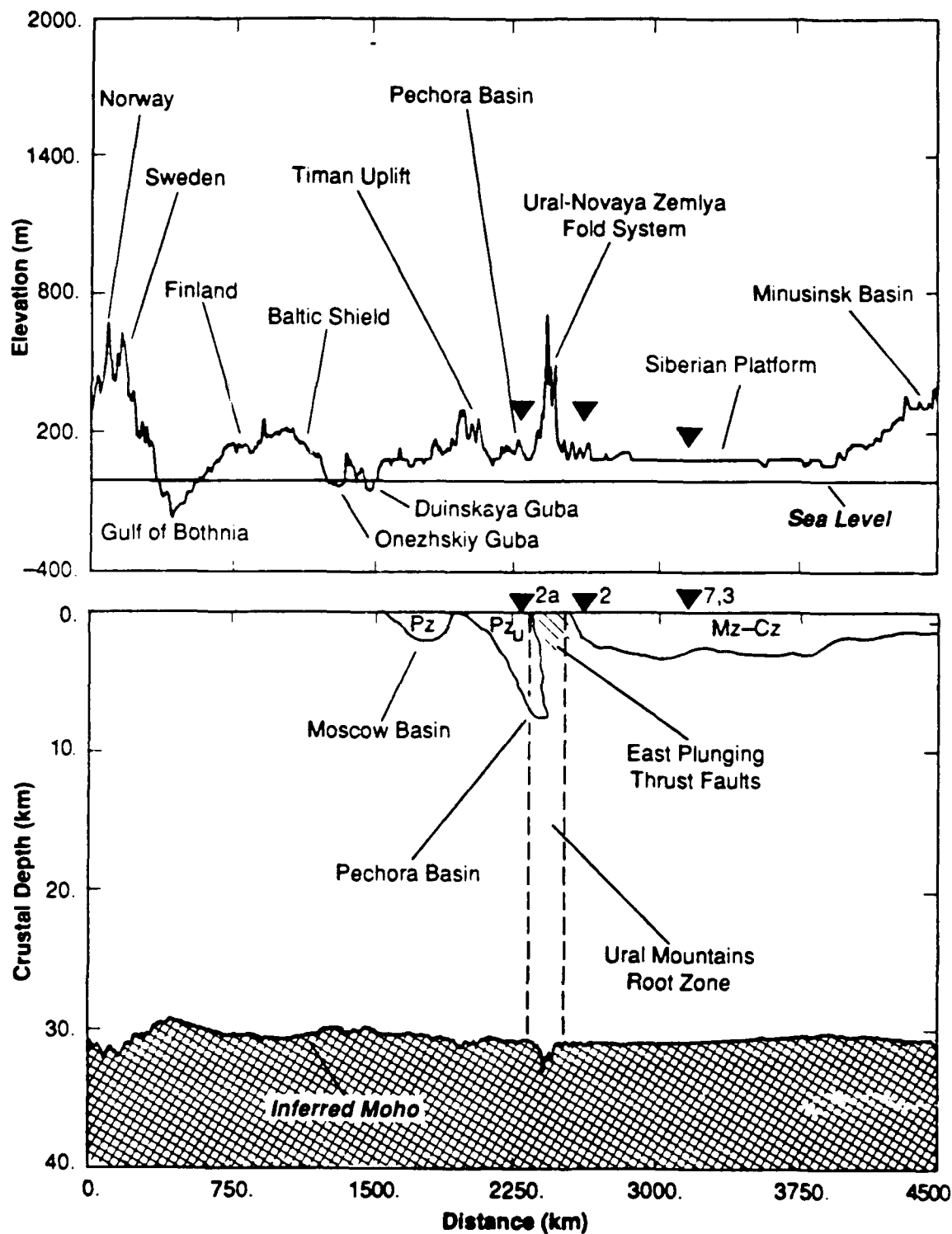
FIGURE 2-15: Crustal cross-section for the events in Figures 2-13 and 2-14. The locations are shown as the triangles.

86
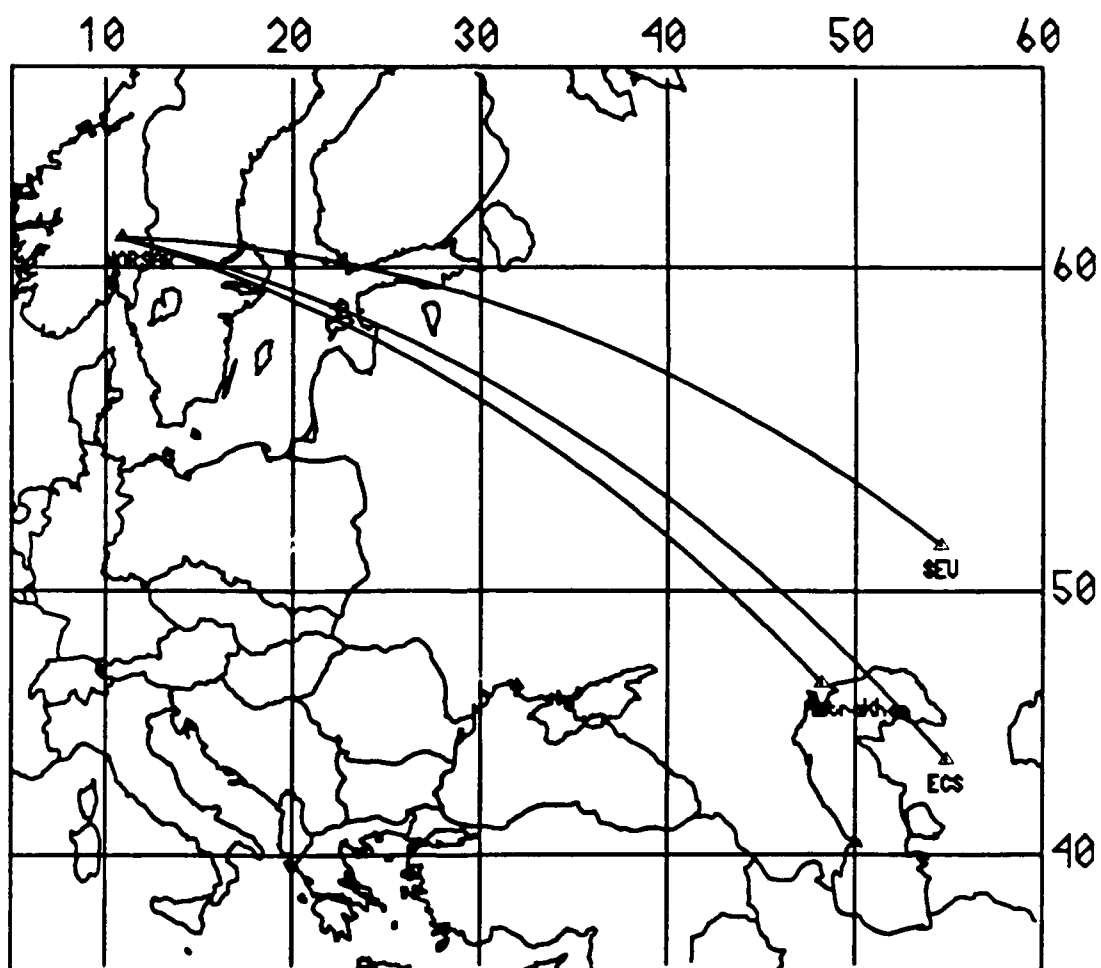
FIGURE 2-16: Propagation paths from two PNEs in the vicinity of the Caspian Sea and in the Southern Urals (SU) to NORSAR.

FIGURE 2-17: Recordings of the PNE located east of the Caspian Sea. (a) Waveforms recorded at the 06C subarray. (b) Incoherent beam.

88

FIGURE 2-18: Comparison of incoherent beams from the Southern Urals and Astrakhan PNEs.

Figure 2-17(a) shows waveforms from the 6C subarray of NORSAR and 2-17(b) shows the incoherent beams, across all subarrays, for the Event 1A. Both plots show that the Lg wave has been virtually blocked, although the Sn-coda waves are strong. As can be seen in Figure 2-16, the Lg propagation path from this event to NORSAR crosses the northern part of the Caspian Sea.
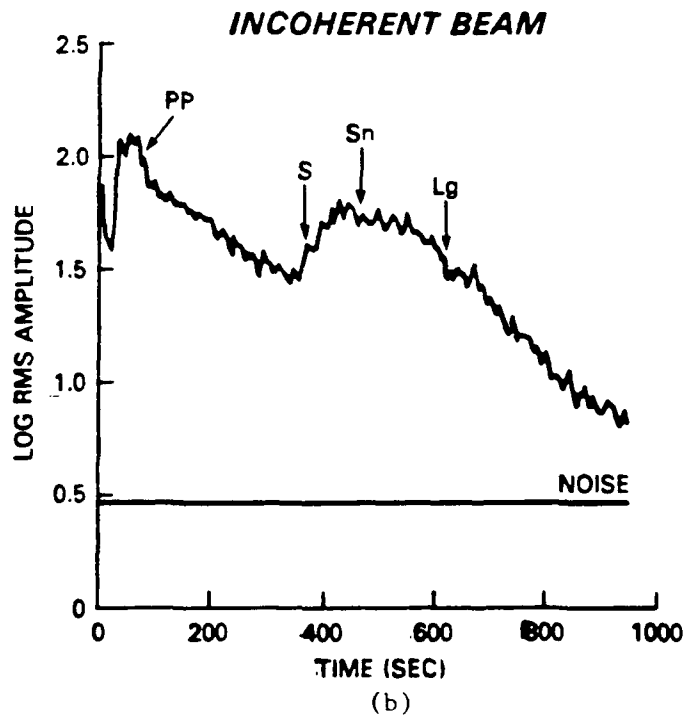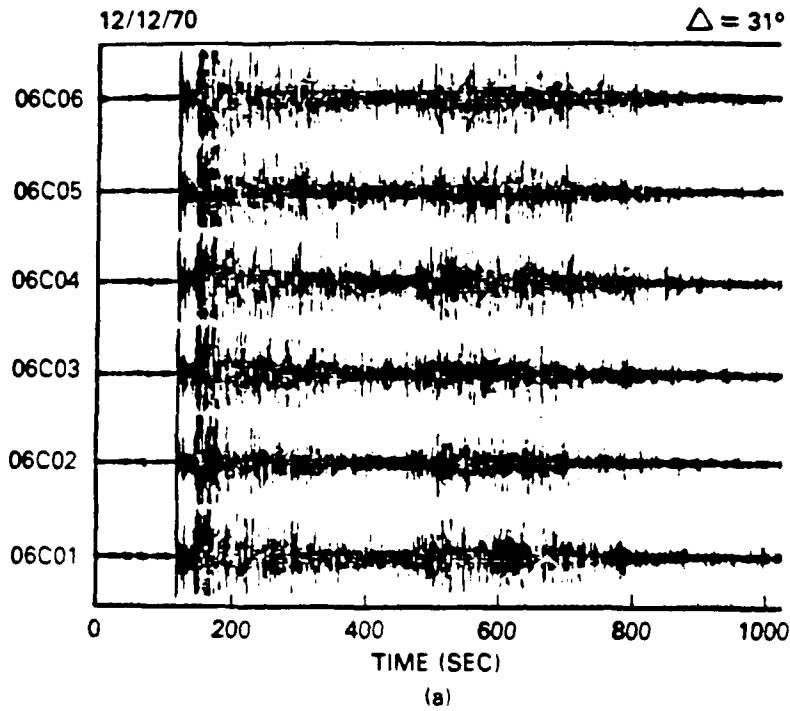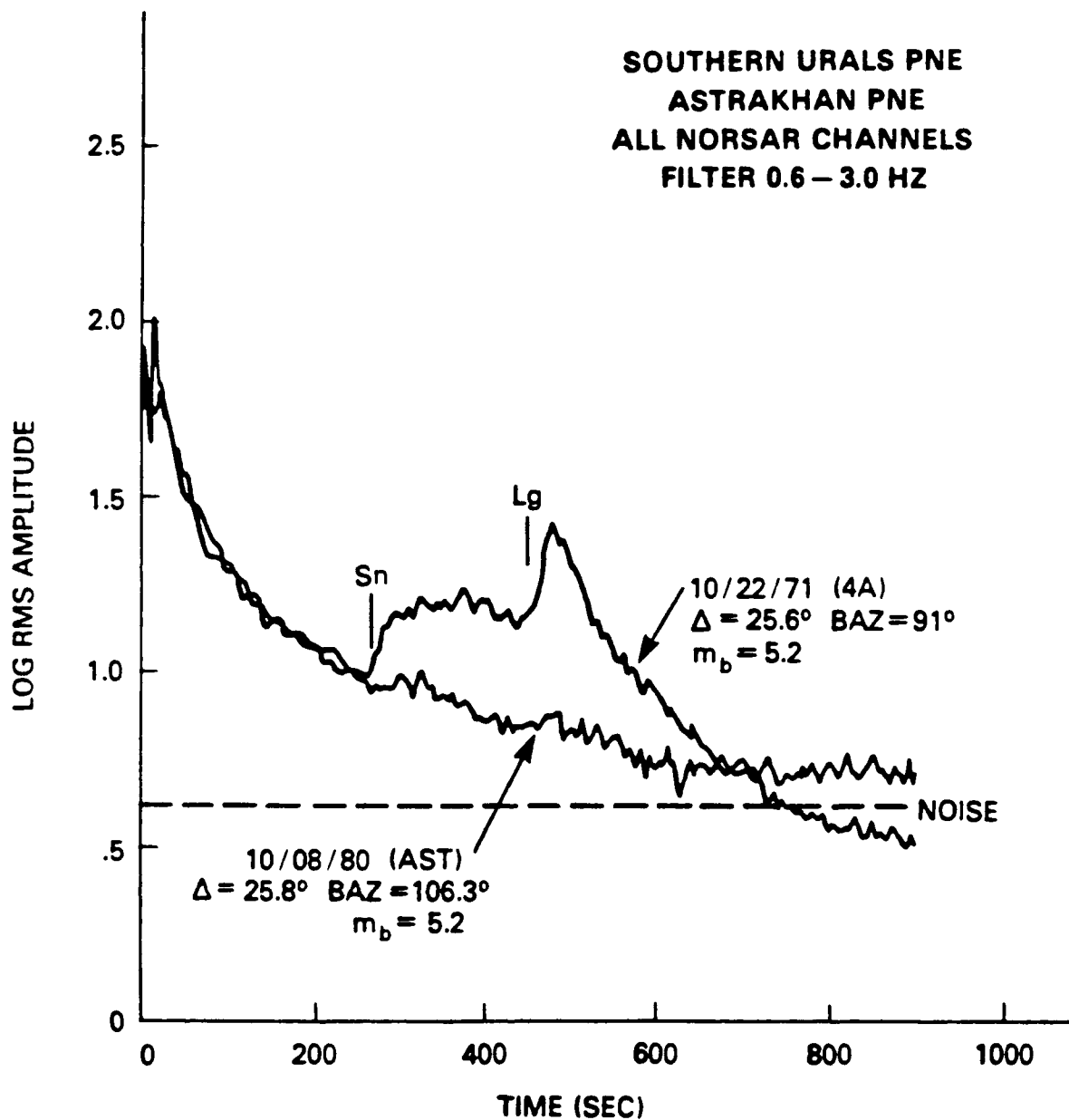
Figure 2-18 compares the incoherent beams of the Astrakhan event with Event 4A, labeled SEU on the map in Figure 2-16, which is located in the southern Urals. Both events have almost the same magnitude and are at the same distance from NORSAR. However, the Southern-Urals event produced a strong Lg, whereas practically no Lg was recorded from the Astrakhan event. The propagation path from the southern Urals region, although the same distance as the Astrakhan path, is well north of the Astrakhan path, as can be seen in Figure 2-16. The two Caspian paths are nearly the same, except for the extra segment across the Caspian Sea for the ECS event. These comparisons suggest that the Lg blockage for the Caspian must lie north and west of the Astrakhan region and is not present in the path from the southern Ural Mountains region to NORSAR.

Figure 2-19 shows the tectonic map of the Caspian region. The map shows (also, see Figure 2-1) that the region northwest of the Caspian includes a large sedimentary basin, called the Pricaspian or North Caspian Depression. Figure 2-20 shows the crustal cross-section from Event 1A, the ECS event, to NORSAR. This Basin is very similar to the Pechora Basin, except the the post-Paleozoic sediments reach extraordinary depths. As shown in Figure 2-20, the USGS maps show depths to the deformed basement of in excess of 15 km. Also, the Basin contains extensive evaporite deposits in the form of salt domes which are exposed at the surface. Figure 2-20 shows that the ECS event happened on the extreme east end of the Basin and thus, Lg would have had to cross this very deep basin before entering the Voronezh Uplift on the Russian Plateau. The Astrakhan event also occurred on the west end of the basin, although north of the Caspian
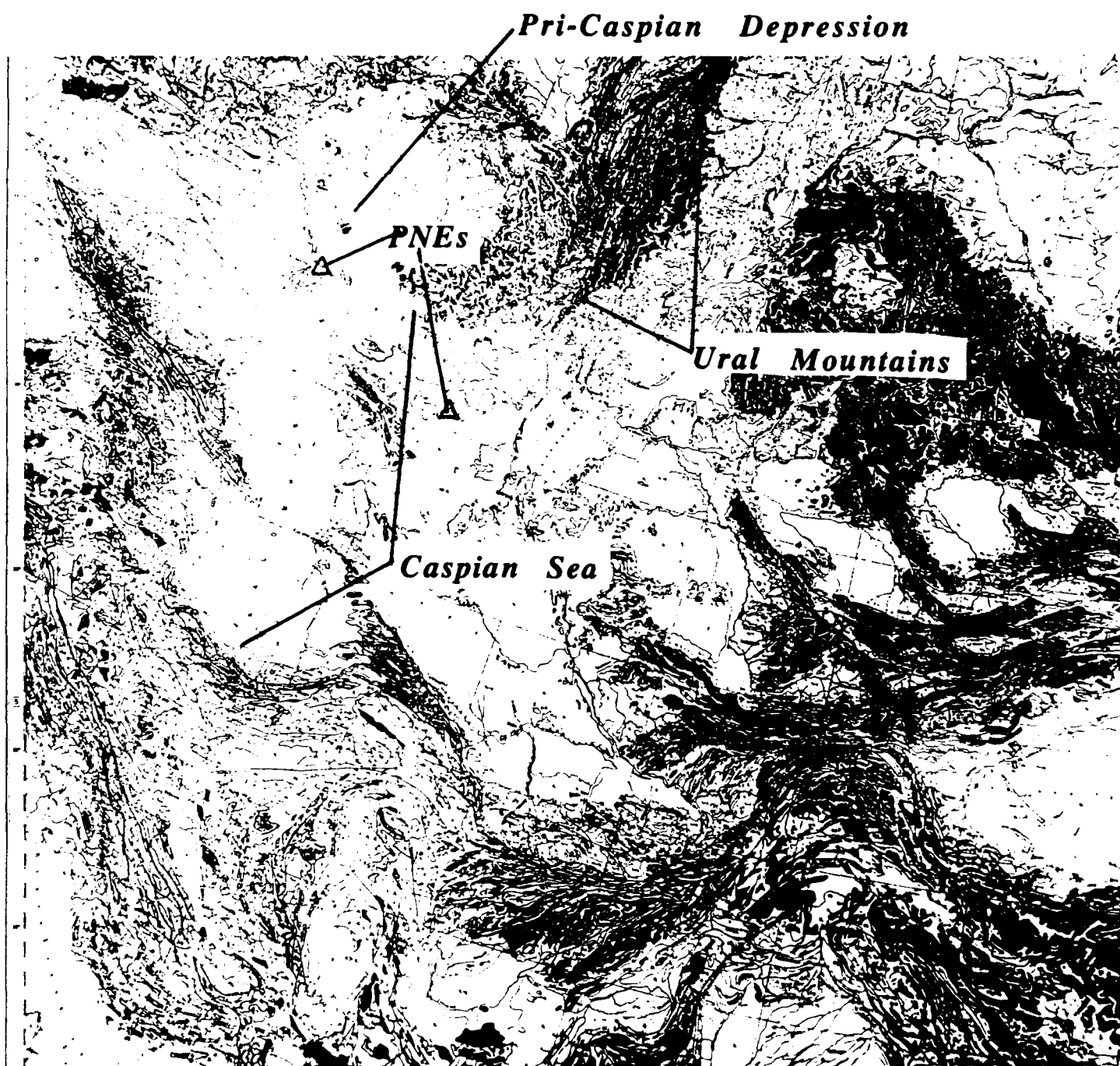
FIGURE 2-19: Geologic map of the Caspian Sea region.
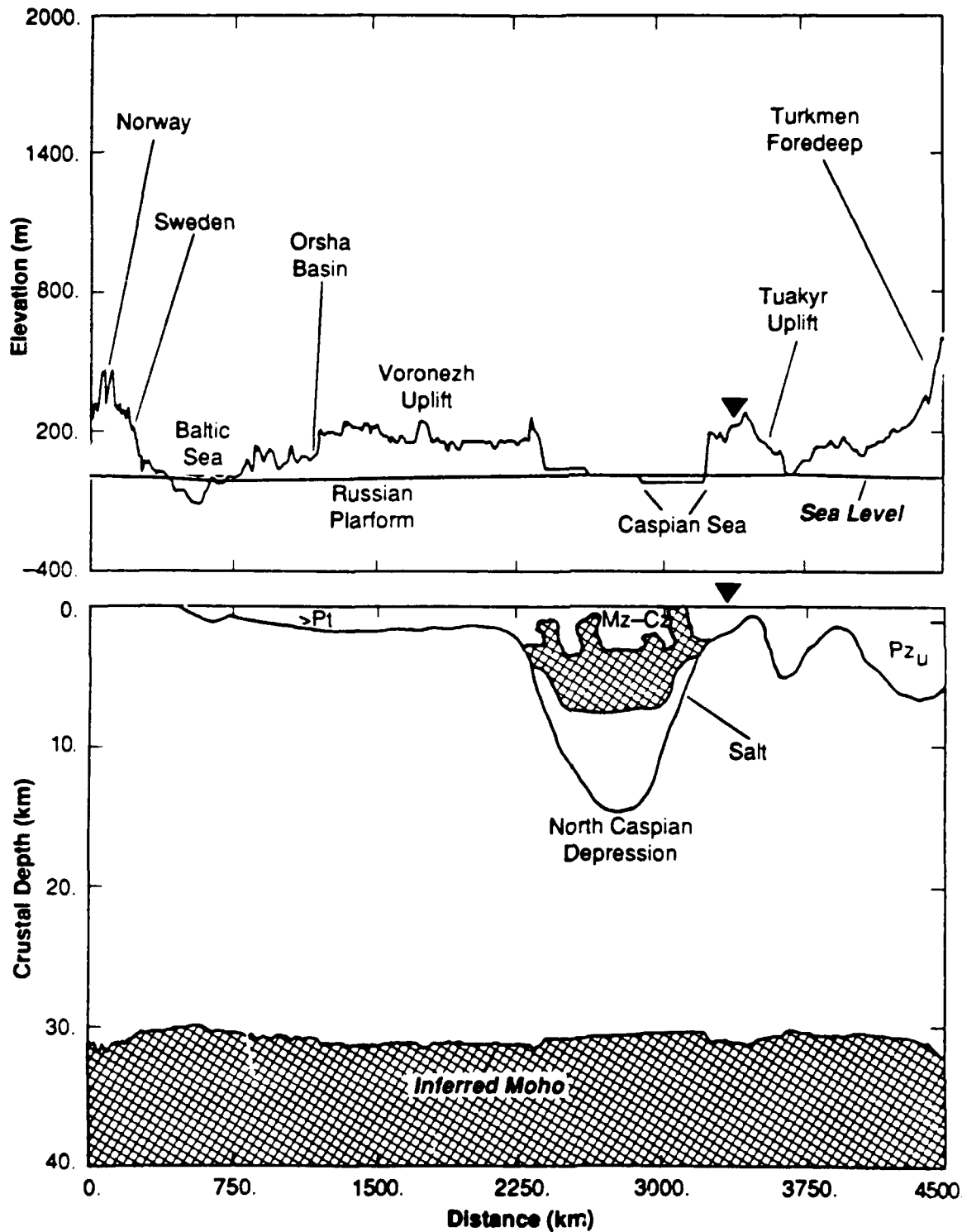
East Caspian Sea
12/23/70

FIGURE 2-20: Crustal cross-section from the Caspian region to NORSAR. Triangle indicates the location of the PNE east of the Caspian. The Astrakhan event occurred on the other side of the Caspian Sea.

Sea, so that its *Lg* propagation path would not have included the water segment. We conclude that it is the North Caspian Depression, not the shallow Caspian Sea itself that blocks the *Lg* propagation across the region.

Figure 2-21 shows the crustal cross-section for the path from the southern Urals region to NORSAR. The southern Urals PNEs also were detonated in a sedimentary basin, called the South Ural Basins, which also contain evaporite deposits. In fact, it is believed that most of the explosions in this basin, as well as those in the Pechora and North Caspian Basins, were probably detonated to generate large cavities in the salt to store natural gas condensate. However, this event occurs in the middle of the basin, as in the case of the South Russian Platform PNE, 5A, which occurred in the middle of the Donbass Basin. In both instances, strong *Lgs*, with amplitudes much greater than the *Sn*, were recorded at NORSAR.

The blockage of *Lg* from the Caspian region can be attributed to the same trapping mechanism that has been proposed for the Barents Basin blockage of *Lg* from the Novaya Zemlya region. The *Lg* waves are composed of shear waves which reverberate in the granitic layer of the crust. When this granitic layer is replaced by a deep, sedimentary basin, containing low-velocity, possibly low-*Q* sediments, the shear waves become trapped in the basin because of the large horizontal impedance contrasts at the edges of the basin. The salt itself may be a factor, since it has *Q* near 70 (Langston, 1983) and compressional seismic velocities near 4.5 km/sec, which are considerably lower than granitic velocities. Another factor is the complexity of the North Caspian Basin itself, where the salt which reaches depths of 8 to 9 km, has several dome structures which extend to the surface, and sediments which extend below the cutoff of the salt. These complexities may cause significant scattering of both *Sn* and *Lg* waves, which result in the blockage of the *Lg* waves and the enhancement of the *P* and *Sn* coda.
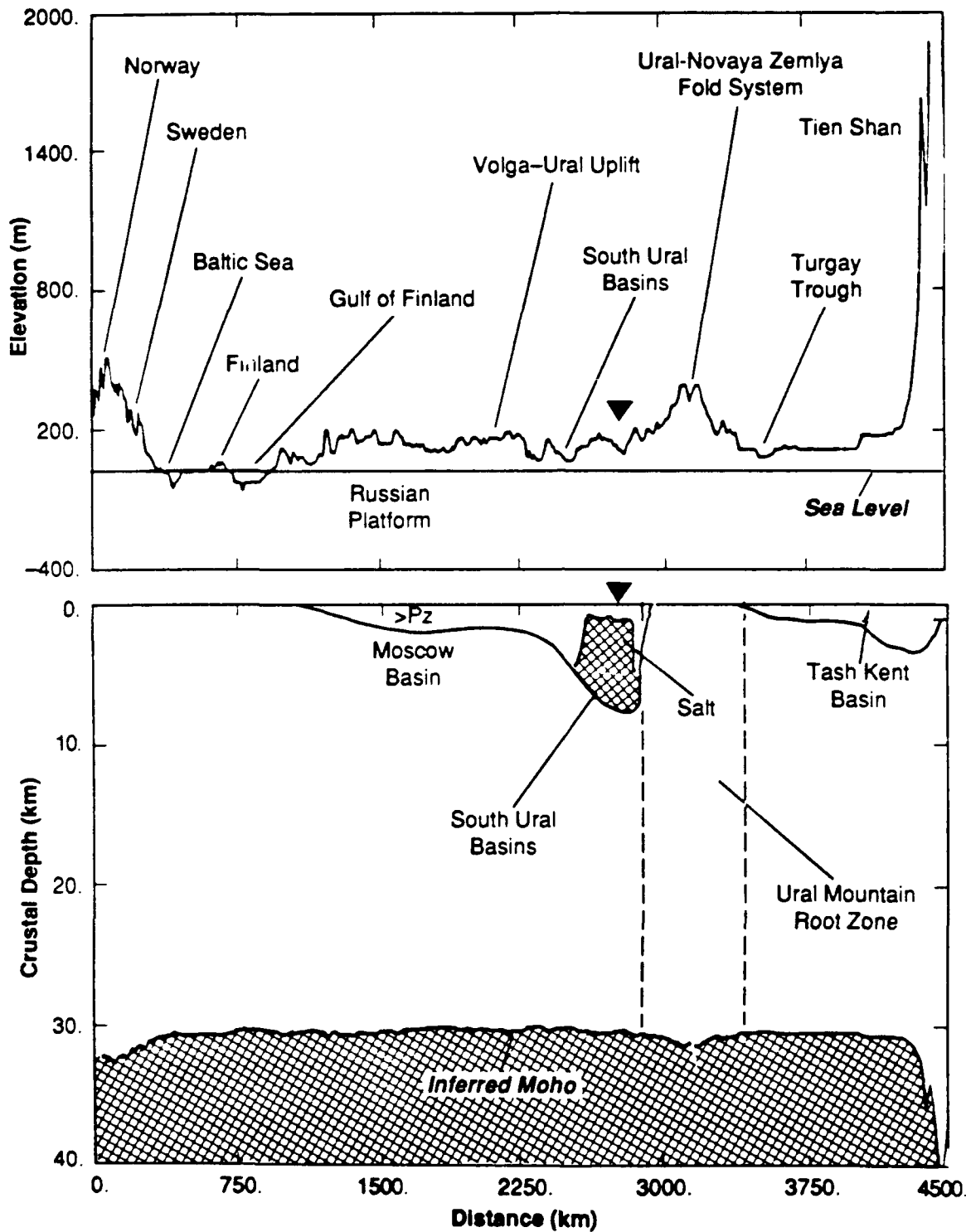
Southern Urals
10/22/71

FIGURE 2-21: Crustal cross-section from the Southern Urals PNE to NORSAR.

One question which arises in this comparison of the southern Urals event with the Caspian events is why the South Ural Basin does not also block *Lg* propagation. The answer may relate to where the event occurs relative to the basin, the depth and width of the basin, how contained the basin is (i.e., how sharply do the sediments cutoff at the edges), and the sharpness of the vertical interface between the basin rocks and the surrounding "granitic layer" rocks. If the event occurs outside the basin and the *Lg* must cross the entire basin, as in the case of the Caspian events, there may be more *Lg* blockage than if the event occurs in the basin itself, as in the case of the SEU PNE in the South Urals Basins and the SRP PNE in the Donbass Basin. In fact, *Lg* may actually be strongly excited if the explosion occurs in the basin itself. The Caspian Basin is considerably larger, both in width and depth, and thus, may be more capable of trapping *Lg* modes, than either the South Urals and Donbass Basins. Also, in the case of the Caspian Basin, there is a sharp topographic interface between the Basin and the adjacent Voronezh Uplift, similar to the Barents Sea - Kola interface, which may significantly backscatter *Lg* waves. This interface could also be a source of *Sn*-to-*Lg* scattering, which may be responsible for the complex *Sn* coda observed from the ECS event. The "bumps" in the *Sn* coda in Figure 2-17 may actually be "early *Lg*" waves produced by this conversion. In the case of the SEU event, the South Ural Basin actually underlies an elevated region, and there is no sharp vertical interface between the Volga-Ural Uplift and the edge of the Basin which could backscatter *Lg*. There is also no such interface in the case of the Russian Platform PNEs.

Lg Waves Which Cross the Urals (WK-N, EK-N, EK-A, SEU-N)

Figure 2-22 shows the locations and *Lg* great-circle propagation paths for a group of explosions which occurred in the vicinity of the Urals and east of the Urals. The *Lg* waves from events east of the Urals crossed some part of the Urals. In the discussion of the Siberian Platform events above, it was suggested that the central part of the Ural mountains blocks and scatters *Lg*
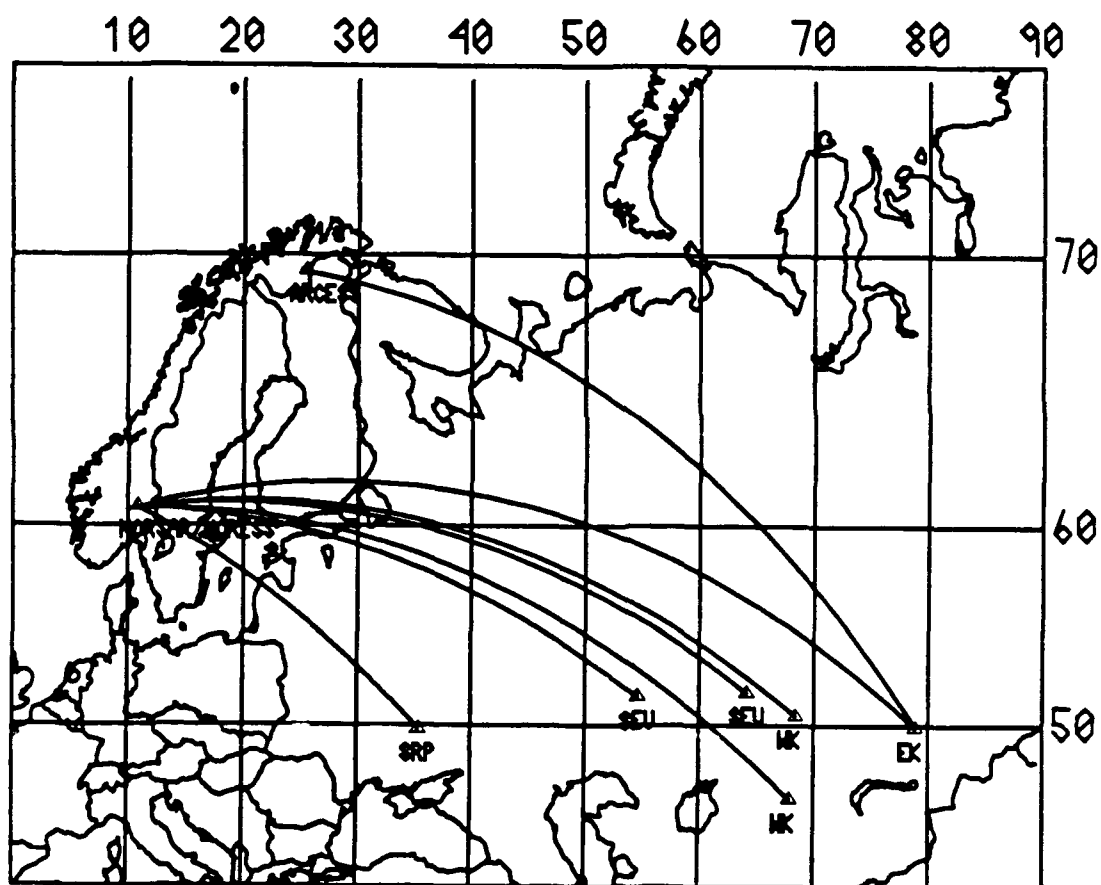
FIGURE 2-22: Propagation paths from the events in the vicinity of the southern Urals to NORSAR, NORESS and ARCESS.

96

waves. The question to be addressed in comparing the events in Figure 2-22 is whether or not the southern Urals block Lg as much as the central and northern Urals.

Figure 2-23 shows the record section for the paths SRP (5A), SU west side of Urals (12A), SEU east side of Urals (8A), WK (10A, 11A) and EK (Shagan River). All the events were recorded at NORSAR, except for the Shagan River explosion recorded at Graefenburg at the bottom of the plot. All these explosions have Lg waves which exceed the Sn levels, although this relative excitation seems to drop somewhat between event 12A and 8A. It appears that the Lg waves from events east of the Urals, which cross the Urals, are somewhat reduced relative to Sn which might suggest a partial blockage in the Urals. Moreover, the P-coda levels ahead of Sn appear to be somewhat higher for events on the west side of the Urals than those on the east side.

Figures 2-24 and 2-25 show the cross-sections for the SEU and WK paths, respectively. Note that the SEU cross-section in Figure 2-24 is very similar to that in Figure 2-21, except that in the former, the event for the path, which is PNE 8A, occurred on the east side of the Urals as opposed to Event 4A, which occurred on the west side in Figure 2-21.

These cross-sections show that the Lg waves from these events encounter a topographic discontinuity in the form of the Ural Foldbelt at the edge of the South Ural Basins. Sediment thicknesses in these basins can reach 8 to 9 km. The Lg waves from these events do not appear to be strongly reduced, which may relate to the small width of this basin compared to that of other basins we have studied which strongly block Lg, such as the South Barents Basin and the North Caspian Basin.

It should also be noted that although the Urals is considered to be a Phanerozoic foldbelt, Figures 2-24 and 2-25 show that it does not appear to have a deep root based on the isostatic compensation model. This is consistent with Soviet deep seismic sounding profiles across the
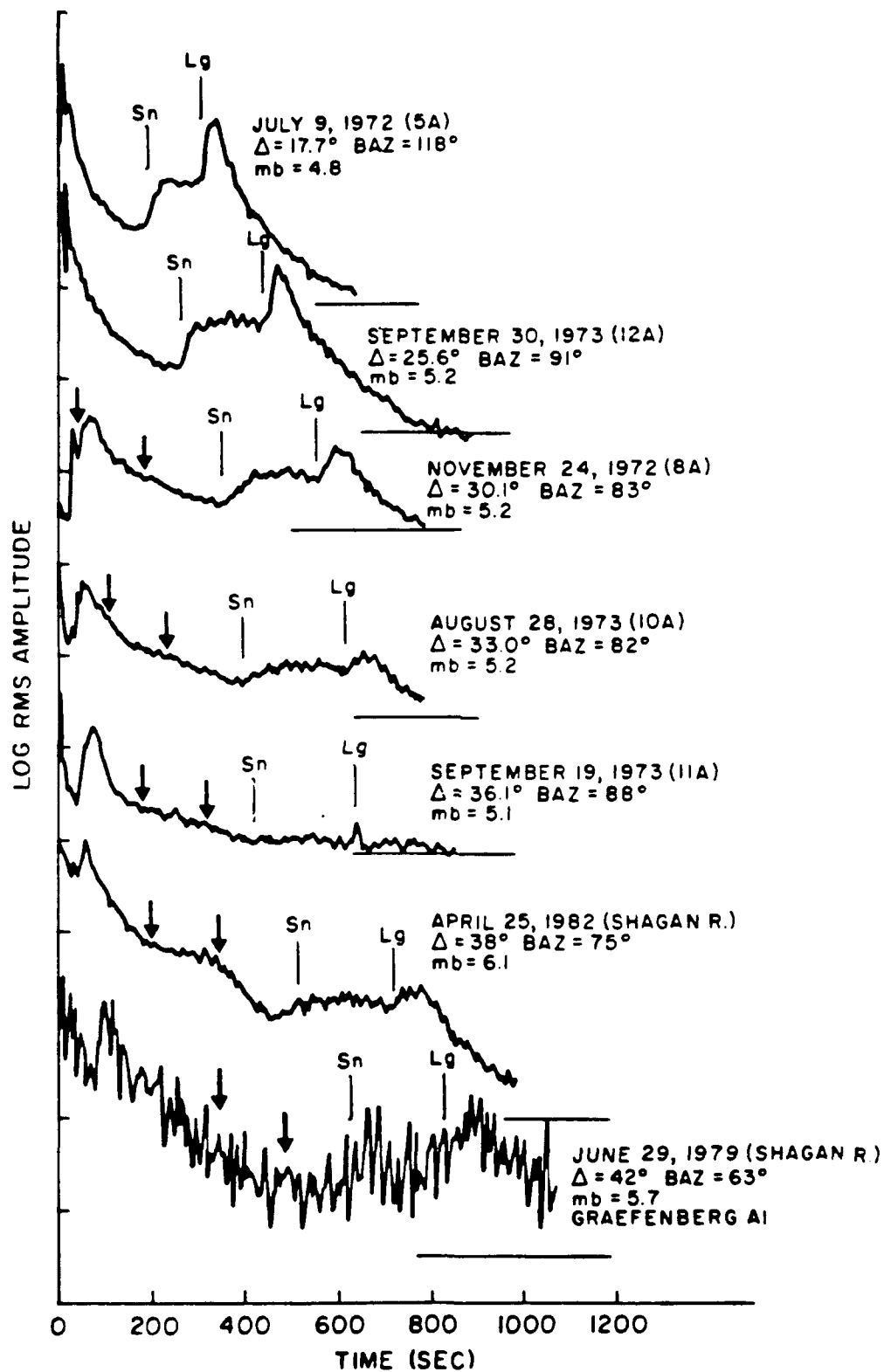
FIGURE 2-23: Record section of incoherent beams from events in the Southern Urals to NORSAR.

South East of Southern Urals
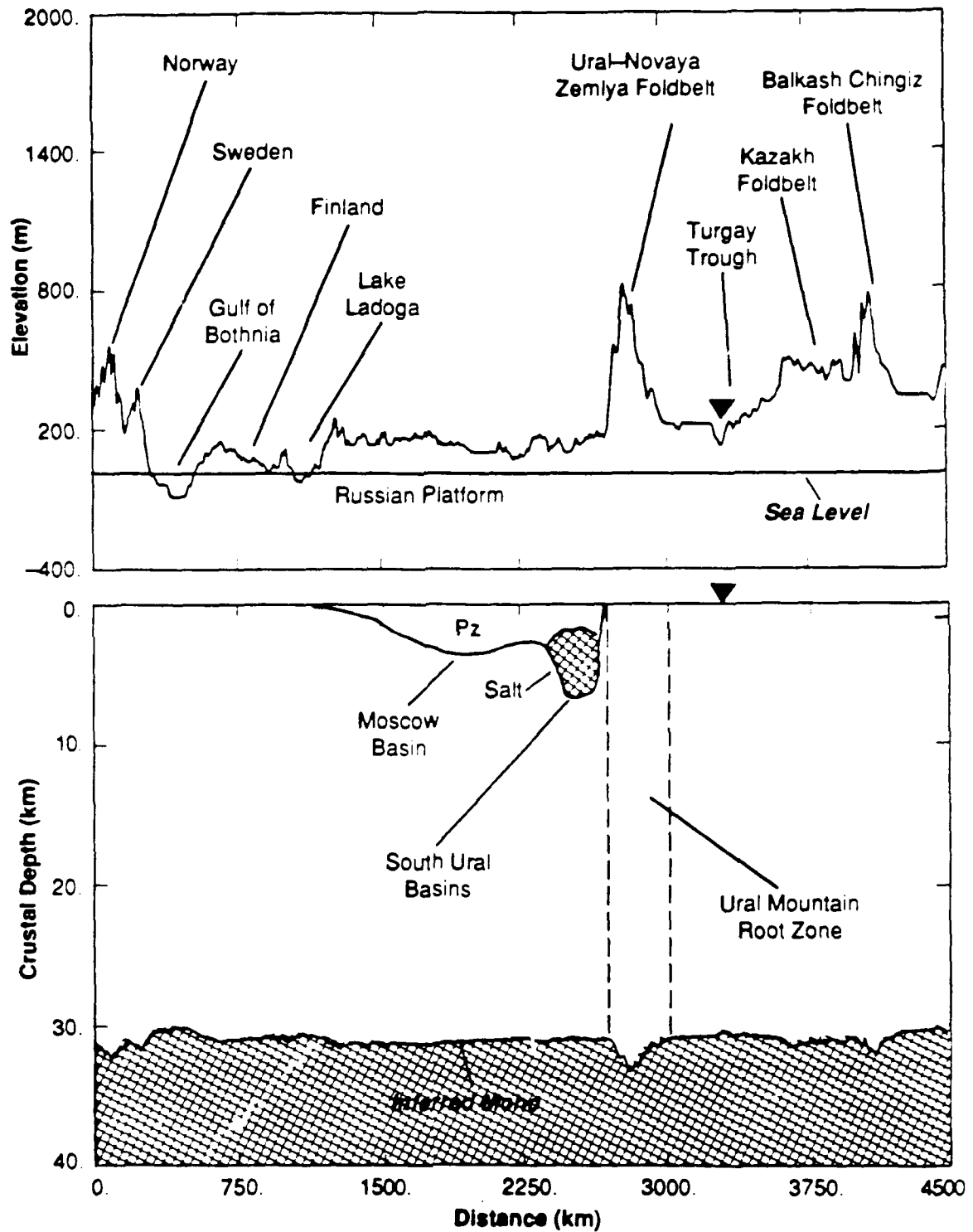## 11/24/72

FIGURE 2-24: Crustal cross-section from the region southeast of the Urals (SEU) to NORSAR.

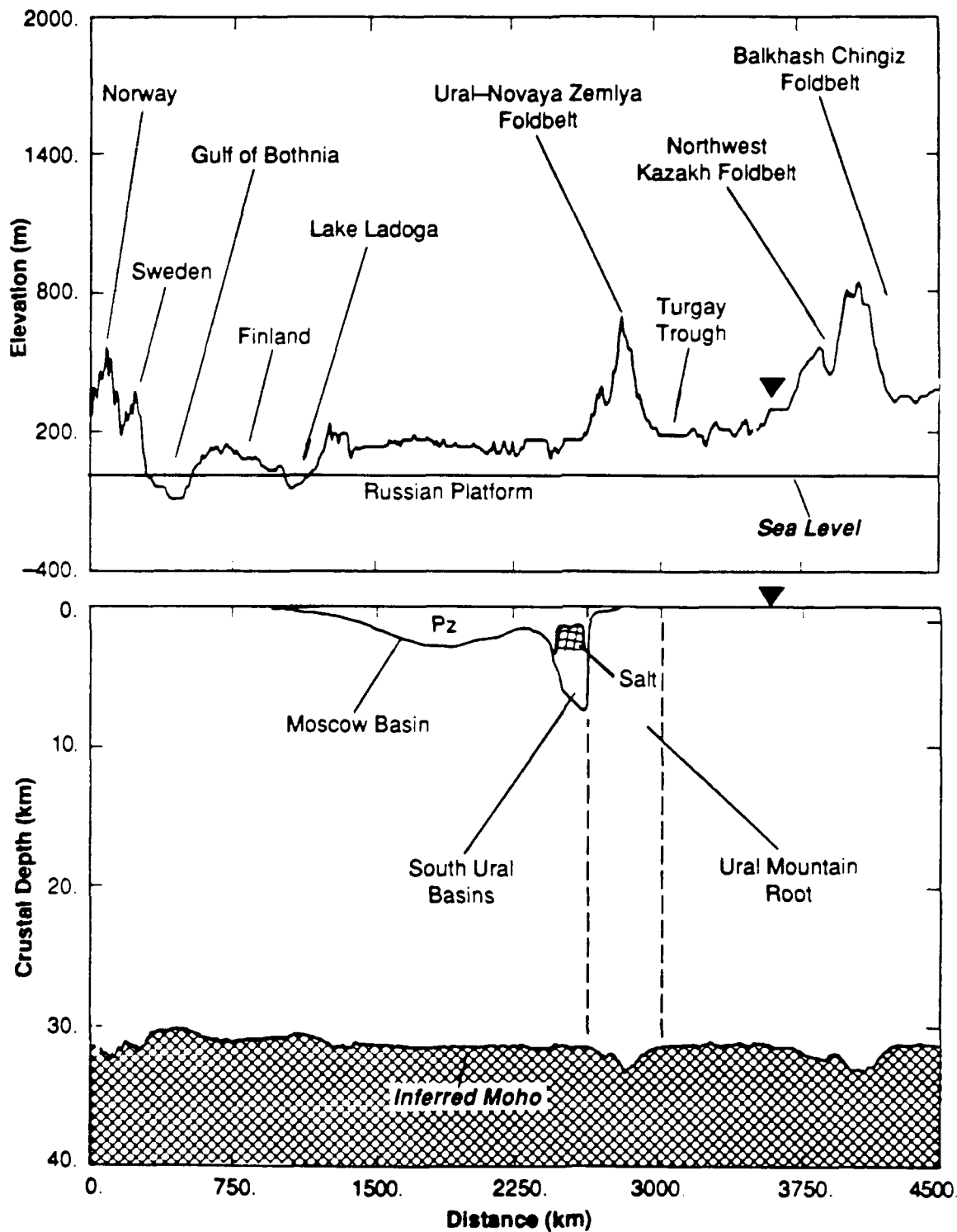# West of Semipalatinsk
08/28/73

FIGURE 2-25: Crustal cross-section from the region west of Semipalatinsk (WS) to NORSAR.

structure (Pinwinskii, 1981) which have not revealed significant increase in crustal thickness associated with the Urals.

The incoherent beams for several NORSAR codas recorded for events near the Soviet test site at Semipalatinsk, after Baumgardt (1985), are shown in Figure 2-26. As shown, the variations in amplitude for these events is very distinctive, which may be caused by different kinds of scattering. Baumgardt (1985) has suggested that the first flat part of the coda may be caused by Lg waves forward scattering into P waves in the vicinity of the Ural Mountains. Baumgardt (1990) has applied FK analysis at NORESS to this part of the coda and measured phase velocities consistent with Pn type modes. However, significant Lg velocities were also measured for this part of the coda, which might have been caused by Pn-to-Lg scattering in the same region. The emergent onset of Sn and hump in the Sn coda is interpreted to be interconversions between Sn and Lg at the Urals and elsewhere along the propagation path.

Figure 2-27 shows a comparison of a NORESS and ARCESS incoherent beams, for an event at Semipalatinsk, first shown by Baumgardt (1990). This comparison shows that both Sn and Lg have very weak onsets for this event, and that the Lg amplitude at ARCESS is less than the Sn amplitude. The Lg amplitude at NORESS exceeds the Sn amplitude, in spite of the fact that it is 8° farther from the source than ARCESS. Thus, the Lg from Semipalatinsk to ARCESS (EK-A) seems to be substantially more blocked than the path from Semipalatinsk to NORESS.

The cross-sections for these two paths are shown in Figures 2-28, for ARCESS (EK-A), and 2-29 for NORESS (EK-N). Comparison of these two paths shows interesting similarities and differences. The paths are similar in that they both cross the Ural Foldbelt and sedimentary basins on the flanks of the Urals. The main difference in the paths, aside from the difference in distance, is the dimensions of the lateral heterogeneities along these paths. First, the elevation of the Ural Foldbelt along the path to ARCESS is around 700 m, almost twice the elevation along the path to
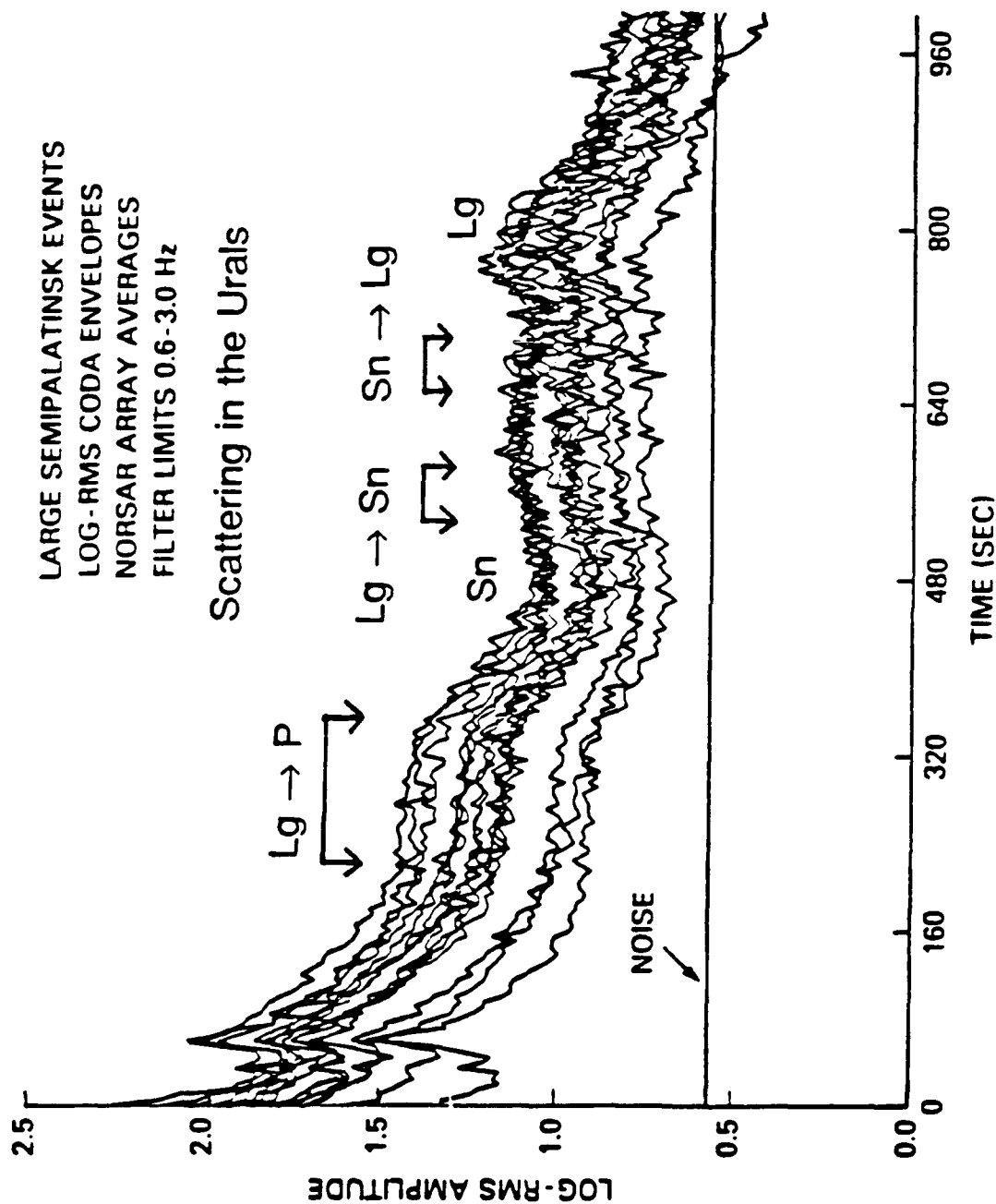
FIGURE 2-26: Incoherent beams of Semipalatinsk event recorded at NORSAR, showing expected arrival times of scattered waves in the vicinity of the Urals (after Baumgardt, 1985a).

Central Kazakh
Incoherent Beams
Filter 0.5-2.5 Hz
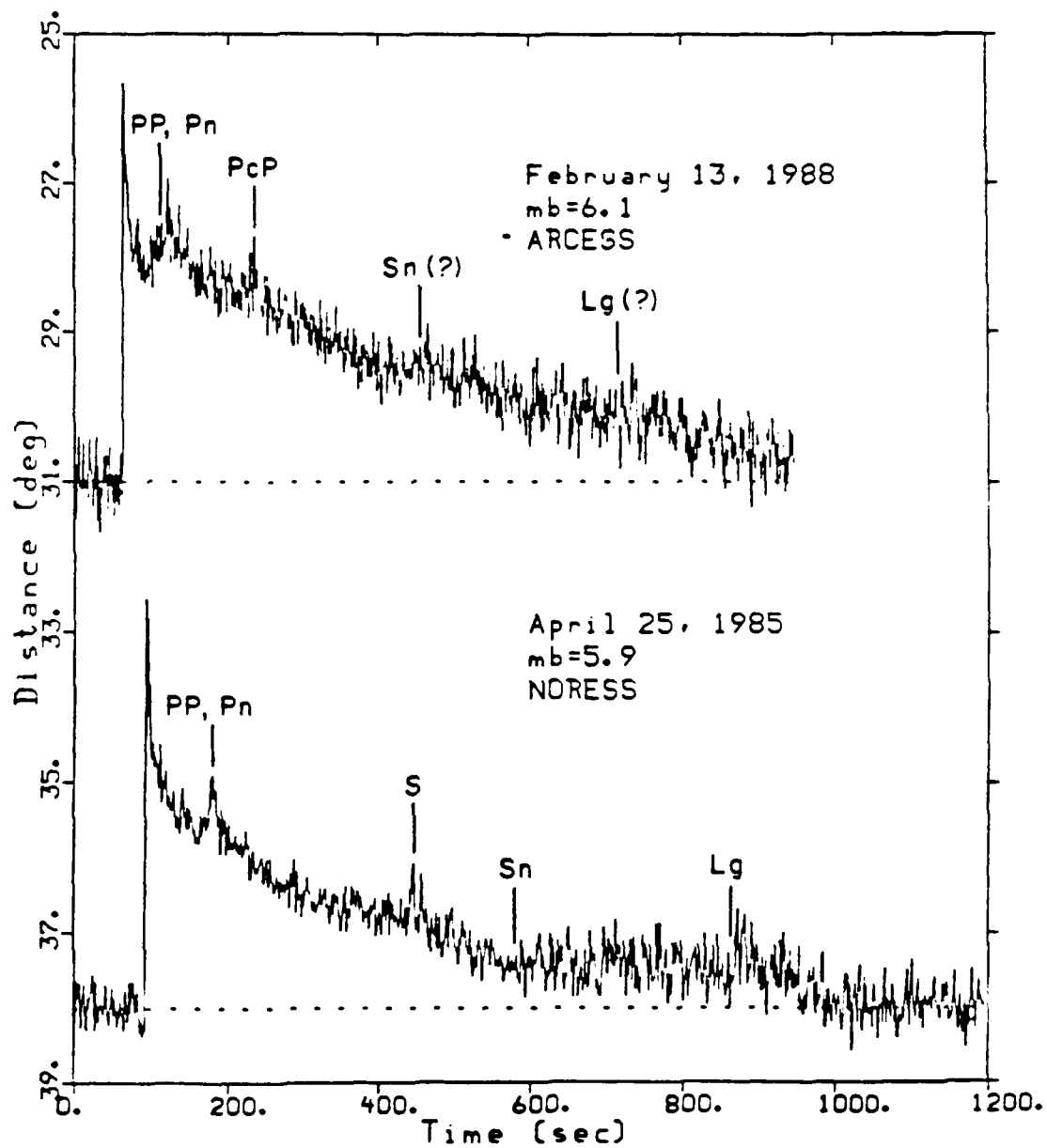
FIGURE 2-27: Record section of incoherent beams of Semipalatinsk events recorded at ARCESS and NORESS.

103

Degelen–Shagan Region
ARCESS Sensors
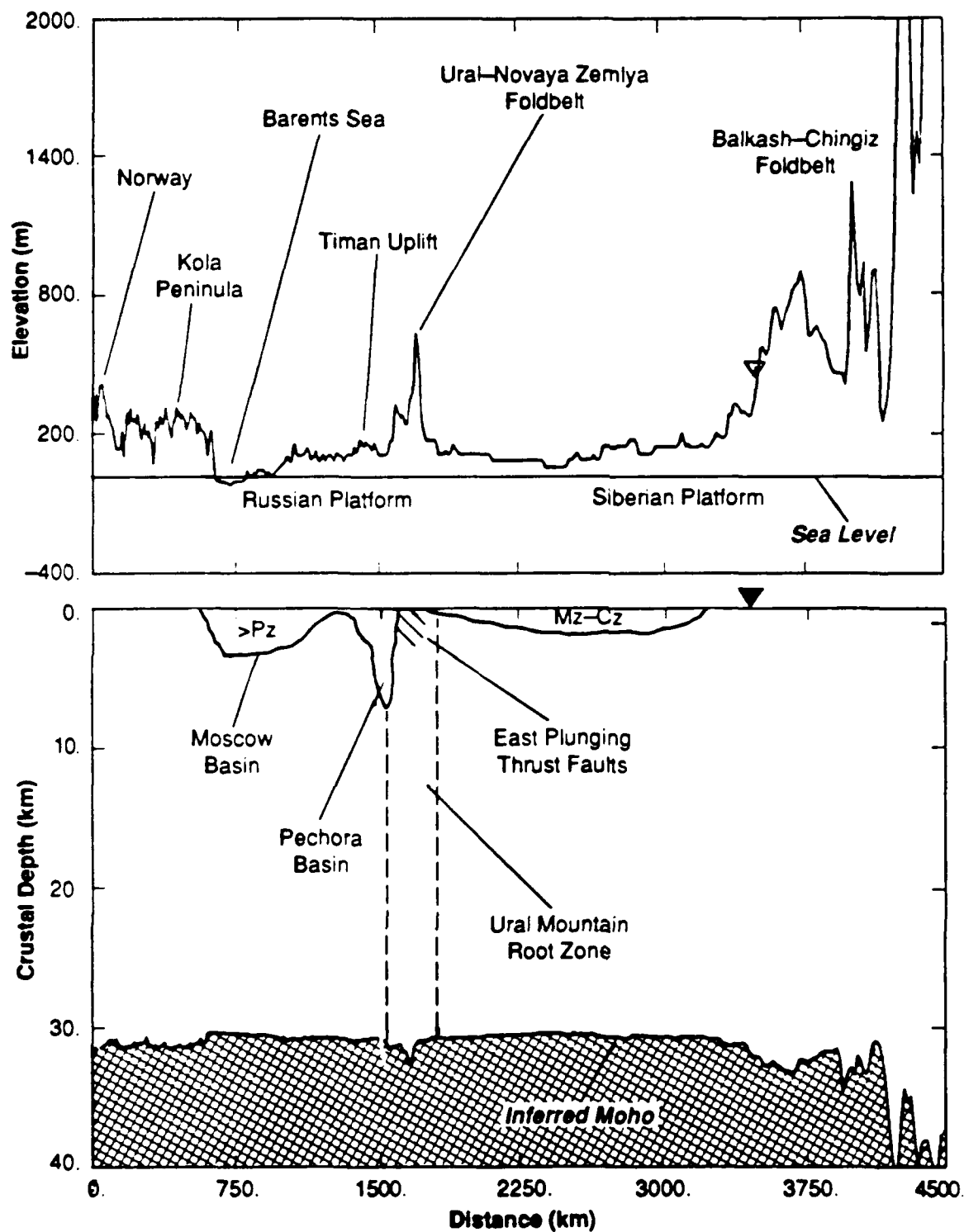
FIGURE 2-28: Crustal cross-section from the Semipalatinsk region to NORESS and NORSAR.

Degelen–Shagan Region
NORSAR/NORESS Sensors
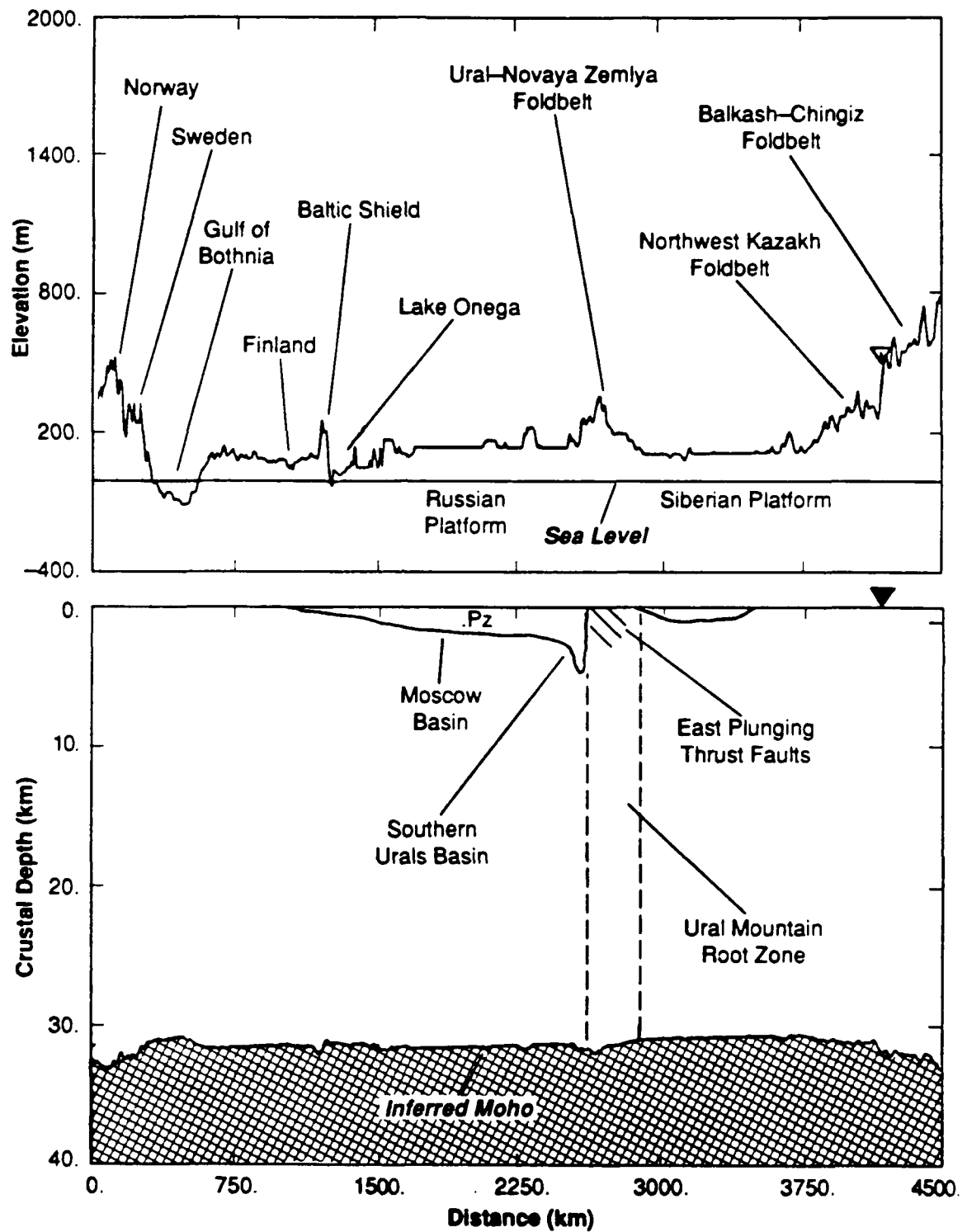
FIGURE 2-29: Crustal cross-section from the Semipalatinsk region to ARCESS.

105

NORESS, where it is about 300 m. Second, the sedimentary basins along the ARCESS path, including the Pechora and Moscow Basins, are deeper than the Urals and Moscow Basins along the NORSAR path. Furthermore, sediments pinch out more sharply in the Pechora and Moscow basins, whereas the sediment thicknesses decrease gradually from the Moscow Basin into the Baltic shield in the case of the path to NORESS. These pinchouts might trap more Lg energy, for the path to ARCESS, compared with the path to NORESS, and the higher elevation of the Urals along the path to ARCESS may scatter more Lg energy into the P coda.

The analysis of these events along with the study of the Siberian Platform events above indicate that the Lg waves which cross the central Urals are more severely blocked than Lg waves which cross the southern parts of the Urals. This result cannot be explained by anelastic attenuation, because Lg clearly decays more rapidly, relative to Sn, across the middle part of the Urals than it does across the southern Urals, even though the distances are shorter in the former case.

2.4   CONCLUSIONS AND RECOMMENDATIONS

This qualitative review of Lg excitation and propagation paths has shown that Lg attenuation, relative to Sn, exhibits significant variation which seems to correlate with the existence of geological heterogeneity along the path. The presence of sedimentary basins along the path, especially when associated with neighboring uplift regions, plays a major role in the blockage of Lg. Basin trapping and scattering from strong vertical inhomogeneities are the proposed mechanisms for Lg blockage and P and Sn coda generation.

The following features seem to be associated with strong *Lg* blockages:

(1)   When the *Lg* must cross a fully contained sedimentary basin, where the sediment thicknesses pinch out to very shallow thicknesses at the edges of the basin.

(2)   When the low-velocity sediment thicknesses replace most of the granitic layer of the crust. Note that this is a variant of the "missing granitic layer" theory for *Lg* blockage, proposed by Piwinskii (1981). However, the missing layer must be contained within a basin where there are significant velocity contrasts between the basin rocks and the rocks surrounding the basin which have granitic velocities. In this setting, the *Lg* waves become trapped in the basin and attenuate as a result of repeated reverberation and scattering in the basin.

(3)   When there are lateral heterogeneities, due to vertical interfaces between uplifted areas and adjacent sedimentary basins. Unusually rough surface topography may also be a source of scattering.

Lg waves are not strongly blocked and propagation is efficient if the following conditions hold:

(1)   There are no sedimentary basins along the path and the granitic layer is relatively stable.

(2)   There are sedimentary basins present with shallow sediments that do not totally replace the granitic layer.

(3)   There are sedimentary basins present, but the sediment velocities are not much different than the granitic velocities.

(4)   Sedimentary basins are present, but they are not contained; i.e., the sediments are not sharply pinched out at the edges. In this study, efficient *Lg* propagation was observed when the basin thins gradually and there are no significant vertical heterogeneities to backscatter *Lg*.

(5)   The event or receiver is actually located in the sedimentary basin, rather than the event occurring outside the basin and its *Lg* waves propagating in and out of the basin. It is well known that surface vibrations are accentuated within the basins themselves, and *Lg* excitation may actually be very strong if the event occurs in the sedimentary basin, or if the receiver is in the sedimentary basin.

The isostatic compensation model for the crustal depth indicates that Moho depths do not vary by more than 5 km in most regions of the Soviet Union which are traversed by these propagation paths. However, significant variations in Lg excitation have been found. Moreover, there is no evidence of any correlation between Moho depth and the nature of Lg excitation. We conclude from this that lower-crustal variations have little effect on Lg excitation, at least in the platform regions of the Soviet craton. This seems logical, since the group velocity of Lg is approximately that of the upper-crustal shear wave velocity and seems to be composed primarily of shear waves reverberating in the upper crust.

An important assumption made in these interpretations is that the source itself has little effect on the excitation of Lg, compared to Sn and coda waves. Since all the events are explosions, there should be no azimuthal or takeoff-angle dependent radiation-pattern effects, like what might be expected for earthquakes. Source effects which could be important include source geology and depth of burial. Regarding source geology, we have pointed out that the explosions which occur within sediments in sedimentary basins may more strongly excite Lg waves than explosions in granite. The depths of burial are unknown for most of the explosions, although some may be estimated based on the presumed purpose of the explosion. For example, explosions in salt probably vere detonated at shallow depths in the salt. Although the effect of depth on absolute Lg excitation has been investigated (Liwall, 1988; Frankel, 1989), the depth dependence of the relative excitation of Sn and Lg has not been studied. Given the modal character of both Sn and Lg, both phases probably have the same depth dependence. Overall, we expect that propagation effects, including those due to near-source geology, will have far greater effect on Lg excitation than source effects.

This study suggests that knowledge of the propagation-path geology can be useful for predicting the efficiency of Lg propagation from a source to receiver and whether or not Lg amplitudes have been partly reduced by blockage effects. This can be important when using Lg

amplitudes for absolute yield estimation, calibrating *Lg* yield curves, or using *Lg* amplitudes for discrimination.

This study has been very qualitative. Future work should attempt to make more quantitative estimates of the effects of geologic heterogeneity on *Lg* amplitude. Data from more paths, using stations inside the Soviet Union, need to be used which traverse other kinds of structures. An attempt should be made to empirically relate the physical characteristics of sedimentary basins, such as their depth, width, sediment velocities, etc., to the degree of *Lg* amplitude reduction, for a given distance.

Attempts should also be made to model theoretically the kinds of conditions which we have found for real propagation paths. Techniques for modeling *Lg* propagation in laterally heterogeneous media are still very limited, given the constraints of current computational capabilities. However, studies of *Lg* excitation and the propagation path characteristics can be very useful in focusing future modeling efforts.

Finally, this study has shown that more precise geological and geophysical information can be very useful for understanding propagation characteristics of *Lg*. Future research should be directed toward acquiring more of this kind of information. With more in-depth data about the surface elevations, lithologies, and seismic velocities for various propagation paths, it should be possible to calibrate *Lg* amplitude measurements for effects of geologic heterogeneity. At the least, conclusions about event yields and event identification utilizing *Lg* amplitudes should be qualified based on knowledge about geologic blockages.

THIS PAGE INTENTIONALLY LEFT BLANK

Frankel, A. (1989). Effects of source depth and crustal structure n the spectral of regional phases determined from synthetic seismograms. *DARPA/AFTAC Annual Seismic Research Review*, 97-118, Patrick Air Force Base, Florida.

Gramberg, I.S. (1988). *The Barents Shelf Plate* (in Russian), Volume 196, Nedra, Leningrad.

Gupta, I.N., B.W. Barker, J.A. Burnetti, and Z.A. Der (1980). A study of regional phases from earthquakes and explosions in Western Russia. *Bull. Seism. Soc. Am.,* **70**, 851-872.

Hansen, R.A., F. Ringdal, and P.G. Richards (1990). The stability of RMS Lg measurements and their potential for accurate estimation of the yields of Soviet underground nuclear explosions. *Bull. Seism. Soc. Am.,* **80**, 2106-2126.

Harjes, H.P. and D. Seidl (1978). Digital recording and analysis of broadband seismic data at the Graefenberg (GRF) array. J. Geophys. Res., **44**, 511-523.

Isacks, B.L. and C. Stephens (1975). Conversion of Sn to Lg at a continental margin. *Bull. Seism. Soc. Am.,* **65**, 224-235.

Kadinsky-Cade, K., M. Barazangi, J. Oliver, and B. Isacks (1981). Lateral variations of high-frequency seismic wave propagation at regional distances across the Turkish and Iranian Plateaus. *J. Geophys. Res.,* **86**, 9377-9396.

Kennett, B.L.N., S. Gregersen, S. Mykkeltveit, and R. Newmark (1985). Mapping of crustal heterogeneity in the North Sea basin via the propagation of Lg waves. *Geophys. J. R. Astr. Soc.,* **83**, 299-306.

Kennett, B.L.N. (1985). On regional S. *Bull. Seism. Soc. Am.,* **75**, 1077-1086.

Kennett, B.L.N. (1986). *Lg* waves and structural boundaries, *Bull. Seism. Soc. Am.,* **76**, 1133-1142.

Kvaerna, T. and D.J. Doornbos (1986). An integrated approach to slowness analysis with arrays and three-component stations. *NORSAR Scientific Report No. 1-85/86,* Kjeller, Norway.

Kvaerna, T. and S. Mykkeltveit (1985). Propagation characteristics of regional phases recorded at NORSAR. *Semi-Annual Technical Summary*, NORSAR, Kjeller, Norway.

Langston, C.A. (1983). Kinematic analysis of strong motion P and SV waves from the Sterling event. *J. Geophys. Res.,* **88**, 3486-3497.

Lilwall, R.C. (1988). Regional mb: M_S, Lg/Pg amplitude ratios and Lg spectral ratios as criteria for distinguishing between earthquakes and explosions: a theoretical study. *Geophys. J.,* **93**, 137-147.

Masse, R.P. and S.S. Alexander (1974). Compressional velocity distribution beneath Scandinavia and western Russia. *Geophys. J. R. Astr. Soc.,* **39**, 587-602.

Mitchell, B. J. and H.J. Hwang (1987). Effect of low-Q sediments and crustal Q on Lg attenuation in the United States. *Bull. Seism. Soc. Am.,* **77**, 1197.

3.0 REFERENCES

Alverson, D.C., D.P. Cox, A.J. Woloshin, M.J. Terman, and C.C. Woo (1967). *Atlas of Asia and Eastern Europe to support detection of underground nuclear testing, Vol II., Tectonics*, prepared by the Department of the Interior, U.S. Geological Survey, for the Advanced Research Projects Agency.

Barazangi, M.J. (1977). Relative excitation of the seismic shear waves Sn and Lg as a function of source depth and their propagation from Melanesia and Banda arcs to Australia. *Annali di Geofisica,* **30**, 385-407.

Bath, M. (1954). The elastic waves, Lg and Rg, along Euroasiatic paths. *Archiv. for Geofysik,* **2**, 295-342.

Baumgardt, D.R. (1985a). Comparative analysis of teleseismic P coda and Lg waves from underground nuclear explosions in Eurasia. *Bull. Seism. Soc. Am.,* **75**, 1413-1433.

Baumgardt, D.R. (1985b). Scattering attenuation of P and Lg waves and P-coda and Lg yield estimation, DARPA/AFGL Seismic Research Symposium, 6 - 8 May 1985, U.S. Air Force Academy, Colorado Springs, CO.

Baumgardt, D.R. (1987). Spectral determination of regional and teleseismic Lg attenuation and source multiplicity in explosions, DARPA/AFGL Seismic Research Symposium, 15 - 18 June 1987, Harbor House, Nantucket, MA.

Baumgardt, D.R. (1990). Investigation of teleseismic Lg blockage and scattering using the NORESS and ARCESS regional arrays. *Bull. Seism. Soc. Am.,* **80**, 2261-2281.

Bennett, T.J., B.W. Barker, K.L. McLaughlin, J.R. Murphy (1989). Regional discrimination of quarry blasts, earthquakes and underground nuclear explosions. *GL-TR-89-0114*, S-Cubed, La Jolla, CA. ADA223148.

Blandford, R.R.(1974). An automatic event detector at the Tonto Forest seismic observatory. *Geophys.,* **39**, 633-643.

Cerveny, V., I.A. Molotkov, and I. Psencik (1977). *Ray Method in Seismology,* Univerzita Karlova, Praha.

Chan, W.W. and B.J. Mitchell (1985). Surface wave dispersion, crustal structure, and sediment thickness variations across the Barents shelf. *Geophys. J. R. Astr. Soc.,* **80**, 329-344.

Chinn, D.S., B.L. Isacks, and M. Barazangi (1980). High-frequency seismic wave propagation in western South America along the continental margin, in the Nazca plate and across the Altiplano. *Geophys. J. R. Astr. Soc.,* **60**, 209-244.

Clarke, J.W. and J. Rachlin (1990). *Geology of the Barents Sea Structural Basin.* U.S. Geological Survey, Military Geology Project, Open-File Report (submitted), July, 1990.

Ewing, M., W.S. Jardetsky and F. Press (1957). *Elastic Waves in Layered Media.* McGraw-Hill, New York.

Ni, J. and M. Barazangi (1983). High-frequency seismic wave propagation beneath the Indian Shield, Himalayan Arc, Tibetan Plateau and surrounding regions: high uppermost mantle velocities and efficient Sn propagation beneath Tibet. *Geophys. J. R. Astr. Soc.*, **72**, 665-689.

Nuttli, O.W. (1986). Lg magnitudes of selected East Kazakhstan underground explosions. *Bull. Seism. Soc. Am.*, **76**, 1241-1251.

Nuttli, O.W. (1988). Lg magnitudes and yield estimates of Novaya Zemlya nuclear explosions. *Bull. Seism. Soc. Am.*, **78**, 873-884.

Piwinskii, A.J. (1981). Deep structure of the earth's crust and upper mantle in the USSR according to geological, geophysical, and seismological data: Dneiper-Donetsk and PriCaspian depressions. *UCID-19203*, Lawrence Livermore Laboratory, Livermore, CA.

Ringdal, F. (1990). Detection and yield estimation studies. *NORSAR Scientific Report, No. 1-90/91*, 1 April - 30 September 1990, Kjeller, Norway.

Ringdal, F. and B.K. Hokland (1987). Magnitudes of large Semipalatinsk explosions using P coda and Lg measurements at NORSAR. *NORSAR Scientific Report, No. 1-87/88*, Kjeller, Norway.

Ringdal, F. and J. Fyen (1988). Comparative analysis of NORSAR and Graefenburg Lg magnitudes of Shagan River explosions. *NORSAR Scientific Report, No. 1-88/89*, Kjeller, Norway.

Ringdal, F. and P.D. Marshall (1989). Yield determination of Soviet underground nuclear explosions at the Shagan River test site. *NORSAR Scientifc Report, No. 2-88/89*, Kjeller, Norway.

Ruzaikin, A., I. Nersesov, V. Khalturin, and P. Molnar (1977). Propagation of Lg and lateral variations in crustal structure in Asia. *J. Geophys. Res.*, **82**, 307-316.

Shumway, R.H. (1971). On detecting a signal in N stationarily correlated noise series. *Technometrics*, **13**, 499-519.

Watson, J. (1976). Eo-Europa: the evolution of a craton, in *Europe from Crust to Core*, D.V. Ager and M. Brooks (eds.), Wiley, London.

113

Prof. Thomas Ahrens
Seismological Lab, 252-21
Division of Geological & Planetary Sciences
California Institute of Technology
Pasadena, CA 91125

Prof. Charles B. Archambeau
CIRES
University of Colorado
Boulder, CO 80309

Dr. Thomas C. Bache, Jr.
Science Applications Int'l Corp.
10260 Campus Point Drive
San Diego, CA 92121   (2 copies)

Prof. Muawia Barazangi
Institute for the Study of the Continent
Cornell University
Ithaca, NY 14853

Dr. Jeff Barker
Department of Geological Sciences
State University of New York
 at Binghamton
Vestal, NY 13901

Dr. Douglas R. Baumgardt
ENSCO, Inc
5400 Port Royal Road
Springfield, VA 22151-2388

Prof. Jonathan Berger
IGPP, A-025
Scripps Institution of Oceanography
University of California, San Diego
La Jolla, CA 92093

Dr. Gilbert A. Bollinger
Department of Geological Sciences
Virginia Polytechnical Institute
21044 Derring Hall
Blacksburg, VA 24061

Dr. Lawrence J. Burdick
Woodward-Clyde Consultants
566 El Dorado Street
Pasadena, CA 91109-3245

Dr. Jerry Carter
Center for Seismic Studies
1300 North 17th St., Suite 1450
Arlington, VA 22209-2308

Dr. Karl Coyner
New England Research, Inc.
76 Olcott Drive
White River Junction, VT 05001

Prof. Vernon F. Cormier
Department of Geology & Geophysics
U-45, Room 207
The University of Connecticut
Storrs, CT 06268

Professor Anton W. Dainty
Earth Resources Laboratory
Massachusetts Institute of Technology
42 Carleton Street
Cambridge, MA 02142

Prof. Steven Day
Department of Geological Sciences
San Diego State University
San Diego, CA 92182

Dr. Zoltan A. Der
ENSCO, Inc.
5400 Port Royal Road
Springfield, VA 22151-2388

Prof. Lewis M. Duncan
Dept. of Physics & Astronautics
Clemson University
Clemson, SC 29634-1901

Prof. John Ferguson
Center for Lithospheric Studies
The University of Texas at Dallas
P.O. Box 830688
Richardson, TX 75083-0688

Dr. Mark D. Fisk
Mission Research Corporation
735 State Street
P. O. Drawer 719
Santa Barbara, CA 93102

Prof. Stanley Flatte
Applied Sciences Building
University of California
Santa Cruz, CA 95064

Dr. Alexander Florence
SRI International
333 Ravenswood Avenue
Menlo Park, CA 94025-3493

1

Dr. Holy K. Given
IGPP, A-025
Scripps Institute of Oceanography
University of California, San Diego
La Jolla, CA 92093

Prof. Henry L. Gray
Vice Provost and Dean
Department of Statistical Sciences
Southern Methodist University
Dallas, TX 75275

Dr. Indra Gupta
Teledyne Geotech
314 Montgomery Street
Alexandria, VA 22314

Prof. David G. Harkrider
Seismological Laboratory
Division of Geological & Planetary Sciences
California Institute of Technology
Pasadena, CA 91125

Prof. Danny Harvey
CIRES
University of Colorado
Boulder, CO 80309

Prof. Donald V. Helmberger
Seismological Laboratory
Division of Geological & Planetary Sciences
California Institute of Technology
Pasadena, CA 91125

Prof. Eugene Herrin
Institute for the Study of Earth and Man
Geophysical Laboratory
Southern Methodist University
Dallas, TX 75275

Prof. Bryan Isacks
Cornell University
Department of Geological Sciences
SNEE Hall
Ithaca, NY 14850

Dr. Rong-Song Jih
Teledyne Geotech
314 Montgomery Street
Alexandria, VA 22314

Prof. Lane R. Johnson
Seismographic Station
University of California
Berkeley, CA 94720

Dr. Richard LaCoss
MIT-Lincoln Laboratory
M-200B
P. O. Box 73
Lexington, MA 02173-0073   (3 copies)

Prof Fred K. Lamb
University of Illinois at Urbana-Champaign
Department of Physics
1110 West Green Street
Urbana, IL 61801

Prof. Charles A. Langston
Geosciences Department
403 Deike Building
The Pennsylvania State University
University Park, PA 16802

Prof. Thorne Lay
Institute of Tectonics
Earth Science Board
University of California, Santa Cruz
Santa Cruz, CA 95064

Prof. Arthur Lerner-Lam
Lamont Doherty Geological Observatory
of Columbia University
Palisades, NY 10964

Lt. Christopher Lynnes
Teledyne Geotech
314 Montgomery Street
Alexandria, VA 22314

Prof. Peter Malin
Department of Geology
Old Chemistry Bldg.
Duke University
Durham, NC 27706

Dr. Randolph Martin, III
New England Research, Inc.
76 Olcott Drive
White River Junction, VT 05001

Prof. Thomas V. McEvilly
Seismographic Station
University of California
Berkeley, CA 94720

Dr. Keith L. McLaughlin
S-CUBED
A Division of Maxwell Laboratory
P.O. Box 1620
La Jolla, CA 92038-1620

Prof. William Menke
Lamont-Doherty Geological Observatory
of Columbia University
Palisades, NY 10964

Stephen Miller
SRI International
333 Ravenswood Avenue
Box AF 116
Menlo Park, CA 94025-3493

Prof. Bernard Minster
IGPP, A-025
Scripps Institute of Oceanography
University of California, San Diego
La Jolla, CA 92093

Prof. Brian J. Mitchell
Department of Earth & Atmospheric Sciences
St. Louis University
St. Louis, MO 63156

Mr. Jack Murphy
S-CUBED, A Division of Maxwell Laboratory
11800 Sunrise Valley Drive
Suite 1212
Reston, VA 22091 (2 copies)

Prof. John A. Orcutt
IGPP, A-025
Scripps Institute of Oceanography
University of California, San Diego
La Jolla, CA 92093

Prof. Keith Priestley
University of Cambridge
Bullard Labs, Dept. of Earth Sciences
Madingley Rise, Madingley Rd.
Cambridge CB3 OEZ, ENGLAND

Dr. Jay J. Pulli
Radix Systems, Inc.
2 Taft Court, Suite 203
Rockville, MD 20850

Prof. Paul G. Richards
Lamont Doherty Geological Observatory
of Columbia University
Palisades, NY 10964

Dr. Wilmer Rivers
Teledyne Geotech
314 Montgomery Street
Alexandria, VA 22314

Prof. Charles G. Sammis
Center for Earth Sciences
University of Southern California
University Park
Los Angeles, CA 90089-0741

Prof. Christopher H. Scholz
Lamont-Doherty Geological Observatory
of Columbia University
Palisades, NY 10964

Thomas J. Sereno, Jr.
Science Application Int'l Corp.
10260 Campus Point Drive
San Diego, CA 92121

Prof. David G. Simpson
Lamont-Doherty Geological Observatory
of Columbia University
Palisades, NY 10964

Dr. Jeffrey Stevens
S-CUBED
A Division of Maxwell Laboratory
P.O. Box 1620
La Jolla, CA 92038-1620

Prof. Brian Stump
Institute for the Study of Earth & Man
Geophysical Laboratory
Southern Methodist University
Dallas, TX 75275

Prof. Jeremiah Sullivan
University of Illinois at Urbana-Champaign
Department of Physics
1110 West Green Street
Urbana, IL 61801

Prof. Clifford Thurber
University of Wisconsin-Madison
Department of Geology & Geophysics
1215 West Dayton Street
Madison, WS 53706

Prof. M. Nafi Toksoz
Earth Resources Lab
Massachusetts Institute of Technology
42 Carleton Street
Cambridge, MA 02142

Prof. John E. Vidale
University of California at Santa Cruz
Seismological Laboratory
Santa Cruz, CA 95064

3

Prof. Terry C. Wallace
Department of Geosciences
Building #77
University of Arizona
Tucson, AZ 85721

Dr. William Wortman
Mission Research Corporation
8560 Cinderbed Rd.
Suite # 700
Newington, VA 22122

Prof. Francis T. Wu
Department of Geological Sciences
State University of New York
at Binghamton
Vestal, NY 13901

Dr. Monem Abdel-Gawad
Rockwell International Science Center
1049 Camino Dos Rios
Thousand Oaks, CA 91360

Prof. Keiiti Aki
Center for Earth Sciences
University of Southern California
University Park
Los Angeles, CA 90089-0741

Prof. Shelton S. Alexander
Geosciences Department
403 Deike Building
The Pennsylvania State University
University Park, PA 16802

Dr. Kenneth Anderson
BBNSTC
Mail Stop 14/1B
Cambridge, MA 02238

Dr. Ralph Archuleta
Department of Geological Sciences
University of California at Santa Barbara
Santa Barbara, CA 93102

Dr. Susan Beck
Department of Geosciences
Bldg. # 77
University of Arizona
Tucson, AZ 85721

Dr. T.J. Bennett
S-CUBED
A Division of Maxwell Laboratory
11800 Sunrise Valley Drive, Suite 1212
Reston, VA 22091

Mr. William J. Best
907 Westwood Drive
Vienna, VA 22180

Dr. N. Biswas
Geophysical Institute
University of Alaska
Fairbanks, AK 99701

Dr. Stephen Bratt
Center for Seismic Studies
1300 North 17th Street
Suite 1450
Arlington, VA 22209

Michael Browne
Teledyne Geotech
3401 Shiloh Road
Garland, TX 75041

Mr. Roy Burger
1221 Serry Road
Schenectady, NY 12309

Dr. Robert Burridge
Schlumberger-Doll Research Center
Old Quarry Road
Ridgefield, CT 06877

Dr. W. Winston Chan
Teledyne Geotech
314 Montgomery Street
Alexandria, VA 22314-1581

Dr. Theodore Cherry
Science Horizons, Inc.
710 Encinitas Blvd., Suite 200
Encinitas, CA 92024 (2 copies)

Prof. Jon F. Claerbout
Department of Geophysics
Stanford University
Stanford, CA 94305

Prof. Robert W. Clayton
Seismological Laboratory
Division of Geological & Planetary Sciences
California Institute of Technology
Pasadena, CA 91125

Prof. F. A. Dahlen
Geological and Geophysical Sciences
Princeton University
Princeton, NJ 08544-0636

Mr. Charles Doll
Earth Resources Laboratory
Massachusetts Institute of Technology
42 Carleton St.
Cambridge, MA 02142

Prof. Adam Dziewonski
Hoffman Laboratory, Harvard Univ.
Dept. of Earth Atmos. & Planetary Sciences
20 Oxford St
Cambridge, MA 02138

5

Prof. John Ebel
Department of Geology & Geophysics
Boston College
Chestnut Hill, MA 02167

Eric Fielding
SNEE Hall
INSTOC
Cornell University
Ithaca, NY 14853

Dr. John Foley
Phillips Laboratory/LWH
Hanscom AFB, MA 01731-5000

Prof. Donald Forsyth
Department of Geological Sciences
Brown University
Providence, RI 02912

Dr. Cliff Frolich
Institute of Geophysics
8701 North Mopac
Austin, TX 78759

Dr. Anthony Gangi
Texas A&M University
Department of Geophysics
College Station, TX 77843

Dr. Freeman Gilbert
IGPP, A-025
Scripps Institute of Oceanography
University of California
La Jolla, CA 92093

Mr. Edward Giller
Pacific Sierra Research Corp.
1401 Wilson Boulevard
Arlington, VA 22209

Dr. Jeffrey W. Given
SAIC
10260 Campus Point Drive
San Diego, CA 92121

Prof. Stephen Grand
University of Texas at Austin
Department of Geological Sciences
Austin, TX 78713-7909

Prof. Roy Greenfield
Geosciences Department
403 Deike Building
The Pennsylvania State University
University Park, PA 16802

Dan N. Hagedorn
Battelle
Pacific Northwest Laboratories
Battelle Boulevard
Richland, WA 99352

Dr. James Hannon
Lawrence Livermore National Laboratory
P. O. Box 808
Livermore, CA 94550

Prof. Robert B. Herrmann
Dept. of Earth & Atmospheric Sciences
St. Louis University
St. Louis, MO 63156

Ms. Heidi Houston
Seismological Laboratory
University of California
Santa Cruz, CA 95064

Kevin Hutchenson
Department of Earth Sciences
St. Louis University
3507 Laclede
St. Louis, MO 63103

Dr. Hans Israelsson
Center for Seismic Studies
1300 N. 17th Street, Suite 1450
Arlington, VA 22209-2308

Prof. Thomas H. Jordan
Department of Earth, Atmospheric
  and Planetary Sciences
Massachusetts Institute of Technology
Cambridge, MA 02139

Prof. Alan Kafka
Department of Geology & Geophysics
Boston College
Chestnut Hill, MA 02167

Robert C. Kemerait
ENSCO, Inc.
445 Pineda Court
Melbourne, FL 32940

William Kikendall
Teledyne Geotech
3401 Shiloh Road
Garland, TX 75041

Prof. Amos Nur
Department of Geophysics
Stanford University
Stanford, CA 94305

Prof. Leon Knopoff
University of California
Institute of Geophysics & Planetary Physics
Los Angeles, CA 90024

Prof. Jack Oliver
Department of Geology
Cornell University
Ithaca, NY 14850

Prof. John Kuo
Aldridge Laboratory of Applied Geophysics
Columbia University
842 Mudd Bldg.
New York, NY 10027

Dr. Kenneth Olsen
P. O. Box 1273
Linwood, WA 98046-1273

Prof. L. Timothy Long
School of Geophysical Sciences
Georgia Institute of Technology
Atlanta, GA 30332

Prof. Jeffrey Park
Department of Geology and Geophysics
Kline Geology Laboratory
P. O. Box 6666
New Haven, CT 06511-8130

Dr. Gary McCartor
Department of Physics
Southern Methodist University
Dallas, TX 75275

Howard J. Patton
Lawrence Livermore National Laboratory
L-205
P. O. Box 808
Livermore, CA 94550

Prof. Art McGarr
Mail Stop 977
Geological Survey
345 Middlefield Rd.
Menlo Park, CA 94025

Prof. Robert Phinney
Geological & Geophysical Sciences
Princeton University
Princeton, NJ 08544-0636

Dr. George Mellman
Sierra Geophysics
11255 Kirkland Way
Kirkland, WA 98033

Dr. Paul Pomeroy
Rondout Associates
P.O. Box 224
Stone Ridge, NY 12484

Prof. John Nabelek
College of Oceanography
Oregon State University
Corvallis, OR 97331

Dr. Norton Rimer
S-CUBED
A Division of Maxwell Laboratory
P.O. Box 1620
La Jolla, CA 92038-1620

Prof. Geza Nagy
University of California, San Diego
Department of Ames, M.S. B-010
La Jolla, CA 92093

Prof. Larry J. Ruff
Department of Geological Sciences
1006 C.C. Little Building
University of Michigan
Ann Arbor, MI 48109-1063

Dr. Keith K. Nakanishi
Lawrence Livermore National Laboratory
L-205
P. O. Box 808
Livermore, CA 94550

Dr. Richard Sailor
TASC Inc.
55 Walkers Brook Drive
Reading, MA 01867

Dr. Susan Schwartz
Institute of Tectonics
1156 High St.
Santa Cruz, CA 95064

Dr. David Taylor
ENSCO, Inc.
445 Pineda Court
Melbourne, FL 32940

John Sherwin
Teledyne Geotech
3401 Shiloh Road
Garland, TX 75041

Dr. Steven R. Taylor
Lawrence Livermore National Laboratory
L-205
P. O. Box 808
Livermore, CA 94550

Dr. Matthew Sibol
Virginia Tech
Seismological Observatory
4044 Derring Hall
Blacksburg, VA 24061-0420

Professor Ta-Liang Teng
Center for Earth Sciences
University of Southern California
University Park
Los Angeles, CA 90089-0741

Dr. Albert Smith
Lawrence Livermore National Laboratory
L-205
P. O. Box 808
Livermore, CA 94550

Dr. Gregory van der Vink
IRIS, Inc.
1616 North Fort Myer Drive
Suite 1440
Arlington, VA 22209

Prof. Robert Smith
Department of Geophysics
University of Utah
1400 East 2nd South
Salt Lake City, UT 84112

Professor Daniel Walker
University of Hawaii
Institute of Geophysics
Honolulu, HI 96822

Dr. Stewart W. Smith
Geophysics AK-50
University of Washington
Seattle, WA 98195

William R. Walter
Seismological Laboratory
University of Nevada
Reno, NV 89557

Donald L. Springer
Lawrence Livermore National Laboratory
L-205
P. O. Box 808
Livermore, CA 94550

Dr. Raymond Willeman
Phillips Laboratory/LWH
Hanscom AFB, MA 01731-5000

Dr. George Sutton
Rondout Associates
P.O. Box 224
Stone Ridge, NY 12484

Dr. Gregory Wojcik
Weidlinger Associates
4410 El Camino Real
Suite 110
Los Altos, CA 94022

Prof. L. Sykes
Lamont-Doherty Geological Observatory
of Columbia University
Palisades, NY 10964

Dr. Lorraine Wolf
Phillips Laboratory/LWH
Hanscom AFB, MA 01731-5000

Prof. Pradeep Talwani
Department of Geological Sciences
University of South Carolina
Columbia, SC 29208

Dr. Gregory B. Young
ENSCO, Inc.
5400 Port Royal Road
Springfield, VA 22151-2388

Dr. Eileen Vergino
Lawrence Livermore National Laboratory
L-205
P. O. Box 808
Livermore, CA 94550

J. J. Zucca
Lawrence Livermore National Laboratory
P. O. Box 808
Livermore, CA 94550

Dr. Ralph Alewine III
DARPA/NMRO
1400 Wilson Boulevard
Arlington, VA 22209-2308

Dr. Dale Glover
DIA/DT-1B
Washington, DC 20301

Mr. James C. Battis
Phillips Laboratory/LWH
Hanscom AFB, MA 01731-5000

Dr. T. Hanks
USGS
Nat'l Earthquake Research Center
345 Middlefield Road
Menlo Park, CA 94025

Harley Benz
U.S. Geological Survey, MS-977
345 Middlefield Rd.
Menlo Park, CA 94025

Dr. Roger Hansen
AFTAC/TT
Patrick AFB, FL 32925

Dr. Robert Blandford
AFTAC/TT
Center for Seismic Studies
1300 North 17th St. Suite 1450
Arlington, VA 22209-2308

Paul Johnson
ESS-4, Mail Stop J979
Los Alamos National Laboratory
Los Alamos, NM 87545

Eric Chael
Division 9241
Sandia Laboratory
Albuquerque, NM 87185

Janet Johnston
Phillips Laboratory/LWH
Hanscom AFB, MA 01731-5000

Dr. John J. Cipar
Phillips Laboratory/LWH
Hanscom AFB, MA 01731-5000

Dr. Katharine Kadinsky-Cade
Phillips Laboratory/LWH
Hanscom AFB, MA 01731-5000

Cecil Davis
Group P-15, Mail Stop D406
P.O. Box 1663
Los Alamos National Laboratory
Los Alamos, NM 87544

Ms. Ann Kerr
IGPP, A-025
Scripps Institute of Oceanography
University of California, San Diego
La Jolla, CA 92093

Mr. Jeff Duncan
Office of Congressman Markey
2133 Rayburn House Bldg.
Washington, DC 20515

Dr. Max Koontz
US Dept of Energy/DP 5
Forrestal Building
1000 Independence Avenue
Washington, DC 20585

Dr. Jack Evernden
USGS - Earthquake Studies
345 Middlefield Road
Menlo Park, CA 94025

Dr. W.H.K. Lee
Office of Earthquakes, Volcanoes,
& Engineering
345 Middlefield Road
Menlo Park, CA 94025

Art Frankel
USGS
922 National Center
Reston, VA 22092

Dr. William Leith
U.S. Geological Survey
Mail Stop 928
Reston, VA 22092

Dr. Richard Lewis
Director, Earthquake Engineering & Geophysics
U.S. Army Corps of Engineers
Box 631
Vicksburg, MS 39180

James F. Lewkowicz
Phillips Laboratory/LWH
Hanscom AFB, MA 01731-5000

Mr. Alfred Lieberman
ACDA/VI-OA'State Department Bldg
Room 5726
320 - 21st Street, NW
Washington, DC 20451

Stephen Mangino
Phillips Laboratory/LWH
Hanscom AFB, MA 01731-5000

Dr. Robert Masse
Box 25046, Mail Stop 967
Denver Federal Center
Denver, CO 80225

Art McGarr
U.S. Geological Survey, MS-977
345 Middlefield Road
Menlo Park, CA 94025

Richard Morrow
ACDA/VI, Room 5741
320 21st Street N.W
Washington, DC 20451

Dr. Carl Newton
Los Alamos National Laboratory
P.O. Box 1663
Mail Stop C335, Group ESS-3
Los Alamos, NM 87545

Dr. Bao Nguyen
AFTAC/TTR
Patrick AFB, FL 32925

Dr. Kenneth H. Olsen
Los Alamos Scientific Laboratory
P. O. Box 1663
Mail Stop D-406
Los Alamos, NM 87545

Mr. Chris Paine
Office of Senator Kennedy
SR 315
United States Senate
Washington, DC 20510

Colonel Jerry J. Perrizo
AFOSR/NP, Building 410
Bolling AFB
Washington, DC 20332-6448

Dr. Frank F. Pilotte
HQ AFTAC/TT
Patrick AFB, FL 32925-6001

Katie Poley
CIA-ACIS/TMC
Room 4X16NHB
Washington, DC 20505

Mr. Jack Rachlin
U.S. Geological Survey
Geology, Rm 3 C136
Mail Stop 928 National Center
Reston, VA 22092

Dr. Robert Reinke
WL/NTESG
Kirtland AFB, NM 87117-6008

Dr. Byron Ristvet
HQ DNA, Nevada Operations Office
Attn: NVCG
P.O. Box 98539
Las Vegas, NV 89193

Dr. George Rothe
HQ AFTAC/TTR
Patrick AFB, FL 32925-6001

Dr. Alan S. Ryall, Jr.
DARPA/NMRO
1400 Wilson Boulevard
Arlington, VA 22209-2308

Dr. Michael Shore
Defense Nuclear Agency/SPSS
6801 Telegraph Road
Alexandria, VA 22310

11

Mr. Charles L. Taylor
Phillips Laboratory/LWH
Hanscom AFB, MA 01731-5000

Phillips Laboratory
Attn: XO
Hanscom AFB, MA 01731-5000

Dr. Larry Turnbull
CIA-OSWR/NED
Washington, DC 20505

Phillips Laboratory
Attn: LW
Hanscom AFB, MA 01731-5000

Dr. Thomas Weaver
Los Alamos National Laboratory
P.O. Box 1663, Mail Stop C335
Los Alamos, NM 87545

DARPA/PM
1400 Wilson Boulevard
Arlington, VA 22209

Phillips Laboratory
Research Library
ATTN: SULL
Hanscom AFB , MA 01731-5000

Defense Technical Information Center
Cameron Station
Alexandria, VA 22314   (2 copies)

Phillips Laboratory
ATTN: SUL
Kirtland AFB, NM 87117-6008   (2 copies)

Defense Intelligence Agency
Directorate for Scientific & Technical Intelligence
Attn: DT1B
Washington, DC 20340-6158

Secretary of the Air Force
(SAFRD)
Washington, DC 20330

AFTAC/CA
(STINFO)
Patrick AFB, FL 32925-6001

Office of the Secretary Defense
DDR & E
Washington, DC 20330

TACTEC
Battelle Memorial Institute
505 King Avenue
Columbus, OH 43201 (Final Report Only)

HQ DNA
Attn: Technical Library
Washington, DC 20305

DARPA/RMO/RETRIEVAL
1400 Wilson Boulevard
Arlington, VA 22209

DARPA/RMO/Security Office
1400 Wilson Boulevard
Arlington, VA 22209

Dr. Peter Basham
Earth Physics Branch
Geological Survey of Canada
1 Observatory Crescent
Ottawa, Ontario, CANADA K1A 0Y3

Dr. Eduard Berg
Institute of Geophysics
University of Hawaii
Honolulu, HI 96822

Dr. Michel Bouchon
I.R.I.G.M.-B.P. 68
38402 St. Martin D'Heres
Cedex, FRANCE

Dr. Hilmar Bungum
NTNF/NORSAR
P.O. Box 51
N-2007 Kjeller, NORWAY

Dr. Michel Campillo
Observatoire de Grenoble
I.R.I.G.M.-B.P. 53
38041 Grenoble, FRANCE

Dr. Kin Yip Chun
Geophysics Division
Physics Department
University of Toronto
Ontario, CANADA M5S 1A7

Dr. Alan Douglas
Ministry of Defense
Blacknest, Brimpton
Reading RG7-4RS, UNITED KINGDOM

Dr. Manfred Henger
Federal Institute for Geosciences & Nat'l Res.
Postfach 510153
D-3000 Hanover 51, FRG

Ms. Eva Johannisson
Senior Research Officer
National Defense Research Inst.
P.O. Box 27322
S-102 54 Stockholm, SWEDEN

Dr. Fekadu Kebede
Geophysical Observatory, Science Faculty
Addis Ababa University
P. O. Box 1176
Addis Ababa, ETHIOPIA

Dr. Tormod Kvaerna
NTNF/NORSAR
P.O. Box 51
N-2007 Kjeller, NORWAY

Dr. Peter Marshall
Procurement Executive
Ministry of Defense
Blacknest, Brimpton
Reading FG7-4RS, UNITED KINGDOM

Prof. Ari Ben-Menahem
Department of Applied Mathematics
Weizman Institute of Science
Rehovot, ISRAEL 951729

Dr. Robert North
Geophysics Division
Geological Survey of Canada
1 Observatory Crescent
Ottawa, Ontario, CANADA K1A 0Y3

Dr. Frode Ringdal
NTNF/NORSAR
P.O. Box 51
N-2007 Kjeller, NORWAY

Dr. Jorg Schlittenhardt
Federal Institute for Geosciences & Nat'l Res.
Postfach 510153
D-3000 Hannover 51, FEDERAL REPUBLIC OF
GERMANY

Universita Degli Studi Di Trieste
Facolta Di Ingegneria
Istituto Di Miniere E. Geofisica Applicata, Trieste,
ITALY

Dr. John Woodhouse
Oxford University
Dept of Earth Sciences
Parks Road
Oxford OX13PR, ENGLAND

Dr. Ramon Cabre, S.J.
Observatorio San Calixto
Casilla 5939
La Paz, Bolivia

Prof. Hans-Peter Harjes
Institute for Geophysik
Ruhr University/Bochum
P.O. Box 102148
4630 Bochum 1, FRG

Prof. Eystein Husebye
NTNF/NORSAR
P.O. Box 51
N-2007 Kjeller, NORWAY

Prof. Brian L.N. Kennett
Research School of Earth Sciences
Institute of Advanced Studies
G.P.O. Box 4
Canberra 2601, AUSTRALIA

Dr. Bernard Massinon
Societe Radiomana
27 rue Claude Bernard
75005 Paris, FRANCE   (2 Copies)

Dr. Pierre Mecheler
Societe Radiomana
27 rue Claude Bernard
75005 Paris, FRANCE

Dr. Svein Mykkeltveit
NTNF/NORSAR
P.O. Box 51
N-2007 Kjeller, NORWAY   (3 copies)